INTERFACE FUNCTIONALIZATION USING SUB-10 NANOMETER STRIPED PHASE FILMS FOR CONTROLLED FUNCTIONAL GROUP PRESENTATION AND ADSORBATE ASSEMBLY

by

Jeremiah Osman Bechtold

A Dissertation

Submitted to the Faculty of Purdue University

In Partial Fulfillment of the Requirements for the degree of

Doctor of Philosophy

Department of Chemistry

West Lafayette, Indiana

May 2021

THE PURDUE UNIVERSITY GRADUATE SCHOOL
STATEMENT OF COMMITTEE APPROVAL

Dr. Shelley A. Claridge, Chair

Department of Chemistry &

Weldon School of Biomedical Engineering

Dr. Jonathan J. Wilker

Department of Chemistry

Dr. Suzanne C. Bart

Department of Chemistry

Dr. Corey M. Thompson

Department of Chemistry

Approved by:

Dr. Christine Hrycyna

For by grace you have been saved through faith. And this is not your own doing; it is the gift of God, not a result of works, so that no one may boast. For we are his workmanship, created in Christ Jesus for good works, which God prepared beforehand, that we should walk in them. (English Standard Version Bible, 2001, Ephesians 2:8–10)

ACKNOWLEDGMENTS

"To God be the glory, great things he hath done"

Fanny Jane Crosby

I have been exceptionally blessed during my time at Purdue and it is for that reason alone I am able to submit this work and conclude my degree at Purdue. Numerous individuals from Purdue University and my local community have invested their time and energy into me. I am incredibly grateful for them and here is my feeble attempt to express that in writing.

To my wife Leah, thank you for being my partner and friend during the adventure graduate school has been for us. I am certain I could not have persevered through this without you. To my parents and brother, thank you for the constant love, prayer and support you have given me throughout my education. I am grateful for all the ways you have worked to provide for me.

To my advisor Professor Shelley Claridge, thank you for the years of investment you made into my professional development. Your professionalism, keen eye for detail, and constant instruction provided me with tools and skills that will benefit me for my entire career. To my current and graduated Purdue colleagues, I am grateful for the support, advise, and criticisms you all provided for me. I greatly benefited from our interaction and while I cannot mention everyone here, you know who you are, and I want to thank you. To Dr. Jae Jin Bang and Dr. Shane Russell, thank you for introducing me to the Claridge lab and for encouraging me to join. Choosing a laboratory to join as a 1st year graduate student is difficult but you made it seem easy. To Dr. Tyson Davis and Dr. Tyler Hayes, I am grateful for our friendship during our time at Purdue and am thankful for the years of advice and support you provided me during my research.

To my friends and Faith church community, my time in Lafayette and at Purdue has been great because of you all. You all have made Lafayette our home.

This is far from an exhaustive list and I hope everyone who knows me and has supported me knows that I am grateful and blessed by you. Thank you.

TABLE OF CONTENTS

LIST OF FIGURES

ABSTRACT

The precise control over interfacial chemistry at the nanoscale will be beneficial for the fabrication of next-generation materials. Noncovalent functionalization of 2D material interfaces may offer a bottom-up nanofabrication technique to control surface structure and functionality. Sub-10 nm chemical patterns of self-assembled amphiphiles are relevant to a range of applications such as biosensors and antifouling coatings where controlling substrate interactions with the environment are essential.

For the high-throughput screening of biomolecular interactions, the specific placement and presentation of functional groups on an interface is desired. In this presented work, we show that nanoscale patterns of self-assembled amphiphiles can be microcontact printed into microscale square arrays as a route to control the placement and presentation of complex functional groups. Within these square arrays the controlled presentation of functional groups is achieved, leveraging the 'sitting' phase orientation of diyne phospholipids, where the protruding headgroup is more available for environmental interactions. Additionally, we examine the effect that molecular structure and printing technique have on the pattern fidelity, demonstrating additional control measures may be applicable for noncovalent microcontact printing.

For elastomeric materials such as polydimethylsiloxane (PDMS), the amorphous surface poorly directs ordered adsorbate assembly, and the hydrophobic surface typically requires hydrophilization for further functionalization. O_2 plasma treatment of PDMS material is widely used to hydrophilize the surface prior to grafting additional functional groups; however, O_2 plasma can damage the material, leading to cracks and lower mechanic stability. PDMS materials are also susceptible to fouling from the nonspecific adsorption of biomaterials and microbes to the surface. These challenges suggest that it would be beneficial for PDMS material applications to control the surface chemistry of the interface at the nanoscale while preserving the advantageous properties of the material.

In this work, we also demonstrate how the nanoscale hierarchical patterns of cationic amphiphiles transferred to PDMS enable us to assemble anionic polyelectrolytes on the surface as a route for fabricating antifouling coatings without the use of O_2 plasma treatment. Here, we assemble two differently functionalized PDMS substrates with antifouling properties and compare their impact on the nonspecific adsorption of fluorescent proteins to the surface.

CHAPTER 1. INTRODUCTION

A central challenge within material fabrication is developing techniques to precisely control interfacial chemistry down to the sub-10 nm scale.[1-4] High resolution interfacial patterning is important to a wide range of applications such as nanoscale electronics,[1-2] organic energy conversion materials,[5] and biosensors.[6-7] For these applications it would be beneficial to control nanoscale interactions at the interface to direct organic and inorganic material assembly or present functional groups in ordered patterns. In fields such as glycobiology, controlling the presentation of complex biologically relevant functionalities benefit from microstructured patterns with nanoscale ordering to better mimic the numerous interactions associated in biological environments.[6-7] Conversely, controlling interfacial interactions may also be beneficial in preserving interfaces from degradation by inhibiting specific biological interactions.[8-10]

Selective interfacial interactions at the nanoscale are routinely expressed within nature, specifically the cell membrane. In the cell membrane, self-assembled amphiphiles organize nanoscopic patterns at sub-10 nm scales, controlling extracellular and intracellular interactions. The structural principles of the cell membrane can be applied to 2D materials (*e.g.*, highly ordered pyrolytic graphite (HOPG)) through the assembly of lying-down striped phase films creating patterns of chemical functionality.[11-12] In this work, we show how microcontact printing can achieve macroscopic templates with sub-10 nm chemical patterns and control the presentation of functional groups at the interface. Next, we examine how the assembly of striped phase films on an interface electrostatically direct the assembly of polyelectrolytes. We then demonstrate how the transfer of striped phase patterns to elastomeric materials may provide a route for fabricating antifouling coatings, leveraging the controlled presentation of functional groups and deposition of polyelectrolyte layers.

In nature, the design of the cell membrane presents, at the sub-10 nm scale, hierarchical ordering of unique chemistries, each engaging in numerous extracellular and intracellular functions. These structural principles can be translated into lying-down striped phases on 2D materials where the entirety of the amphiphile is exposed to the environment. The self-assembly of these striped patterns are commonly studied on HOPG, where the film is stabilized through noncovalent interactions with the substrate (*i.e.,* van der Waals forces from epitaxial matching with the graphite lattice) and intermonolayer interactions (*i.e.*, close packing of alkyl chains and

headgroup dimerization).[13] The Claridge group has shown that further monolayer stability is achieved through diacetylene (DA) groups within each monomer photopolymerized into a polydiacetylene backbone (PDA) throughout the monolayer.[14] These striped phases present a route for noncovalent high-resolution patterning for controlling local interfacial chemistry and directing assembly of adsorbates.[13, 15-16]

Diyne phospholipids represent a crucial component of the cell membrane and exhibit unique and advantageous properties within their self-assembled striped phase templates. Striped phase films of diyne phospholipids adopt a 'sitting' orientation on the HOPG surface where the headgroup protrudes a few Ångströms from the surface.[13, 17] The 'sitting' orientation provides striped phase films of diyne phospholipids greater access to the surrounding environment. Previous work in the Claridge group has shown that the headgroups of diyne phospholipids, in comparison to single chain fatty acids, when adjacent to a nonpolar surface exhibit $pK_{1/2}$ values similar to the solution values.[13] Therefore the protruding headgroups enable the striped phase film to control wetting, direct assembly, and control the interfacial chemistry of materials.[15-16, 18]

Assembling the noncovalent functionalization of striped phases on 2D materials is often accomplished through Langmuir–Blodgett and Langmuir–Schaefer (LS) conversion from the air/water interface.[13-14, 19-22] The Claridge group has shown that thermally regulated LS conversion improves the monolayer ordering to length scales >100 nm.[14] The assembled striped phase films are often characterized using atomic force microscopy (AFM) or scanning tunneling microscopy (STM).[23-24] In the AFM micrograph each stripe of the lamellar pattern represents rows of paired lying-down molecules ~1-nm wide with a sub-10 nm pitch. The Claridge group has also shown that scanning electron microscopy (SEM) can resolve the lying-down striped phase film at a broad range of 1 mm to ~10 nm.[19-20] In the SEM image, visible cracking, formed by conformation changes that occur during polymerization, in the long-range ordered monolayer illustrate µm-scale lamellar orientation.[20]

Within biological environments, complex biological entities are spatially ordered at both the nanoscale and microscale and presented at controlled orientations.[6-7, 25-26] For high-throughput screening of complex biomolecule interactions, mimicking the controlled placement and presentation of chemical entities would be beneficial.[6-7, 17, 25-26] Microcontact printing has been a broadly applied methodology to template geometrically controlled functionalities with sub micrometer accuracy to surfaces.[27-29] In Chapter 2, we demonstrate the microcontact printing of

striped phases as a route for controlling the macroscopic placement of function groups exhibiting nanoscopic ordered patterns on an interface. To control microscale placement, we microcontact print nanoscale patterned striped phase films to demonstrate the fabrication of geometrically constrained sub-10 nm chemical patterns. We then examine the relationship between molecular structure (*e.g.*, alkyl chain length, single and dual chain amphiphiles) and the fidelity of the printed pattern. Finally, we utilize the 'sitting' phase orientation of diyne phospholipids and a saturated phosphoinositol to demonstrate the control of functional group presentation and identify parameters to modulate the pattern fidelity and orientation.

For many biomedical applications, elastomeric materials (*i.e.*, polydimethylsiloxane (PDMS)) are utilized for their advantageous properties such as biocompatibility, low cost, and the ease of fabrication.[30] The PDMS surface, however, poorly directs adsorbate assembly and is susceptible to fouling in biological environments, and the inert hydrophobic surface typically requires hydrophilization via O_2 plasma treatment for further functionalization.[8-9, 31-33] Commonly applied techniques for reducing the fouling of PDMS materials are antimicrobial and antiadhesive coatings.[32, 34-35] Generally, antiadhesive coatings are used to reduce nonspecific adsorption by forming a thermodynamically unfavorable surface composed of well-hydrated, neutral or weakly negative, and sterically bulky adsorbates.[8, 10] These coatings can be fabricated through both top-down and bottom-up methodologies, but often require hydrophilization of the PDMS surface. While O_2 plasma treatment of PDMS is routinely used to hydrophilize the surface prior to the grafting process for fabricating antifouling coatings, this technique can create surface cracks and lower mechanical stability of the material.[31, 33]

The amorphous nature of the PDMS surface may also present challenges for directing patterning on the surface. The fabrication of a nanostructured PDMS surface may be beneficial for directing adsorbate assembly on the surface. The Claridge group has previously demonstrated a route to transfer stiped phase films from HOPG to PDMS through a polydiacetylene-on-amorphous material transfer (PATRN) process.[18] This striped phase film transfer to PDMS functions as a 'skin' on the surface altering the interfacial properties. The nanostructured arrays of sub-10 nm chemical patterns on PDMS may enable the controlled wetting and presentation of chemical functional groups as well as direct assembly of adsorbates on the surface.

In Chapter 3, we demonstrate the directed assembly of polyions to striped phase functionalized PDMS and illustrate its potential benefit for antifouling coating applications by

measuring the reduction of nonspecific adsorption of BSA proteins. First, we examine the adsorption of polyelectrolytes on striped phase films utilizing AFM. Next, we demonstrate that both weak and strong polyelectrolytes readily adsorb to striped phase functionalized PDMS but minimally to bare PDMS surfaces. We then expose the PDMS substrates to fluorescent labeled BSA protein solutions and characterize the surface of PDMS with fluorescence microscopy. Finally, we estimate the nonspecific adsorption of BSA to bare PDMS and functionalized PDMS substrates with a PSS coating or a microcontact printed zwitterion film and assess the antifouling properties of each interface.

CHAPTER 2. HIERARCHICALLY PATTERNED STRIPED PHASES OF POLYMERIZED LIPIDS: TOWARD CONTROLLED CARBOHYDRATE PRESENTATION AT INTERFACES

A version of this chapter has been published in *Faraday Discussions*
DOI: 10.1039/c9fd00022d

2.1 Introduction

Interfaces with precisely constructed chemical environments at the micrometer and nanometer scales are required for applications ranging from the design of electronic devices to the controlled display of complex biomolecules.[17] Increasingly, the goals of controlling interfacial structure may include not only positioning functional groups on the surface, but also controlling their orientation, clustering, or placement relative to other functional groups, mimicking complex structures such as those in cell membranes.

Monolayers of molecules such as alkanethiols have been broadly utilized to structure interfacial chemistry, particularly on coinage metals.[36] In alkanethiol monolayers, ordered lattices of alkyl chains position terminal functional groups with nearest-neighbor distances ~0.5 nm, tilted at angles influenced by the bond between the thiol and the substrate.[36] Lattices displaying simple functional groups (*e.g.* carboxylic acids) influence further assembly at the interface (*e.g.* selecting for specific crystal facets of calcite); microcontact printing enables geometrically patterned assembly over microscopic (or large nanoscopic) areas.[37-39]

Controlling presentation of more complex, biologically relevant functionalities raises new challenges. In biological environments, polysaccharides, peptides, and other entities are presented in controlled orientations, with both nanoscale and microscale spatial ordering. To mimic elements of these environments for applications such as high-throughput screening of biomolecular interactions,[6-7] it would be useful to present microstructured areas of surface containing nanostructured clusters of specific ligand chemistries, enabling multivalent binding similar to molecular recognition events in the glycocalyx.[25-26, 28, 40-46]

However, even monosaccharides occupy interfacial footprints substantially greater than that of an alkyl chain in an alkanethiol monolayer (~0.25 nm^2). Thus, creating simple lattices of these larger moieties becomes less straightforward. Designing complex clusters of functional

groups at biologically relevant scales— with linear dimensions large relative to alkyl chain nearest neighbor distances in standing phases (>0.5 nm) but small relative to those typically achieved through microcontact printing (significantly <100 nm)—becomes especially challenging.

One complementary strategy for clustering structures with larger footprints arises from a transformation to the monolayer structure.[17] Since at least the 1960s, it has been known that long chain alkanes can adopt lying down orientations on graphite and other layered materials such as MoS_2 and WS_2.[47-48] More recently, the surface chemistry of 2D materials (particularly graphite and graphene) has been regulated using striped phases of functional alkanes,[47-52] in which the alkyl chains extend horizontally across the substrate. Scanning probe microscopy studies[47-52] have shown that this arrangement produces nm-wide stripes of headgroups with 0.5 or 1 nm lateral periodicity along the row (for single-chain and dual-chain amphiphiles, respectively), separated by wider (~5 nm, dependent on chain length) stripes of exposed alkyl chains. Assembly of functional alkanes containing an internal diyne allows the monolayer to be photopolymerized, creating a conjugated ene–yne polymer backbone that has been studied extensively in the context of molecular electronics.[24, 50, 52] Polymerization also stabilizes the noncovalently adsorbed monolayer, increasing potential utility of patterns of functional groups displayed at the interface.[13-14, 53]

Just as clustering of functional groups at biological active sites creates unique chemical environments to promote specific interactions, precise positioning of functional groups in striped phases also creates unique chemical environments (Fig. 2.1). We have observed that striped phases of diyne phospholipids[13] exhibit distinct characteristics in comparison with striped phases composed of other amphiphiles.[54] Phospholipids can adopt a 'sitting' orientation in which the terminal amine in the headgroup protrudes a few Ångströms from the interface.[13]

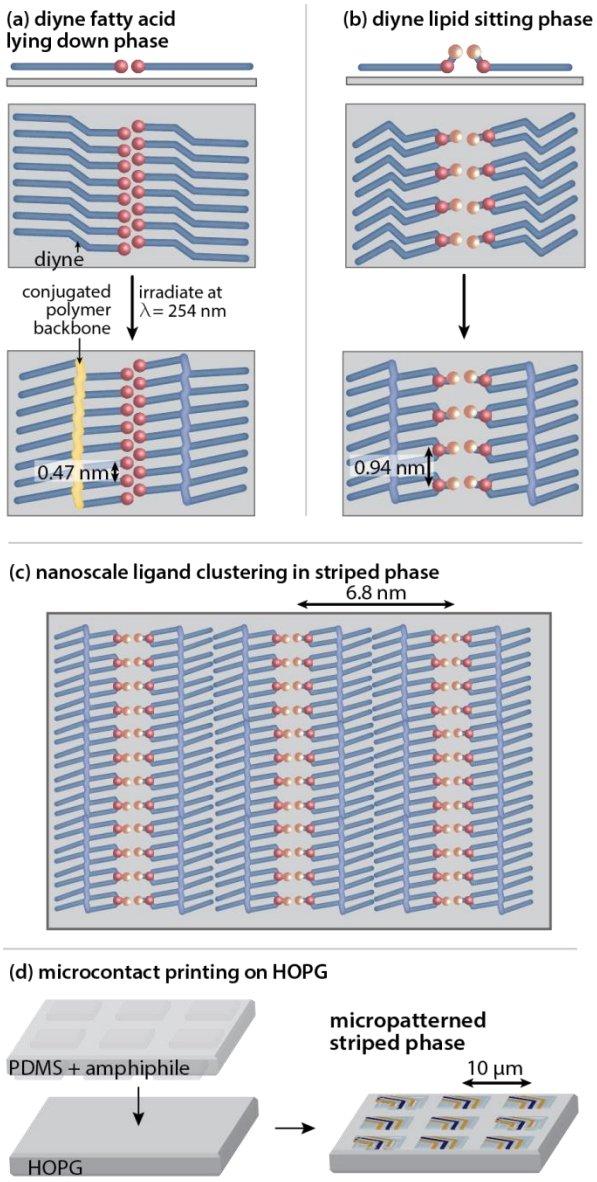

Figure 2-1 Illustrations of: (a) striped phase of diynoic acids on HOPG, showing a 0.47 nm distance between functional groups along the stripe direction; (b) striped phase of diyne phospholipids, showing a 0.94 nm distance between functional groups along the row; (c) multiple rows of the striped phase, showing lamellar periodicity, a route to nanoscale ordering of complex functional groups; and (d) illustration of poly(dimethylsiloxane) (PDMS) transfer of amphiphiles to HOPG to form striped phases.

The phosphate and ester functional groups create a tailored chemical environment around the amine. Both head and chain structures influence nano- and micro-scale assembly of striped phases,[14, 19-20] and chain elements including the position of the polymer backbone can be used to modulate solvent availability of the polar headgroups.[54] Flexible 1D zwitterionic arrays formed by

the striped phase also impact further assembly of inorganic and organic nanostructures at the interface.[15-16] More broadly, the striped phospholipid polymer architecture represents a potential means for flexible yet controlled presentation of ligands at the interface.

Microcontact printing of striped phases (Fig. 2.1d) has the potential to combine microscopic geometric control over surface chemistry with molecular-scale control over ligand presentation, a capability of potential use in glycobiology. However, the strong focus on molecular-scale structure in noncovalent striped-phase monolayers on highly oriented pyrolytic graphite (HOPG) has meant that such monolayers are typically ordered and characterized at length scales< 100 nm.[29, 55-56] Recently, we have shown that some amphiphiles order into striped phases with edge lengths > 10 mm,[14] scales relevant to controlling interactions with biological entities, and that monolayer ordering can be characterized by scanning electron microscopy (SEM), making it possible to characterize surface functionalization up to mm scales.[19-20, 57] Some noncovalent monolayers can also be robust enough to survive vigorous solution processing and other environmental interactions.[14, 16]

Here, we demonstrate microcontact printing of striped phases of amphiphiles on HOPG, utilizing both diyne amphiphiles (*e.g.* diynoic acids, diyne phospholipids) and a saturated phosphoinositol. This approach generates hierarchical molecular-scale and microscale interfacial clustering of functional ligands, including carbohydrates, prototyping a strategy of potential relevance for controlled presentation of carbohydrates at interfaces.

2.2 Results and Discussion

2.2.1 Preparation of striped monolayers on HOPG

Striped monolayers of both single-chain amphiphiles (*e.g.* 10,12-pentacosadiynoic acid (PCDA), Fig. 2.2a and b) and dual-chain amphiphiles (*e.g.* 1,2-bis(10,12- tricosadiynoyl)-sn-glycero-3-phosphocholine (diyne PC), Fig. 2.2a and c) are typically prepared via drop-casting or Langmuir–Schaefer (LS) conversion,[13-14, 16, 52, 58-59] then polymerized via UV irradiation and characterized by atomic force microscopy (AFM) (Fig. 2.2d and e). In AFM images, striped lamellar patterns are oriented at 120° angles, in epitaxy with the HOPG lattice; each stripe represents a row of lying-down molecules. SEM images of striped phases (Fig. 2.2f–i) typically exhibit brighter areas representing the molecular domains, against a darker background of HOPG.

Long linear features along the image diagonals in Fig. 2.2f and g represent step edges in the HOPG substrates. Higher-resolution SEM images (Fig. 2.2h and i) reveal linear defects within the ordered molecular domains, highlighting the directionality of the molecular rows.[20] Use of this combination of techniques enables us to characterize both microscopic and nanoscopic ordering in striped phases, including those with carbohydrate headgroups (*vide infra*).

2.2.2 Preparation of pattered striped monolayers on HOPG by microcontact printing

Microscopic patterns of striped phase monolayers were prepared on HOPG by microcontact printing,[45] as shown in Fig. 2.3. Stamps used for microcontact printing of alkanethiols on gold are commonly prepared with a 10 : 1 ratio of elastomer base to crosslinker, resulting in a nominal elastic modulus of ~2.6 ± 0.02 MPa at commonly used curing conditions (65 °C, 1 h).[60] For transfer to HOPG, which has relatively low local surface roughness, we often found that stamps prepared with a 10 : 2 ratio of base to crosslinker (nominal elastic modulus 3.6 ± 0.1 MPa)[60] improved transfer fidelity, while still enabling conformal contact.

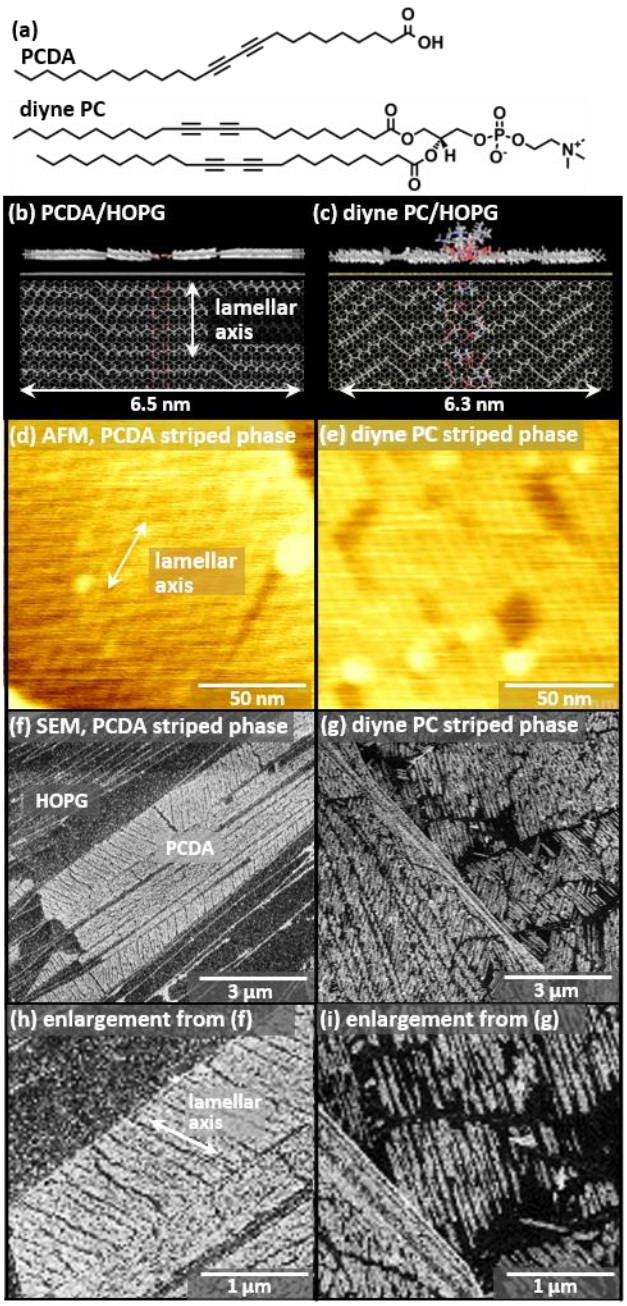

Figure 2-2 (a) Structures of PCDA and diyne PC. (b, c) Molecular models of striped phases of (b) PCDA and (c) diyne PC on HOPG. (d, e) AFM images of striped phases of (d) PCDA and (e) diyne PC, illustrating the lamellar pattern. (f–i) SEM images of striped phases of (f, h) PCDA and (g, i) diyne PC, illustrating long-range ordering.

A number of studies have previously examined factors relating to ink delivery to the substrate, with the goals of limiting diffusion of the ink outside the stamp contact area,[27, 61-62] and limiting delivery of impurities from the PDMS stamp.[62-63] Delivering a controlled amount of diyne

amphiphile to the substrate is especially important in assembling noncovalent monolayers; screening several possible methods for controlling diyne amphiphile delivery, we found that immersing the stamp in a solution of amphiphile in carrier solvent (1.1 mM for PCDA and single-chain amphiphiles, 0.55 mM for diyne PC and dual chain amphiphiles, maintaining the concentration of alkyl chains) generally maximized coverage of striped phase inside the contact area while minimizing coverage outside the contact area.

Ink concentrations used here are similar to those typically utilized for assembly of standing phases of alkanethiols on Au (1–10 mM),[36] although fewer molecules are required to fill a given area of the surface: the molecular footprint of an alkyl chain in a lying-down phase (1.5 nm^2 for PCDA) is much larger than for a standing phase (~0.25 nm^2). Fig. 2.3a and b show SEM images of a pattern of squares transferred to HOPG using the stamp preparation and inking conditions described above. Fig. 2.3b shows a higher-resolution image of the square pattern.

High coverage is observed within the squares; AFM is used to verify that molecular coverage is comprised of striped domains (Fig. 2.3b, inset, and Appendix A). Areas between the square stamp contact areas (channel regions) contain low number-densities of long, narrow molecular domains characteristic of submonolayer island nucleation and growth under conditions of low surface monomer concentrations.[64] Areas between squares also contain material that appears in dark contrast in SEM images. Similar features appear on substrates brought into contact with stamps wetted with the carrier solvents in the absence of amphiphile (see Appendix A). Deposition of impurities is also common in microcontact printing of alkanethiols on gold. Previous studies suggest that the deposited material is the oligomeric PDMS crosslinker, in which hydrosilyl groups undergo oxidation to form more polar species exhibiting increased solubility in the ink or carrier solvent.[63, 65]

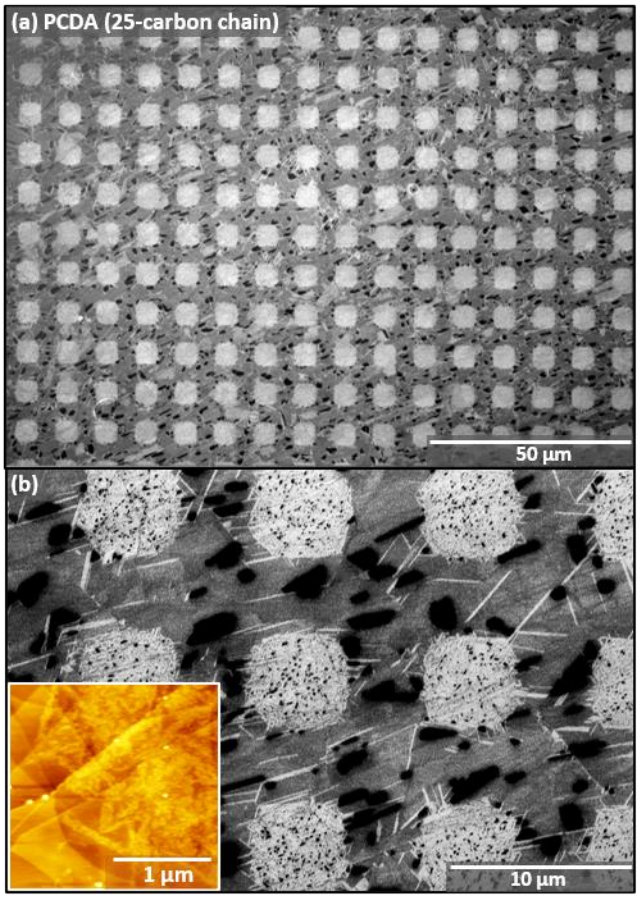

Figure 2-3 (a) SEM image of microscopic areas of PCDA striped phases assembled on HOPG by microcontact printing. (b) Higher-resolution SEM image illustrating coverage in the square interior and the small fractional coverage of molecular domains assembled outside the stamp contact area. An AFM image (inset in (b)) shows the striped phase structure.

2.2.3 Transfer characteristics of single-chain amphiphiles based on chain length

In using a striped phase to pattern functionality at an interface, shorter chain lengths correspond to smaller stripe pitch values, and thus shorter distances between linear clusters of functional groups on the surface (Fig. 2.4a). However, chain length also impacts dynamics in the self-assembly process. In previous demonstrations of microcontact printing to form standing phases (*e.g.* alkanethiols on Au), others have observed that molecular diffusion around the stamp contact area increases for molecular inks with shorter chains.[66-68] Here, we tested the transfer and assembly of 10,12-diynoic acids with chain lengths from 21 to 29 carbons to form noncovalently adsorbed striped phases to better understand the range of pitches that can reasonably be established, and the fidelity of patterning (Fig. 2.4b–d). In the Figure, areas exhibiting linear

defects typical of striped phases (similar to those in Fig. 2.2h) have been colored yellow as a guide to the eye. Image segmentation was used to estimate the average distance over which each amphiphile spread outside the stamped area in areas with good stamp contact (Fig. 2.4d, see ESI† for example AFM images used for segmentation). The average band through which molecules diffuse decreases in width from ~600 nm for HCDA to ~50 nm for NCDA. For all four carboxylic acids, the number density of domains was 10–20 per mm^2 within the contact area, which is reasonable given that the monomer concentration in the ink solution was the same for each molecule.

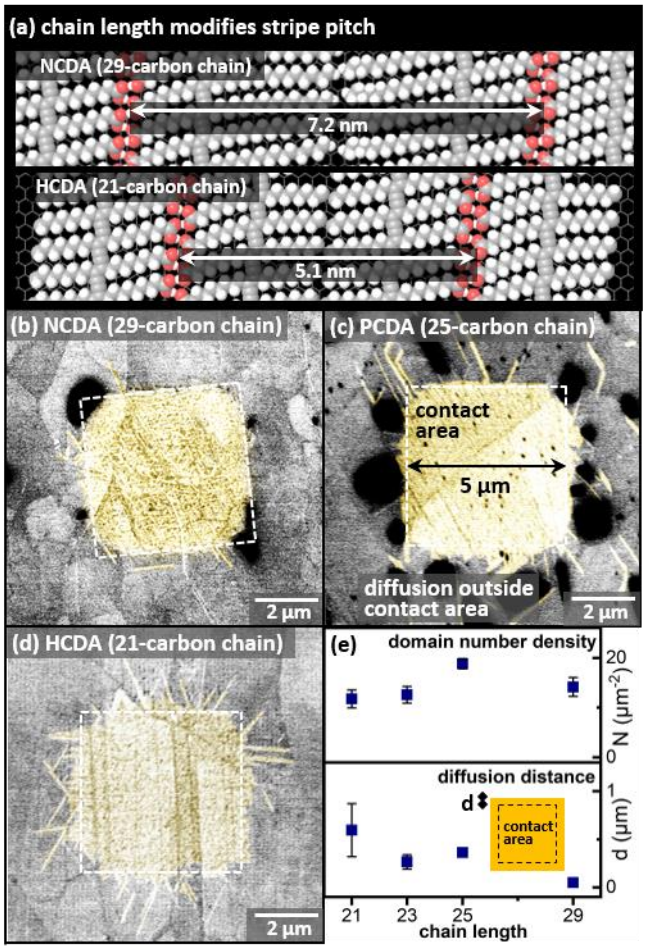

Figure 2-4 (a) Molecular models of diynoic acid striped phases with the longest (29 carbon) and shortest (21 carbon) chains utilized in these experiments. (b–d) SEM images of 10,12- diynoic acids: (b) nonacosadiynoic acid (NCDA, 29-carbon chain), (c) pentacosadiynoic acid (PCDA, 25-carbon chain), (d) henicosadiynoic acid (HCDA, 21-carbon chain). (e) Average domain number density per mm2, N, and average distance molecular

2.2.4 Transfer dual-chain amphiphiles

Commercially available diyne phospholipids have two alkyl chains and a zwitterionic headgroup, which would be expected to modulate molecular transfer and spreading on the substrate in comparison with the single-chain carboxylic acids transferred above. Here, we test the transfer behavior of two diyne phospholipids, 23:2 diyne phosphocholine (diyne PC, Fig. 2.5) and 23:2 diyne phosphoethanolamine(diyne PE, Fig. 2.6). The phospholipid structures are identical with the exception that the bulky terminal quaternary ammonium in the PC headgroup (Fig. 2.5a) limits molecular packing in comparison with PE, which has a smaller terminal primary amine.

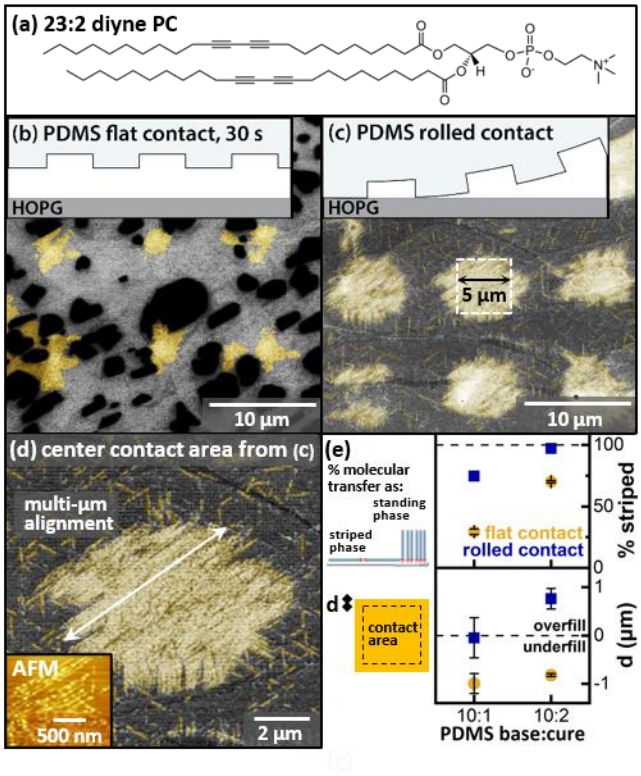

Figure 2-5 (a) Structure of diyne PC. (b–d) SEM images of 0.5mMdiyne PC in EtOH transferred to HOPG using (b) 30 s flat contact and (c, d) rolled contact (stamp prepared at 10 : 2 base : crosslinker ratio). (e) Comparison of % striped phase (vs. standing phase) molecular transfer with flat and rolled stamp contact, and fill of contact area, for PDMS stamps prepared with 10 : 1 and 10 : 2 base : crosslinker ratios.

Transfer conditions similar to those optimized for single-chain amphiphiles result in a large fraction of standing phase formation (bright areas in square centers) (Fig. 2.5b, highlighted in yellow as a guide to the eye; also see Appendix A). This is reasonable given the large number of

alkyl carbons per molecule, promoting interchain interactions leading to standing phase formation. To mechanically destabilize interchain interactions (*e.g.* standing phases) on the stamp, and to initiate domain growth from a limited area (to increase post-transfer molecular alignment), we tested molecular delivery by rolling the stamp along the HOPG surface (Fig. 2.5c and d, see Appendix A for more experimental detail regarding the rolling procedure). Testing transfer from stamps prepared with both 10 : 1 and 10 : 2 PDMS elastomer base : crosslinker ratios, we found that rolled contact increased the percentage of molecular transfer that produced striped phases (to near 100% for 10 : 2 stamps with rolled contact, Fig. 2.5e). Flat contact typically resulted in under filling of the stamp contact area, while rolled contact resulted in average coverage zones extending nearly 1 μm outside the stamp contact area (as visible in Fig. 2.5d). In some cases (again, see Fig. 2.5d), rolled contact produced molecular alignment across the stamp contact areas (i.e., lamellar axes aligned from upper left to lower right in Fig. 2.5d). Using other contact geometries, we have not observed this behavior, so with further optimization, rolled contact may represent a means of achieving long-range molecular alignment in printed striped phases, for applications in which such alignment is desirable.

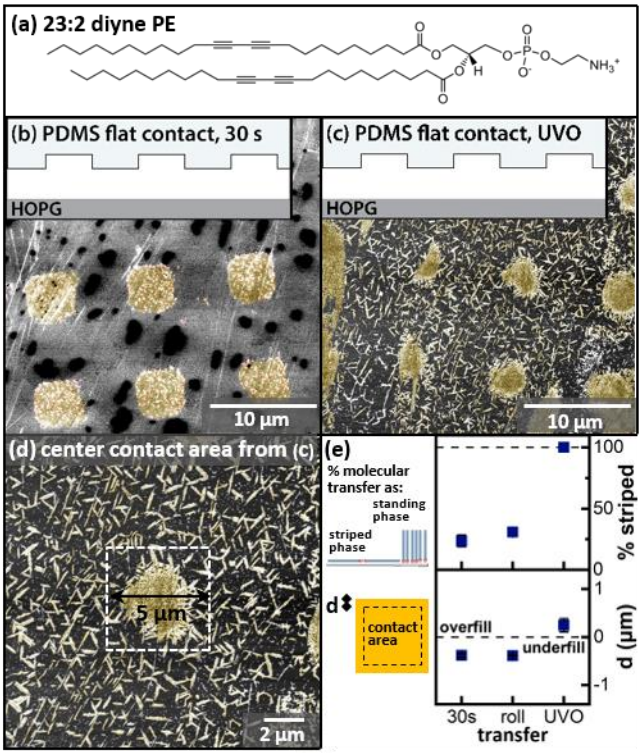

Figure 2-6 (a) Structure of diyne PE. (b–d) SEM images of 0.5 mM diyne PE in EtOH transferred to HOPG using (b) 30 s flat contact and (c, d) flat contact with stamp hydrophilicity increased with UV ozone (stamp prepared at 10 : 2 base : crosslinker ratio). (e) Comparison of % striped phase (vs. standing phase) molecular transfer with flat contact, rolled contact, and flat contact with UV ozone, and fill of contact area, for PDMS stamps prepared with 10 : 2 base : crosslinker ratios.

Figure 2-7 (a) Structure of 18:0 phosphoinositol (18:0 PI). (b–d) Minimized molecular models of striped phase of 18:0 PI on HOPG, illustrating: (b) lamellar width, (c) projection of inositol rings, in side view, (d) spacing of inositol rings (45° tilted view). (e–h) SEM images of PI striped phases formed using (e, f) rolling contact and (g, h) UV ozone-treated stamps for microcontact printing. (i) AFM image of PI striped phase, and line scans illustrating (j) domain height and (k) lamellar width.

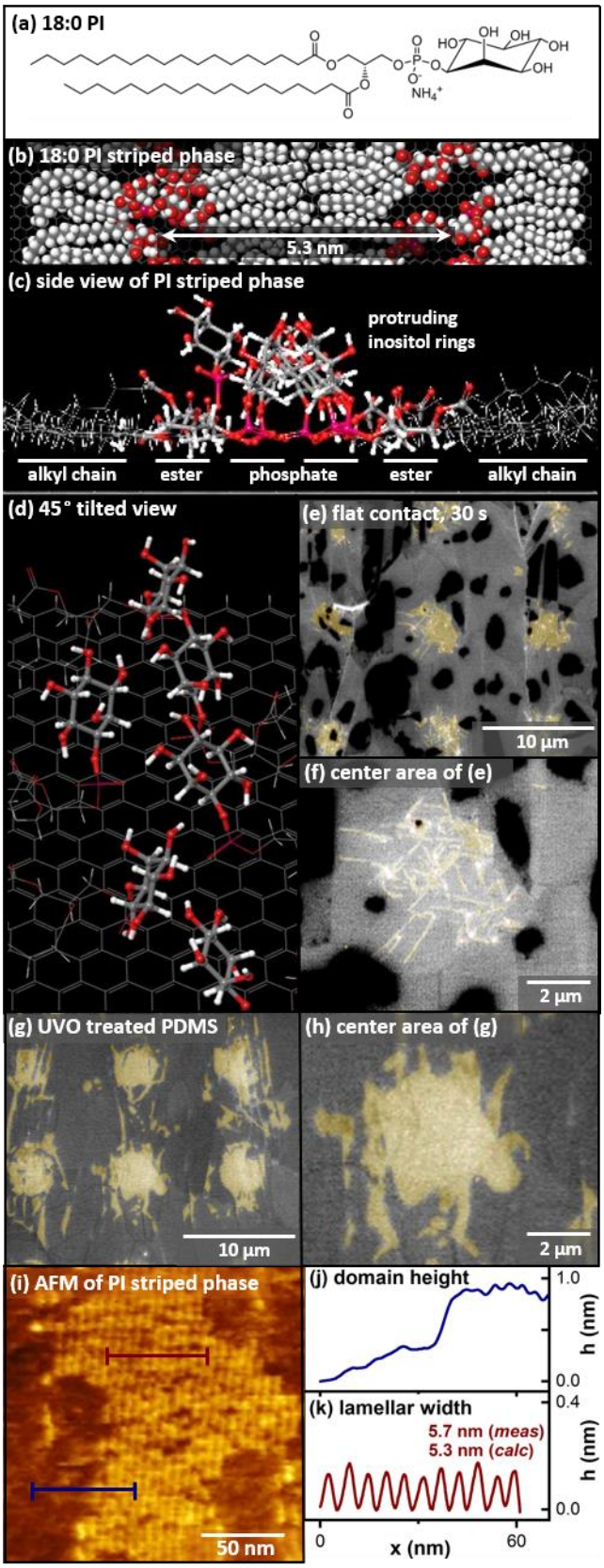
(a) 18:0 PI
(b) 18:0 PI striped phase
5.3 nm
(c) side view of PI striped phase
protruding
inositol rings
alkyl chain
ester
phosphate
ester
alkyl chain
(d) 45° tilted view
(e) flat contact, 30 s
10 µm
(f) center area of (e)
2 µm
(g) UVO treated PDMS
10 µm
(h) center area of (g)
2 µm
(i) AFM of PI striped phase
50 nm
(j) domain height
1.0
0.0
h (nm)
(k) lamellar width
5.7 nm (meas)
5.3 nm (calc)
0.4
0.0
h (nm)
0
x (nm)
60

Diyne PE (Fig. 2.6a) has a smaller terminal amine group that enables stronger lateral interactions between headgroups in standing phases, in comparison with the PC headgroup (which is bulky enough to limit packing). Importantly, the primary amine can also act as a functional handle for further coupling reactions, of potential utility in elaborating headgroups for glycobiological applications. Microcontact transfers of diyne PE in the conventional flat contact geometry also produced large areas of molecules assembled in standing phases (Fig. 2.6b). For transfer of diyne PE, the highest percentages of striped phase were observed for transfers in which the stamp surface hydrophilicity was increased by treatment with UV ozone plasma (a process which has been used previously to transfer hydrophilic molecules to create standing phase self-assembled monolayers (SAMs)). While multiple factors may contribute to the observed improvement in striped phase assembly during transfer, one possibility is that the hydrophilic stamp enables PE to assemble with polar headgroups oriented toward the stamp surface, with tails oriented favorably to mediate the initial stages of adsorption to HOPG for striped phase assembly. The differences in transfer behavior observed for molecules as structurally similar as diyne PE and diyne PC suggests a need to carefully balance molecule–stamp, molecule–molecule, and molecule–substrate interaction strengths for transfer of complex amphiphiles such as those relevant to glycobiology.

2.2.5 Striped phases from carbohydrate-conjugated lipids

The procedures developed above are also useful for microcontact printing of phospholipids incorporating carbohydrates in the headgroups. Here, we demonstrate that 1,2-distearoyl-sn glycero-3-phosphoinositol (18:0 PI, Fig. 2.7a), a phospholipid with an O-linked monosaccharide appended to the phosphate, can assemble into striped phases through microcontact printing (Fig. 2.7b–d, models; Fig. 2.7e–h, SEM). As with other phospholipids, bringing the stamp into flat contact with the HOPG substrate resulted in assembly of standing phases (see Appendix A), while rolling contact or stamps treated with UV ozone produced striped phases with domain lengths in some cases >2 mm (Fig. 2.7f). Characterization of domain structure based on SEM images is more challenging for these amphiphiles, since they lack the polymerizable diyne group, and thus do not exhibit cracking defects under the electron beam. However, AFM images (Fig. 2.7i) reveal a lamellar structure consistent with that predicted by molecular models, with average peak domain

heights of ~0.8 nm (Fig. 2.7j, corresponding to inositol headgroup ridges), and measured lamellar widths of 5.7 nm (Fig. 2.7j), similar to the modeled values of 5.3 nm.

2.3 Conclusions

Here, we have demonstrated that it is feasible to use microcontact printing to create microscale striped patterns of amphiphiles. Stripes were printed using diynoic acids with chain lengths from 21–29 carbons, diyne phospholipids with phosphocholine and phosphoethanolamine headgroups, and phosphoinositol with 18-carbon saturated chains. The lamellar structures assembled in this way present 1 nm-wide stripes of functional headgroups with pitches from 5–10 nm determined by alkyl chain length. In the cell membrane, amphiphiles with diverse headgroup chemistry, including pendant carbohydrates, are used to mediate interactions with other cells and the extracellular matrix. Our findings point to the possibility that similarly diverse headgroup chemistries could be installed in striped phases, either directly through Langmuir–Schaefer conversion, or through post-assembly modification using common coupling chemistries. Overall, this illustrates a new route for controlled molecular-scale clustering of complex ligands such as carbohydrates at interfaces.

CHAPTER 3. POLYELECTROLYTE ADSORPTION TO STRIPED PHASE FILMS ON ELASTOMERIC MATERIAL: TOWARD ANTIADHESIVE COATING FABRICATION

3.1 Introduction

Extensive research has investigated mechanisms to control the nanoscale surface chemistry of materials for fabrication applications.[2, 5, 17, 69-72] Increasingly, the goals of controlling interfacial interactions include not only directing adsorption for fabrication but limiting future unwanted environmental interactions.[8-10] Nanostructured films generated by techniques such as Langmuir–Schaefer (LS) and Langmuir–Blodgett (LB) transfer have been investigated for controlling interfacial chemistry as the nanoscale.[13, 19-20, 73] Nanostructured films are commonly assembled on rigid crystalline 2D materials aimed to modify select properties of the substrate and fabricate high resolution patterns.[49, 74-77]

Commonly applied techniques for reducing nonspecific adsorption of biomaterials are antimicrobial and antiadhesive coatings that typically require controlled interfacial interactions through a variety of top-down and bottom-up fabrication strategies.[32, 34, 78] For example, biomedical applications preventing biofilm formation requires surface functionalization to reduce the rate of biomaterial and microbial adsorption.[8, 10, 32, 79-80]

Generally, antiadhesion coatings are fabricated to form a thermodynamically unfavorable surface for biomaterial adsorption by creating well hydrated, neutral or weakly negative, sterically bulky coatings.[8, 10, 32] Polyethylene glycol (PEG) derivatives and zwitterions are commonly grafted on substrates for general antiadhesive coating applications. The adsorption of polyelectrolytes via Layer-by-Layer (LBL) deposition has also been implemented to incorporate antifouling components within multilayers creating opportunity for the modular design of coatings.[32, 34-35, 81]

Elastomeric materials (*e.g.*, poly(dimethylsiloxane), PDMS) exhibit advantageous material properties for biomedical applications such as nontoxicity, biocompatibility, ease of fabrication, and low cost.[30] The hydrophobic surface of PDMS requires functionalization in order to protect the material from fouling. The grafting of zwitterions and PEG coatings typically requires the hydrophilization of the PDMS surface (e.g. O_2 plasma treatment) prior to functionalization.[9, 30, 32] However, plasma treatment functionalization of PDMS is susceptible to engulfment, can induce surface cracks, and lower mechanical stability.[31, 33]

Controlling structure at sub-10 nm scales is central to many areas of material chemistry ranging from nanoscale electronics to organic energy conversion materials.[1-2, 5] Striped phases assembled by long alkyl chains with a terminal functional group and other noncovalent functionalization chemistries are an important method for fabricating high resolution interfacial patterns (Fig. 3.1b).[17, 48-49] On highly ordered pyrolytic graphite (HOPG) these patterns are stabilized by van der Waals forces between the alkyl chains in epitaxy with the graphene lattice and intermolecular headgroup dimers (Fig. 3.1b).

Previously, we have found that striped phase films on HOPG can orient the assembly of adsorbates and direct nanoscale wetting.[15-16, 75] Applying striped phase functionality to PDMS may be beneficial to indue the material with high resolution chemical patterns and potentially avoiding the challenges associated with O_2 plasma treatment.

Previous work with nanostructured saturated amphiphiles demonstrated that the templates would electrostatically direct the adsorption orientation of polyions on HOPG.[75] The directed assembly of polyions illustrated a potential mechanism for controlled polymer interactions at the interface. In our lab, we have fabricated polydiacetylene (PDA) nanoscale templates, with a ~1-nm wide chemical pattern and sub-10 nm pitch on 2D materials. Utilizing these templates, we directed the assembly of AuNWs through strong dipole directing effects.[15] The introduction of photopolymerizable diacetylene (DA) groups in noncovalent templates may improve solution stability during polyion adsorption over saturated amphiphile templates (*vide infra*). Recently, we transferred these nanoscale templates to elastomeric materials (*i.e.*, PDMS) providing a route to chemically pattern PDMS without O_2 plasma treatment.[18] The transferred films were shown to be stable against engulfment, and were fluorescently labeled, demonstrating the potential for further surface modification.

In this study, we first examine strong and weak anionic polyions (*e.g.*, poly(styrenesulfonate) (PSS) and poly(acrylate) (PAA), Fig. 3.1a) adsorbing to (cationic) PDA striped phase patterns. These polyions were selected to compare the impact different electrolyte structures and solution charge properties (*i.e.*, complete vs. partial dissociation) has on adsorption. The ~1-nm wide chemical pattern electrostatically directs the adsorption of PSS to the surface (Fig. 3.1b) creating anisotropic regions of the polymer in epitaxy with the underlying striped phase template (Fig. 3.1c).

Additionally, we then characterize and measure the surface wetting behavior of both HOPG and PDMS functionalized substrates to examine the properties of transferred ammonium groups. Finally, we fabricate and expose polyelectrolyte and zwitterionic coatings to fluorescent proteins to examine the antifouling properties of each surface and compare with a bare PDMS control.

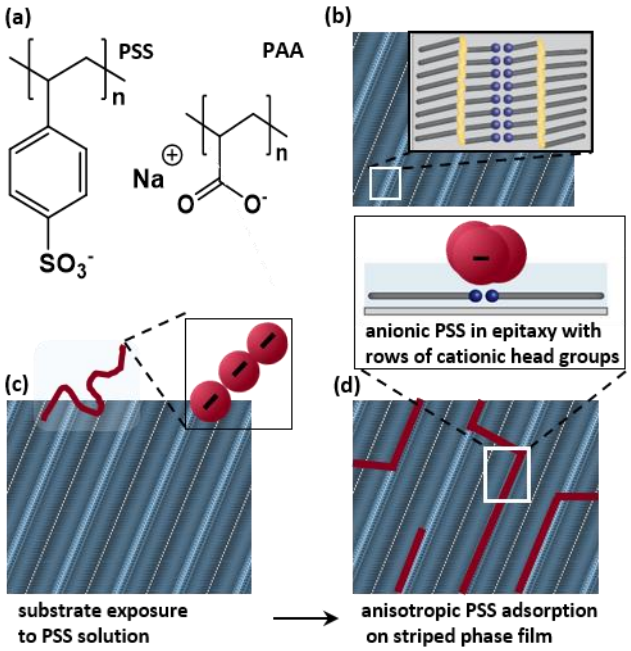

Figure 3-1 (a) Structures of poly(styrenesulfonate) (PSS) and polyacrylate (PAA). (b) Cartoon of a striped phase film, (c) the interactions between striped phase patterns on HOPG and PSS in solution, and (d) of the anisotropic alignment of PSS and enlarged schematic of the electrostatic interactions in epitaxy with striped amine template.

3.2 Results and Discussion

3.2.1 Preparation and assembling of a striped phase monolayer on HOPG

Striped phase monolayers of 10,12-pentacosadiynamine (PCD-NH_2, Fig. 3.2a), 10,12-tricosadiynamine (TCD-NH_2, Fig. 3.2a), and 1,2-bis(10,12-tricosadiynoyl)-*sn*-glycero-3-phosphocholine (dPC, Fig. 3.2a) were prepared via Langmuir–Schaefer (LS) conversion, using previously reported procedures.[13-14] Briefly, LS conversion begins by generating a standing phase Langmuir film on water, after which a freshly cleaved HOPG substrate is slowly lowered onto the hydrophobic face of the film. A fraction of molecules in the Langmuir film undergo transfer to the HOPG substrate, forming structured striped phases (Fig. 3.2b–e).

Here, assembly of PCD-NH_2 and TCD-NH_2, which have amine headgroups, generates highly structured polyelelectrolyte-templated surfaces containing 1-nm-wide stripes of amines with a pitch of ~5.8 nm (Fig. 3.2b). Because the molecules include an internal diacetylene (DA) group (Fig. 3.2b, highlighted in gold), the monolayers can be photopolymerized *via* UV irradiation, generating conjugated polydiacetylene (PDA) backbones oriented parallel to the lamellar axes (Fig. 3.2c, highlighted in gold). Characterized by atomic force microscopy (AFM), the visible striped pattern represents rows of paired lying-down molecules (Fig. 3.2d). The measured lamellar periodicity of ~5.3 nm (Fig. 3.2d) is commensurate with the theoretical ~5.8 nm pitch in the molecular model (Fig. 3.2c).

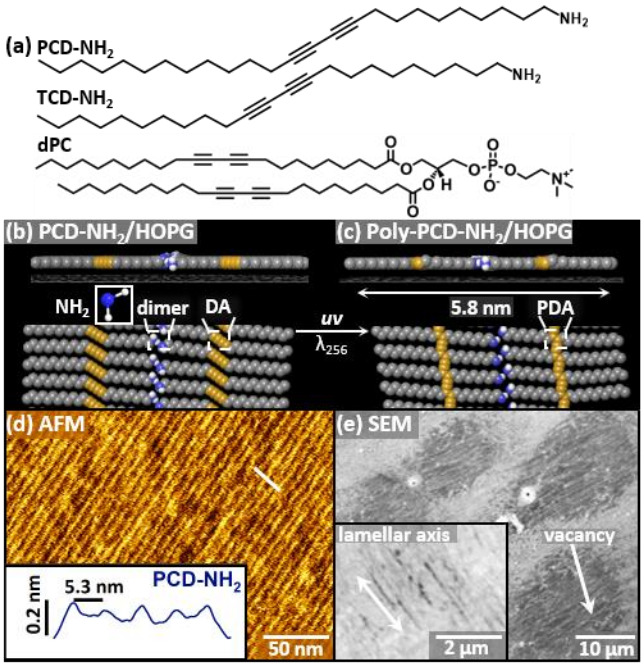

Figure 3-2 (a) Structures of PCD-NH_2 and TCD-NH_2 (b, c) Molecular models of striped phases of PCD-NH_2 (d) AFM micrographs of striped phases of PCD-NH_2 illustrating the lamellar pattern. (e) SEM images of PCD-NH_2 film illustrating vacancies within assembled film. Insets in (d) show line profile from lamellar pattern. (e) Striped phases illustrating oval vacancies within monolayer. Inset illustrates lamellar orientation parallel to the crack defects in the monolayer after polymerization.

Although striped phases are typically studied at small length scales (<10 μm) by scanning tunnel microscopy (STM) and AFM,[23-24] SEM enables characterization of broader topographical features (*e.g.*, the long-range ordering of domains, 10–100 μm).[20] Conductive HOPG appears dark

in SEM images, while striped phase molecular domains scatter electrons and appear as bright regions.[19-20] For LS conversion, we chose conditions we have previously found to produce monolayers of various characteristics (*e.g.*, long-range ordering, and large oval vacancies).[14, 20] These film conditions facilitate characterization of striped films *via* SEM or fluorescence microscopy by creating easily identified and reproducible surface features. In Fig. 3.2e, we show an assembled PCD-NH_2 monolayer with oval vacancies consistent with domain structure transitioning from complete to low density coverage on the HOPG. For long-range ordered films, the μm-scale lamellar orientation is illustrated in the SEM image (Fig. 3.2e; inset) based on visible cracks parallel to the lamellar axis that evolve during polymerization.[14]

3.2.2 Anisotropic polyelectrolyte adsorption on striped phase films

We compared polyelectrolyte adsorption on structured striped phase templates on HOPG, utilizing spin coating and dip coating techniques. While dip coating is more scalable (and thus more industrially compatible), non-covalent films may be more susceptible to desorption during the longer solution exposure times associated with dip-coating. In this experiment, we also compared polyelectrolyte adsorption on polymerized and non-polymerizable striped phase films. Adsorption of PSS on octadecylamine (ODAm)/HOPG was reported previously.[75, 82] Here, we made a direct comparison with adsorption of PSS to PCD-NH_2/HOPG. In other work, we have found that striped monolayer polymerization improved stability toward solvent exposure in comparison with unpolymerized films;[14] here, that effect could potentially stabilize the films for PSS dip coating. In comparison with ODAm films, PCD-NH_2 films provide additional advantages, including covalent transfer to other substrates,[83] as described below.

First, we compared assembly of (anionic) PSS on (cationic) PCD-NH_2/HOPG and ODAm/HOPG films through spin-coating (see Appendix B for more experimental detail), to benchmark assembly with minimal solvent exposure. PCD-NH_2 and ODAm films utilized for these experiments exhibited ordered domains with length scales >300 nm (Fig. 3.3a,b, and Figure S.B. 1). PSS adsorbed to PCD-NH_2/HOPG and ODAm/HOPG at a similar surface density (Fig. 3.3a,b). However, the adsorbed morphologies on the two films were very different. On ODAm striped templates, we observed greater epitaxial alignment between PSS and ODAm, with segmental lengths >200 nm (Fig. 3.3b) in comparison to PCD-NH_2 (segmental lengths <100 nm). One

possible interpretation would be that non-polymerized lamellae in the ODAm film restructure to accommodate interactions with adsorbing PSS, improving adsorbate alignment.

Dip coating, common in LBL film preparation,[35, 72, 84] increases the solvent exposure and adsorption time associated with polyelectrolyte deposition. Anisotropic alignment of PSS was somewhat decreased for both film types (Fig. 3.3c,d), to segmental lengths ~50 nm on PCD-NH_2/HOPG and ~100 nm on ODAm/HOPG. Desorption of the ODAm film was greater under the same conditions (Fig. 3.3d), producing large vacancies where PSS typically aligned along the edge and decreasing aligned segment lengths to ~100 nm. Overall, the disordering of non-covalent films on HOPG after dip coating suggests increased monolayer stability would be beneficial for processes requiring extensive solution exposure.

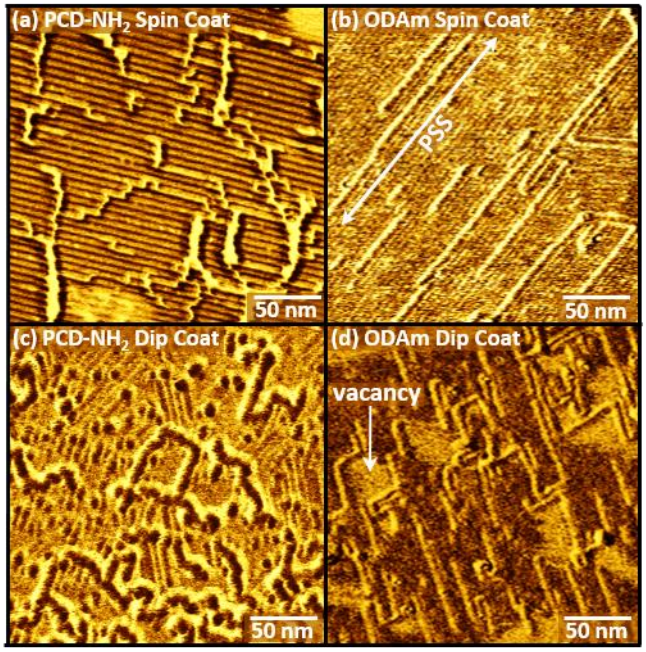

Figure 3-3 AFM micrographs of (a,c) PCD-NH_2/HOPG and (c,d) ODAm/HOPG films with strong polyelectrolyte PSS adsorbed to the surface. Spin coat: A 50 µL aqueous PSS solution of 4 µg/mL was spin coated at 2400 rpm on (a) PCD-NH_2/HOPG and (b) ODAm/HOPG. Dip coat: Substrates of (c) PCD-NH_2/HOPG and (d) ODAm/HOPG were immersed in a PSS solution of 4 µg/mL for 30 s, blown dry with UHP N_2, and immediately imaged.

3.2.3 Comparison of surface wetting after transfer to PDMS

It would be reasonable to expect that generating covalent bonds between the functional monolayer and the substrate would increase the solution stability of the monolayer. We recently

demonstrated the transfer of striped phase films from HOPG to PDMS through a polydiacetylene-on-amorphous material transfer (PATRN) process (Fig. 3.4a);[83] here, we anticipated that transferring stripes of charged groups to the hydrophobic PDMS surface would enable us to control adsorption of polyelectrolytes on PDMS without O_2 plasma hydrophilization.[18]

To transfer striped phase films from HOPG to PDMS (Fig. 3.4a), a mixture of PDMS crosslinker and base polymer is cured in contact with a striped phase film. Curing results from Pt-catalyzed hydrosilylation, forming bonds between Si-H and C-C multiple bonds. In the bulk PDMS mixture, these are vinyl groups in the PDMS base polymer; however, at the interface, the PDA backbone of the striped phase film can participate in the crosslinking reaction, covalently linking the monolayer to the PDMS. Following crosslinking, the functionalized PDMS is gently exfoliated from the HOPG substrate.

Modulating polyelectrolyte adsorption parameters such as the solution charge state (*e.g.*, controlled through the pH and ionic strength of solution) and the surface charge density (*e.g.*, controlled by altering the density of functionalities on a surface) are important for LBL coating fabrication.[84-85] In striped monolayers, differences in alkyl chain length modulate the surface density of charged functional groups.[86] Here, we selected two amphiphiles with terminal amines of different alkyl chain lengths. AFM images of PCD-NH_2/HOPG and TCD-NH_2/HOPG (Fig. 3.4b) illustrate domain sizes >100 nm, typical for thermally regulated LS conversion of single-chain amphiphiles.[14]

Transfer of the PDA layer to PDMS can be characterized based on fluorescence emission from the conjugated PDAs. Regions of low fluorescence visible in transferred films (Fig. 3.4c) are morphologically consistent with vacancies observed in films on HOPG prior to transfer (Fig. 3.2e and Figure S.B. 6a).

After characterization of the striped phase films, we measured the wetting properties of PCD-NH_2/HOPG and TCD-NH_2/HOPG controls as well as PCD-NH_2/PDMS and TCD-NH_2/PDMS for comparison. Our group has previously shown an increase of $pK_{1/2}$ values for carboxylic acid functional groups directly adjacent to the nonpolar interface.[13] Due to the lower stability of charged groups adjacent to the nonpolar HOPG surface, we expected a decrease in the $pK_{1/2}$ values for the amine functional groups compared to solution values (~10.5 pH).[87]

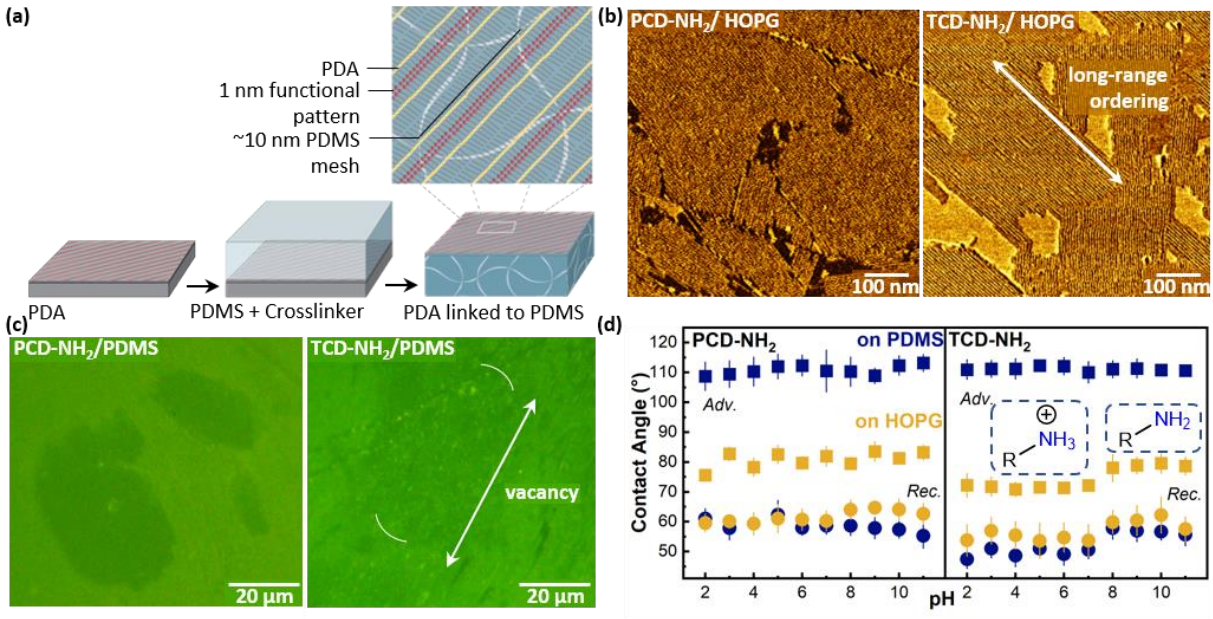

Figure 3-4 (a) Cartoon of the PATRN transfer process illustrating a striped monolayer on HOPG is crosslinked *in situ* and exfoliated onto PDMS. (b) AFM micrographs of PCD-NH_2/HOPG, and TCD-NH_2/HOPG exhibiting ordered striped phase domains. (c) Fluorescence images of PCD-NH_2/PDMS, and TCD-NH_2/PDMS illustrating vacancies in transferred film. (d) Contact angle titrations for PCD-NH_2 (left), and TCD-NH_2, (right) are shown on HOPG (gold) and on PDMS (blue) for comparison.

The advancing contact angles (Fig. 3.4d, gold squares) for PCD-NH_2/HOPG are higher than TCD-NH_2/HOPG (low pH ~8 °, high pH ~3 °) while the values for PCD-NH_2/PDMS and TCD-NH_2/PDMS substrates are similar to bare PDMS values (~110 °, blue square) consistent with our previous work.[18] Similarly, the receding angles (Fig. 3.4d, gold circles) for PCD-NH_2/HOPG are higher than TCD-NH_2/HOPG (low pH~6 °, high pH ~4 °) and for PCD-NH_2/PDMS (Fig. 3.4d, blue circles) the angles were higher than TCD-NH_2/PDMS (low pH ~10 °, high pH ~1 °). The lower contact angles observed for TCD-NH_2/HOPG may be consistent with greater headgroup accessibility, as we have found previously for striped phases of carboxylic acids.[13] All the receding angles except for PCD-NH_2/PDMS indicate $pK_{1/2}$ values (~7.5 pH) lower than the reported solution values, consistent with our predictions. The increase of the contact angles above pH 8 indicate the deprotonation of the ammonium groups on the surface. The wetting behavior for PCD-NH_2/PDMS is consistent with a charged ammonium group present across the entire pH range measured. From the data, we expected that the charged state of the transferred films would enable us to adsorb anionic polyelectrolytes to the functionalized PDMS surface.

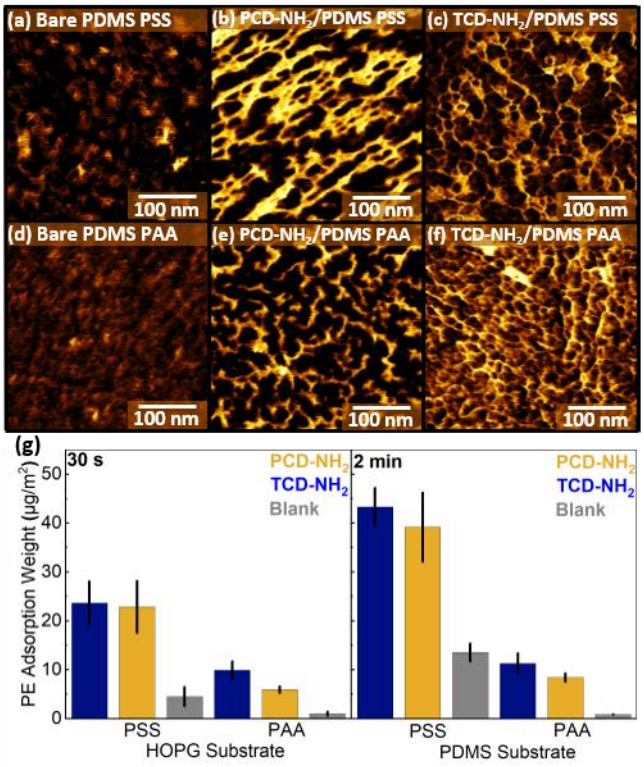

Figure 3-5 Top: AFM micrographs of (b,e) PCD-NH_2/PDMS, (c,f) TCD-NH_2/PDMS, and (a,d) bare PDMS with strong polyelectrolyte PSS (a–c) and weak polyelectrolyte PAA (d–f) adsorbed to the surface. Functionalized PDMS substrates were immersed in a polyelectrolyte solution of either PSS (4 µg/mL) or PAA (2 µg/mL) for 2 min, blown dry with UHP N_2, and immediately imaged. Bottom: The bar graph compares the estimated adsorption mass of polyelectrolytes PSS and PAA on HOPG (left) and PDMS (right) functionalized with PCD-NH_2, or TCD-NH_2 films in comparison to the bare substrate.

3.2.4 Polyelectrolyte adsorption on functionalized PDMS

We were interested how surface wetting behavior would impact polyion adsorption to functionalized PDMS. In this experiment (Fig. 3.5), we compared the adsorption of strong (PSS) and weak (PAA) electrolytes to bare and functionalized PDMS. To establish a baseline of adsorption, we estimated the adsorbed mass (m) on bare PDMS ($m_{PSS\ PDMS}$, $m_{PAA\ PDMS}$) substrates by measuring the total length of polymers visible in AFM micrographs and comparing with the mass of a full monolayer (1200 µg/m^2 for PSS, and 1400 µg/m^2 for PAA). Using this method, we estimated $m_{PSS\ PDMS}$ = 13 ± 1.8 µg/m^2 (~1 % of a full monolayer) and $m_{PAA\ PDMS}$ = 0.8 ± 0.05 µg/m^2 (<0.1 % of a full monolayer) (Fig. 3.5g). This observation of minimal adsorption is consistent with a relatively hydrophobic and inert surface weakly interacting with the electrolyte solution.

Next, we examined the adsorbed mass of polyelectrolytes on functionalized PCD-NH_2/PDMS ($m_{PSS\ P\text{-}PDMS}$, $m_{PAA\ P\text{-}PDMS}$) and TCD-NH_2/PDMS ($m_{PSS\ T\text{-}PDMS}$, $m_{PAA\ T\text{-}PDMS}$) (Fig. 3.5b,c,e,f). The $m_{PSS\ P\text{-}PDMS} = 40 \pm 0.7\ \mu g/m^2$ (Fig. 3.5b) and $m_{PAA\ P\text{-}PDMS} = 8 \pm 0.8\ \mu g/m^2$ (Fig. 3.5e). We estimated $m_{PSS\ T\text{-}PDMS} = 43 \pm 3.8\ \mu g/m^2$ (Fig. 3.5c) and $m_{PAA\ T\text{-}PDMS} = 11 \pm 2.1\ \mu g/m^2$ (Fig. 3.5f). Our data suggests that strong electrolytes more readily adsorbed to charged surfaces than weak. The m_{PSS} increased marginally on TCD-NH_2/PDMS but for m_{PAA} there was a ~37 % increase.

For comparison with PDMS substrates, we measured the adsorbed mass of polyelectrolytes on both TCD-NH_2/HOPG ($m_{PSS\ T\text{-}HOPG}$, $m_{PAA\ T\text{-}HOPG}$) and PCD-NH_2/HOPG ($m_{PSS\ P\text{-}HOPG}$, $m_{PAA\ P\text{-}HOPG}$). The results from Fig. 3.3 (*i.e.*, the monolayer desorption observed with dip coating) led us to shorten the exposure time of HOPG samples to 30 s to reduce monolayer disordering. First, we estimated the adsorbed mass of PSS ($m_{PSS\ HOPG}$) and PAA ($m_{PAA\ HOPG}$) on bare HOPG. Based on the analysis of AFM images in Fig. 3.5, we estimated $m_{PSS\ HOPG} = 5 \pm 1.9\ \mu g/m^2$ and $m_{PAA\ HOPG} = 1 \pm 0.4\ \mu g/m^2$. On functionalized HOPG m_{PSS} increased ~5-fold ($m_{PSS\ T\text{-}HOPG} = 23 \pm 4.4\ \mu g/m^2$ and $m_{PSS\ P\text{-}HOPG} = 22 \pm 5.3\ \mu g/m^2$). For m_{PAA}, a ~10-fold ($m_{PAA\ T\text{-}HOPG} = 10 \pm 1.7\ \mu g/m^2$ for and $m_{PAA\ P\text{-}HOPG} = 6 \pm 0.6\ \mu g/m^2$) increase was observed. The data suggests the TCD-NH_2/PDMS surface has stronger solution interactions with weakly charged adsorbates (*i.e.*, PAA) than PCD-NH_2/PDMS. This preferential adsorption of weak polyelectrolytes on both TCD-NH_2/HOPG and TCD-NH_2/PDMS is also consistent with the lower receding angle values observed in Fig. 3.4 suggesting stronger solution interactions.

3.2.5 Comparison of the non-specific adsorption of TRITC-BSA on PDMS

Quantification of non-specific adsorption of biomolecules is commonly used to evaluate the antifouling properties of coatings. In Fig. 3.6 we characterized the non-specific adsorption of BSA on bare PDMS (Fig. 3.6a,d,g,j). We then fabricated and characterized PDMS surfaces designed to exhibit antifouling properties using a dip coated PSS layer (TCD-NH_2/PDMS+PSS, Fig. 3.6b, e, and h) or a transferred microcontact printed (μCP) striped phase film of dPC (Fig. 3.6c,f,i,k). The antifouling properties of these surfaces were subsequently tested and compared with bare PDMS (Fig. 3.6j).

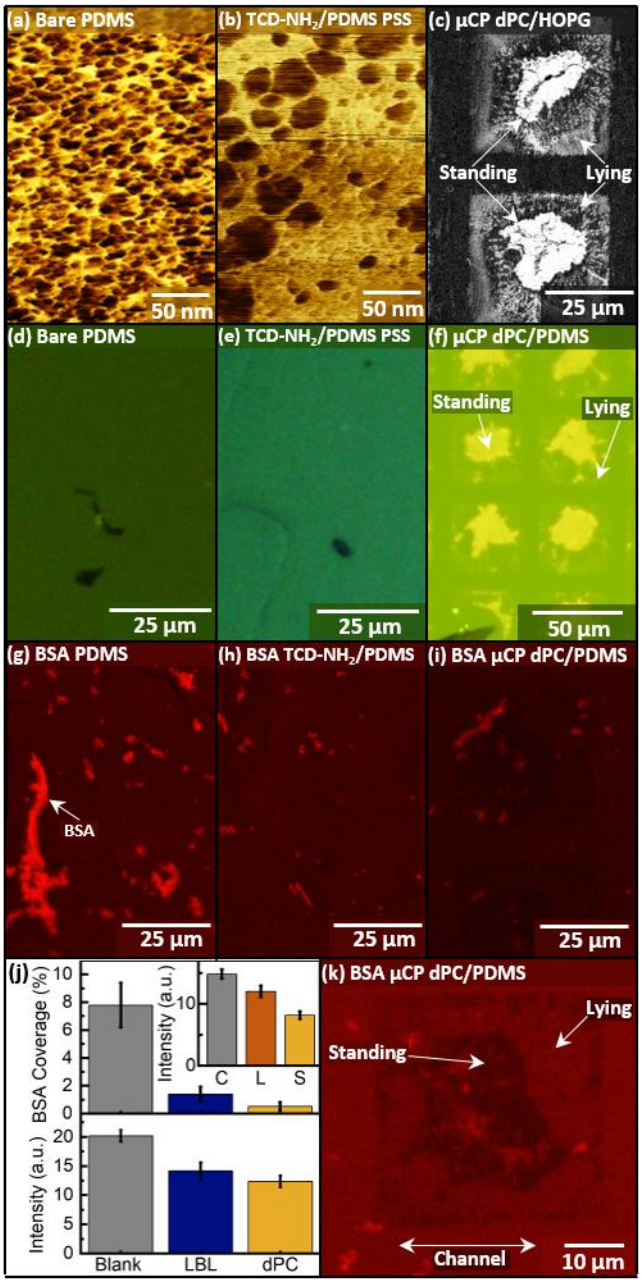

Figure 3-6 (a,b) AFM micrographs of (a) bare PDMS, and (b) TCD-NH_2 film with dip coated PSS layers. (c) SEM images of µcp dPC film on HOPG displaying standing phase (bright contrast) and lying down phase (grey contrast) within square stamped pattern. (d,e,f) Fluorescence images of (d) bare PDMS, and PDMS functionalized with (e) TCD-NH_2 film, and (f) µcp dPC film. Fluorescence images of PDMS substrates with TRITC-BSA adsorption on (g) bare PDMS, (h) TCD-NH_2 films with dip coated PSS layers, and (i) µcp dPC film. (k) A high contrast image of (i) enlarged to µcp dPC film features. (j) Bar graph illustrating the coverage percentage of BSA on the various surfaces. Inset: The percentage of BSA adsorption on the three different surface features of the µcp dPC film (i.e., bare PDMS (B), lying down phase (L), standing phase (S)).

Prior to BSA exposure, we characterized each PDMS substrate; all substrates were cured under the same PATRN process conditions (see Appendix B for more experimental detail). The cured PDMS forms a crosslinked network with a mesh size of 9.8 ± 0.5 nm, as shown in the bare PDMS AFM micrograph (Fig. 3.6a). For TCD-NH_2/PDMS, we fabricated a PSS multilayer via repeated surface dip coatings modified from reported LBL conditions.[32] These modifications enabled us to assess the anionic multilayer impact on non-specific adsorption and demonstrate the possibility of LBL fabrication on striped phase films. In the AFM micrographs, we observed ~ 50 % coverage of the TCD-NH_2/PDMS+PSS (Fig. 3.6b).

To examine zwitterion functionalized PDMS, we transferred μCP dPC to PDMS. Utilizing μCP conditions we have previously reported,[88] we stamped an array of 50 μm x 50 μm square pattern of dPC on the HOPG surface. SEM images reveal regions of both standing and lying-down phases in the dPC square patterns as illustrated in the SEM image (Fig. 3.6c). These regions enabled us to assess how the difference in charge density between standing and lying-down phases in a monolayer, (molecular footprints of ~0.4 nm^2 and ~3.9 nm^2, respectively) impacted the adsorption of BSA**.** The area between the square patterns (channel region) exhibited unpatterned, low number-density of molecular domains. The unpatterned assembly of dPC is caused by amphiphiles spreading out from the stamp contact areas during the μCP transfer (Figure S.B. 7).[88]

Fluorescence micrographs (Fig. 3.6d–f) illustrated the transfer of striped phase features to PDMS from the HOPG surface. In contrast to bare PMDS, we observed the fluorescent emission from the PDA backbones within the transferred film (Fig. 3.6e, and f). This is consistent with our previous observations that bare PDMS fluorescence spectra lack the additional PDA emission peaks (Figure S.B. 10).[18]

For μCP dPC films, we can differentiate standing and lying-down phases transferred to PDMS by comparing the fluorescence intensity. Standing phase contains a much higher density of molecules, and thus a higher density of PDA backbones, producing stronger fluorescence intensity than the surrounding lying-down phase, as highlighted in Fig. 3.6f. High density regions of zwitterions were reported to produce increased antifouling properties.[8, 10, 89] Therefore, we were interested in whether the greater density of zwitterions associated with transferred standing phase regions of dPC would produce a noticeable difference in non-specific adsorption, in comparison with transferred striped phases of dPC.

To compare the antifouling properties of PDMS surfaces, we deposited fluorescent TRITC-BSA proteins and quantified the adsorption. For the images in Fig. 3.6g–i, each substrate was exposed to 0.5 mg/mL TRIC-BSA in 10 mM potassium phosphate buffer. From the fluorescence images, we then estimated the area covered by BSA and the intensity of fluorescence (Fig. 3.6j). After 10 minute exposure, the average total surface coverage (Fig. 3.6g–k) was reduced for TCD-NH_2/PDMS+PSS (1.4 ± 0.5 %) and μCP dPC (0.5 ± 0.3 %) compared to the coverage observed on bare PDMS (7.8 ± 1.6 %).

We then estimated the fluorescence intensity of each functionalized substrate (Fig. 3.6j, bottom). For bare PDMS, the background fluorescence intensity of the substrate was = 20 ± 1.0 a.u. The estimated intensity was reduced on PSS dip coated TCD-NH_2/PDMS substrates to 14 ± 1.4 a.u. and further reduced on μCP dPC substrates to = 12 ± 1.0 a.u. We also estimated the fluorescence intensity of the standing, lying-down, and channel regions of the μCP dPC substrates. The fluorescence intensity of the channel region was = 15 ± 0.75 a.u. compared to the 12 ± 0.9 a.u. of the lying-down phase, and 8.2 ± 0.61 a.u. of the standing phase (Fig. 3.6j, inset).

These results represent a ~30 % reduction in the fluorescence intensity between the lying-down and standing phase regions of the pattern and ~46 % reduction between the channel and standing phase region. Furthermore, the channel regions showed a reduction in fluorescence intensity by ~25 % from the bare PDMS substrate. In previous work, higher functional group densities of a surface coating have shown to increase the overall the antimicrobial activity.[10, 90-91] These findings are consistent with previous reports suggesting that functionalized regions with the highest functional group density have the most impact on non-specific adsorption.

Overall, we observed the reduction of both the BSA surface coverage and the fluorescence intensity on PSS dip coated TCD-NH_2/PDMS and μCP dPC films. These results suggest the dip coated PSS layers on TCD-NH_2/PDMS and μCP dPC film both reduced the non-specific adsorption of BSA to the PDMS surface. In summary, we demonstrated the reduction of non-specific adsorption of BSA to functionalized PDMS surfaces utilizing PATRN transferred striped phase films.

3.3 Conclusions

Here, we have demonstrated that it is feasible to adsorb polyelectrolytes to striped phase functionalized PDMS as a route for creating antiadhesive coatings and reduced the non-specific

adsorption of proteins to the functionalized PDMS surface. Our findings point to the possibility that striped phase functionalized PDMS could be utilized to fabricate antiadhesive coatings through polyelectrolyte LBL deposition, or through PDMS functionalization using zwitterions or other functional diacetylenes. Overall, this illustrates a new route for antiadhesive coating fabrication using controlled polyelectrolyte adsorption to striped phase functionalized PDMS.

REFERENCES

1. Asenov, A.; Kaya, S.; Brown, A. R., Intrinsic parameter fluctuations in decananometer mosfets introduced by gate line edge roughness. *IEEE Trans. Electron Devices* **2003,** *50* (5), 1254-1260.

2. Shin, C., State-of-the-art silicon device miniaturization technology and its challenges. *IEICE Electron. Express* **2014,** *11* (10), 11.

3. Biswas, A.; Bayer, I. S.; Biris, A. S.; Wang, T.; Dervishi, E.; Faupel, F., Advances in top-down and bottom-up surface nanofabrication: Techniques, applications & future prospects. *Advances in Colloid and Interface Science* **2012,** *170* (1-2), 2-27.

4. Vieu, C.; Carcenac, F.; Pepin, A.; Chen, Y.; Mejias, M.; Lebib, A.; Manin-Ferlazzo, L.; Couraud, L.; Launois, H., Electron beam lithography: Resolution limits and applications. *Applied Surface Science* **2000,** *164*, 111-117.

5. Ostroverkhova, O., Organic optoelectronic materials: Mechanisms and applications. *Chemical Reviews* **2016,** *116* (22), 13279-13412.

6. Liang, R.; Yan, L.; Loebach, J.; Ge, M.; Uozumi, Y.; Sekanina, K.; Horan, N.; Gildersleeve, J.; Thompson, C.; Smith, A.; Biswas, K.; Still, W. C.; Kahne, D., Parallel synthesis and screening of a solid phase carbohydrate library. *Science* **1996,** *274* (5292), 1520-1522.

7. Oyelaran, O.; Gildersleeve, J. C., Glycan arrays: Recent advances and future challenges. *Current Opinion in Chemical Biology* **2009,** *13* (4), 406-413.

8. Banerjee, I.; Pangule, R. C.; Kane, R. S., Antifouling coatings: Recent developments in the design of surfaces that prevent fouling by proteins, bacteria, and marine organisms. *Adv. Mater.* **2011,** *23* (6), 690-718.

9. Neoh, K. G.; Li, M.; Kang, E. T.; Chiong, E.; Tambyah, P. A., Surface modification strategies for combating catheter-related complications: Recent advances and challenges. *Journal of Materials Chemistry B* **2017,** *5* (11), 2045-2067.

10. Schlenoff, J. B., Zwitteration: Coating surfaces with zwitterionic functionality to reduce nonspecific adsorption. *Langmuir* **2014,** *30* (32), 9625-9636.

11. Butler, S. Z.; Hollen, S. M.; Cao, L. Y.; Cui, Y.; Gupta, J. A.; Gutierrez, H. R.; Heinz, T. F.; Hong, S. S.; Huang, J. X.; Ismach, A. F.; Johnston-Halperin, E.; Kuno, M.; Plashnitsa, V. V.; Robinson, R. D.; Ruoff, R. S.; Salahuddin, S.; Shan, J.; Shi, L.; Spencer, M. G.; Terrones, M.; Windl, W.; Goldberger, J. E., Progress, challenges, and opportunities in two-dimensional materials beyond graphene. *Acs Nano* **2013,** *7* (4), 2898-2926.

12. Geim, A. K., Graphene: Status and prospects. *Science* **2009,** *324* (5934), 1530-1534.

13. Bang, J. J.; Rupp, K. K.; Russell, S. R.; Choong, S. W.; Claridge, S. A., Sitting phases of polymerizable amphiphiles for controlled functionalization of layered materials. *J. Am. Chem. Soc.* **2016,** *138* (13), 4448-4457.

14. Hayes, T. R.; Bang, J. J.; Davis, T. C.; Peterson, C. F.; McMillan, D. G.; Claridge, S. A., Multimicrometer noncovalent monolayer domains on layered materials through thermally controlled langmuir-schaefer conversion for noncovalent 2d functionalization. *Acs Applied Materials & Interfaces* **2017,** *9* (41), 36409-36416.

15. Porter, A. G.; Ouyang, T.; Hayes, T. R.; Biechele-Speziale, J.; Russell, S. R.; Claridge, S. A., 1-nm-wide hydrated dipole arrays regulate aunw assembly on striped monolayers in nonpolar solvent. *Chem* **2019,** *5* (8), 2264-2275.

16. Choong, S. W.; Russell, S. R.; Bang, J. J.; Patterson, J. K.; Claridge, S. A., Sitting phase monolayers of polymerizable phospholipids create dimensional, molecular-scale wetting control for scalable solution based patterning of layered materials. *Acs Applied Materials & Interfaces* **2017,** *9* (22), 19326-19334.

17. Claridge, S. A., Standing, lying, and sitting: Translating building principles of the cell membrane to synthetic 2d material interfaces. *Chemical Communications* **2018,** *54* (50), 6681-6691.

18. Davis, T. C. a. B. J. O. a. S. A. a. L. E. N. a. S. A. a. C. S. A., One nanometer wide functional patterns with a sub-10 nanometer pitch transferred to an amorphous elastomeric material. *ACS Nano* **2021,** *15* (1), 1426-1435.

19. Bang, J. J.; Porter, A. G.; Davis, T. C.; Hayes, T. R.; Claridge, S. A., Spatially controlled noncovalent functionalization of 2d materials based on molecular architecture. *Langmuir* **2018,** *34* (19), 5454-5463.

20. Davis, T. C.; Bang, J. J.; Brooks, J. T.; McMillan, D. G.; Claridge, S. A., Hierarchically patterned noncovalent functionalization of 2d materials by controlled langmuir-schaefer conversion. *Langmuir* **2018,** *34* (4), 1353-1362.

21. Chen, X. D.; Lenhert, S.; Hirtz, M.; Lu, N.; Fuchs, H.; Chi, L. F., Langmuir-blodgett patterning: A bottom-up way to build mesostructures over large areas. *Accounts of Chemical Research* **2007,** *40* (6), 393-401.

22. Okawa, Y.; Mandal, S. K.; Hu, C. P.; Tateyama, Y.; Goedecker, S.; Tsukamoto, S.; Hasegawa, T.; Gimzewski, J. K.; Aono, M., Chemical wiring and soldering toward all-molecule electronic circuitry. *J. Am. Chem. Soc.* **2011,** *133* (21), 8227-8233.

23. Okawa, Y.; Aono, M., Materials science - nanoscale control of chain polymerization. *Nature* **2001,** *409* (6821), 683-684.

24. Okawa, Y.; Akai-Kasaya, M.; Kuwahara, Y.; Mandal, S. K.; Aono, M., Controlled chain polymerisation and chemical soldering for single-molecule electronics. *Nanoscale* **2012,** *4* (10), 3013-3028.

25. Park, S.; Gildersleeve, J. C.; Blixt, O.; Shin, I., Carbohydrate microarrays. *Chemical Society Reviews* **2013,** *42* (10), 4310-4326.

26. Kiessling, L. L., Chemistry-driven glycoscience. *Bioorganic & Medicinal Chemistry* **2018,** *26* (19), 5229-5238.

27. Libioulle, L.; Bietsch, A.; Schmid, H.; Michel, B.; Delamarche, E., Contact-inking stamps for microcontact printing of alkanethiols on gold. *Langmuir* **1999,** *15* (2), 300-304.

28. Perl, A.; Reinhoudt, D. N.; Huskens, J., Microcontact printing: Limitations and achievements. *Adv. Mater.* **2009,** *21* (22), 2257-2268.

29. Hovis, J. S.; Boxer, S. G., Patterning and composition arrays of supported lipid bilayers by microcontact printing. *Langmuir* **2001,** *17* (11), 3400-3405.

30. Demming, S.; Lesche, C.; Schmolke, H.; Klages, C. P.; Buttgenbach, S., Characterization of long-term stability of hydrophilized peg-grafted pdms within different media for biotechnological and pharmaceutical applications. *Physica Status Solidi a-Applications and Materials Science* **2011,** *208* (6), 1301-1307.

31. Adly, N. Y.; Hassani, H.; Tran, A. Q.; Balski, M.; Yakushenko, A.; Offenhausser, A.; Mayer, D.; Wolfrum, B., Observation of chemically protected polydimethylsiloxane: Towards crack-free pdms. *Soft Matter* **2017,** *13* (37), 6297-6303.

32. Vaterrodt, A.; Thallinger, B.; Daumann, K.; Koch, D.; Guebitz, G. M.; Ulbricht, M., Antifouling and antibacterial multifunctional polyzwitterion/enzyme coating on silicone catheter material prepared by electrostatic layer-by-layer assembly. *Langmuir* **2016,** *32* (5), 1347-1359.

33. Tan, S. H.; Nguyen, N. T.; Chua, Y. C.; Kang, T. G., Oxygen plasma treatment for reducing hydrophobicity of a sealed polydimethylsiloxane microchannel. *Biomicrofluidics* **2010,** *4* (3).

34. Seon, L.; Lavalle, P.; Schaaf, P.; Boulmedais, F., Polyelectrolyte multi layers: A versatile tool for preparing antimicrobial coatings. *Langmuir* **2015,** *31* (47), 12856-12872.

35. Zhu, X. Y.; Loh, X. J., Layer-by-layer assemblies for antibacterial applications. *Biomaterials Science* **2015,** *3* (12), 1505-1518.

36. Love, J. C.; Estroff, L. A.; Kriebel, J. K.; Nuzzo, R. G.; Whitesides, G. M., Self-assembled monolayers of thiolates on metals as a form of nanotechnology. *Chemical Reviews* **2005,** *105* (4), 1103-1169.

37. Aizenberg, J.; Black, A. J.; Whitesides, G. M., Control of crystal nucleation by patterned self-assembled monolayers. *Nature* **1999,** *398* (6727), 495-498.

38. Han, Y. J.; Aizenberg, J., Face-selective nucleation of calcite on self-assembled monolayers of alkanethiols: Effect of the parity of the alkyl chain. *Angewandte Chemie-International Edition* **2003,** *42* (31), 3668-3670.

39. Pokroy, B.; Aizenberg, J., Calcite shape modulation through the lattice mismatch between the self-assembled monolayer template and the nucleated crystal face. *Crystengcomm* **2007,** *9* (12), 1219-1225.

40. Kiessling, L. L.; Pohl, N. L., Strength in numbers: Non-natural polyvalent carbohydrate derivatives. *Chemistry & Biology* **1996,** *3* (2), 71-77.

41. Gestwicki, J. E.; Cairo, C. W.; Strong, L. E.; Oetjen, K. A.; Kiessling, L. L., Influencing receptor-ligand binding mechanisms with multivalent ligand architecture. *J. Am. Chem. Soc.* **2002,** *124* (50), 14922-14933.

42. Kiessling, L. L.; Gestwicki, J. E.; Strong, L. E., Synthetic multivalent ligands as probes of signal transduction. *Angewandte Chemie-International Edition* **2006,** *45* (15), 2348-2368.

43. Kumar, A.; Whitesides, G. M., Features of gold having micrometer to centimeter dimensions can be formed through a combination of stamping with an elastomeric stamp and an alkanethiol ink followed by chemical etching. *Applied Physics Letters* **1993,** *63* (14), 2002-2004.

44. Kumar, A.; Biebuyck, H. A.; Whitesides, G. M., Patterning self-assembled monolayers - applications in materials science. *Langmuir* **1994,** *10* (5), 1498-1511.

45. Xia, Y. N.; Whitesides, G. M., Soft lithography. *Angewandte Chemie-International Edition* **1998,** *37* (5), 550-575.

46. Han, X.; Zheng, Y. T.; Munro, C. J.; Ji, Y. W.; Braunschweig, A. B., Carbohydrate nanotechnology: Hierarchical assembly using nature's other information carrying biopolymers. *Current Opinion in Biotechnology* **2015,** *34*, 41-47.

47. Groszek, A. J., Preferential adsorption of normal hydrocarbons on cast iron. *Nature* **1962,** *196* (4854), 531-&.

48. Groszek, A. J., Preferential adsorption of long-chain normal paraffins on mos2 ws2 + graphite from n-heptane. *Nature* **1964,** *204* (495), 680-&.

49. Rabe, J. P.; Buchholz, S., Commensurability and mobility in 2-dimensional molecular-patterns on graphite. *Science* **1991,** *253* (5018), 424-427.

50. Grim, P. C. M.; De Feyter, S.; Gesquiere, A.; Vanoppen, P.; Rucker, M.; Valiyaveettil, S.; Moessner, G.; Mullen, K.; De Schryver, F. C., Submolecularly resolved polymerization of diacetylene molecules on the graphite surface observed with scanning tunneling microscopy. *Angewandte Chemie-International Edition* **1997,** *36* (23), 2601-2603.

51. Cyr, D. M.; Venkataraman, B.; Flynn, G. W., Stm investigations of organic molecules physisorbed at the liquid-solid interface. *Chemistry of Materials* **1996,** *8* (8), 1600-1615.

52. Okawa, Y.; Aono, M., Linear chain polymerization initiated by a scanning tunneling microscope tip at designated positions. *Journal of Chemical Physics* **2001,** *115* (5), 2317-2322.

53. Li, B.; Tahara, K.; Adisoejoso, J.; Vanderlinden, W.; Mali, K. S.; De Gendt, S.; Tobe, Y.; De Feyter, S., Self-assembled air-stable supramolecular porous networks on graphene. *Acs Nano* **2013,** *7* (12), 10764-10772.

54. Villarreal, T. A.; Russell, S. R.; Bang, J. J.; Patterson, J. K.; Claridge, S. A., Modulating wettability of layered materials by controlling ligand polar headgroup dynamics. *J. Am. Chem. Soc.* **2017,** *139* (34), 11973-11979.

55. Workman, R. K.; Schmidt, A. M.; Manne, S., Detection of a diffusive two-dimensional gas of amphiphiles by lateral force microscopy. *Langmuir* **2003,** *19* (8), 3248-3253.

56. Workman, R. K.; Manne, S., Molecular transfer and transport in noncovalent microcontact printing. *Langmuir* **2004,** *20* (3), 805-815.

57. Russell, S. R.; Davis, T. C.; Bang, J. J.; Claridge, S. A., Spectroscopic metrics for alkyl chain ordering in lying-down noncovalent monolayers of diynoic acids on graphene. *Chemistry of Materials* **2018,** *30* (8), 2506-2514.

58. Miura, A.; De Feyter, S.; Abdel-Mottaleb, M. M. S.; Gesquiere, A.; Grim, P. C. M.; Moessner, G.; Sieffert, M.; Klapper, M.; Mullen, K.; De Schryver, F. C., Light- and stm-tip-induced formation of one-dimensional and two-dimensional organic nanostructures. *Langmuir* **2003,** *19* (16), 6474-6482.

59. Giridharagopal, R.; Kelly, K. F., Substrate-dependent properties of polydiacetylene nanowires on graphite and mos2. *Acs Nano* **2008,** *2* (8), 1571-1580.

60. Wang, Z. X.; Volinsky, A. A.; Gallant, N. D., Crosslinking effect on polydimethylsiloxane elastic modulus measured by custom-built compression instrument. *Journal of Applied Polymer Science* **2014,** *131* (22).

61. Xia, Y. N.; Whitesides, G. M., Use of controlled reactive spreading of liquid alkanethiol on the surface of gold to modify the size of features produced by microcontact printing. *J. Am. Chem. Soc.* **1995,** *117* (11), 3274-3275.

62. Sharpe, R. B. A.; Burdinski, D.; Huskens, J.; Zandvliet, H. J. W.; Reinhoudt, D. N.; Poelsema, B., Spreading of 16-mercaptohexadecanoic acid in microcontact printing. *Langmuir* **2004,** *20* (20), 8646-8651.

63. Graham, D. J.; Price, D. D.; Ratner, B. D., Solution assembled and microcontact printed monolayers of dodecanethiol on gold: A multivariate exploration of chemistry and contamination. *Langmuir* **2002,** *18* (5), 1518-1527.

64. Doudevski, I.; Hayes, W. A.; Schwartz, D. K., Submonolayer island nucleation and growth kinetics during self-assembled monolayer formation. *Phys. Rev. Lett.* **1998,** *81* (22), 4927-4930.

65. Sharpe, R. B. A.; Burdinski, D.; van der Marel, C.; Jansen, J. A. J.; Huskens, J.; Zandvliet, H. J. W.; Reinhoudt, D. N.; Poelsema, B., Ink dependence of poly(dimethylsiloxane) contamination in microcontact printing. *Langmuir* **2006,** *22* (13), 5945-5951.

66. Claridge, S. A.; Liao, W. S.; Thomas, J. C.; Zhao, Y. X.; Cao, H. H.; Cheunkar, S.; Serino, A. C.; Andrews, A. M.; Weiss, P. S., From the bottom up: Dimensional control and characterization in molecular monolayers. *Chemical Society Reviews* **2013,** *42* (7), 2725-2745.

67. Srinivasan, C.; Mullen, T. J.; Hohman, J. N.; Anderson, M. E.; Dameron, A. A.; Andrews, A. M.; Dickey, E. C.; Horn, M. W.; Weiss, P. S., Scanning electron microscopy of nanoscale chemical patterns. *Acs Nano* **2007,** *1* (3), 191-201.

68. Delamarche, E.; Schmid, H.; Bietsch, A.; Larsen, N. B.; Rothuizen, H.; Michel, B.; Biebuyck, H., Transport mechanisms of alkanethiols during microcontact printing on gold. *Journal of Physical Chemistry B* **1998,** *102* (18), 3324-3334.

69. Rydzek, G.; Ji, Q. M.; Li, M.; Schaaf, P.; Hill, J. P.; Boulmedais, F.; Ariga, K., Electrochemical nanoarchitectonics and layer-by-layer assembly: From basics to future. *Nano Today* **2015,** *10* (2), 138-167.

70. Nguyen, B. H.; Nguyen, V. H., Promising applications of graphene and graphene-based nanostructures. *Adv. Nat. Sci.-Nanosci Nanotechnol* **2016,** *7* (2), 15.

71. Cai, J. M.; Ruffieux, P.; Jaafar, R.; Bieri, M.; Braun, T.; Blankenburg, S.; Muoth, M.; Seitsonen, A. P.; Saleh, M.; Feng, X. L.; Mullen, K.; Fasel, R., Atomically precise bottom-up fabrication of graphene nanoribbons. *Nature* **2010,** *466* (7305), 470-473.

72. Boudou, T.; Crouzier, T.; Ren, K. F.; Blin, G.; Picart, C., Multiple functionalities of polyelectrolyte multilayer films: New biomedical applications. *Adv. Mater.* **2010,** *22* (4), 441-467.

73. Tao, A. R.; Huang, J. X.; Yang, P. D., Langmuir-blodgettry of nanocrystals and nanowires. *Accounts of Chemical Research* **2008,** *41* (12), 1662-1673.

74. MacLeod, J. M.; Rosei, F., Molecular self-assembly on graphene. *Small* **2014,** *10* (6), 1038-1049.

75. Severin, N.; Okhapkin, I. M.; Khokhlov, A. R.; Rabe, J. P., Adsorption of polyelectrolyte molecules to a nanostructured monolayer of amphiphiles. *Nano Letters* **2006,** *6* (5), 1018-1022.

76. Dubrovin, E. V.; Gerritsen, J. W.; Zivkovic, J.; Yaminsky, I. V.; Speller, S., The effect of underlying octadecylamine monolayer on the DNA conformation on the graphite surface. *Colloid Surf. B-Biointerfaces* **2010,** *76* (1), 63-69.

77. Long, B.; Manning, M.; Burke, M.; Szafranek, B. N.; Visimberga, G.; Thompson, D.; Greer, J. C.; Povey, I. M.; MacHale, J.; Lejosne, G.; Neumaier, D.; Quinn, A. J., Non-covalent functionalization of graphene using self-assembly of alkane-amines. *Adv. Funct. Mater.* **2012,** *22* (4), 717-725.

78. Phan, H. T. M.; Bartelt-Hunt, S.; Rodenhausen, K. B.; Schubert, M.; Bartz, J. C., Investigation of bovine serum albumin (bsa) attachment onto self-assembled monolayers (sams) using combinatorial quartz crystal microbalance with dissipation (qcm-d) and spectroscopic ellipsometry (se). *Plos One* **2015,** *10* (10).

79. Zhang, H. B.; Chiao, M., Anti-fouling coatings of poly(dimethylsiloxane) devices for biological and biomedical applications. *Journal of Medical and Biological Engineering* **2015,** *35* (2), 143-155.

80. Mi, L.; Jiang, S. Y., Integrated antimicrobial and nonfouling zwitterionic polymers. *Angewandte Chemie-International Edition* **2014,** *53* (7), 1746-1754.

81. Schmolke, H.; Demming, S.; Edlich, A.; Magdanz, V.; Buttgenbach, S.; Franco-Lara, E.; Krull, R.; Klages, C. P., Polyelectrolyte multilayer surface functionalization of poly(dimethylsiloxane) (pdms) for reduction of yeast cell adhesion in microfluidic devices. *Biomicrofluidics* **2010,** *4* (4).

82. Severin, M.; Barner, J.; Kalachev, A. A.; Rabe, J. P., Manipulation and overstretching of genes on solid substrates. *Nano Letters* **2004,** *4* (4), 577-579.

83. Davis, T. C.; Bechtold, J. O.; Shi, A.; Lang, E. N.; Singh, A.; Claridge, S. A., One nanometer wide functional patterns with a sub-10 nanometer pitch transferred to an amorphous elastomeric material. *ACS Nano* **2021,** *15* (1), 1426-1435.

84. Richardson, J. J.; Cui, J. W.; Bjornmalm, M.; Braunger, J. A.; Ejima, H.; Caruso, F., Innovation in layer-by-layer assembly. *Chemical Reviews* **2016,** *116* (23), 14828-14867.

85. Hammond, P. T., Engineering materials layer-by-layer: Challenges and opportunities in multilayer assembly. *Aiche Journal* **2011,** *57* (11), 2928-2940.

86. Phillipson, R.; de la Rosa, C. J. L.; Teyssandier, J.; Walke, P.; Waghray, D.; Fujita, Y.; Adisoejoso, J.; Mali, K. S.; Asselierghs, I.; Huyghebaert, C.; Uji-i, H.; De Gendt, S.; Feyter, S., Tunable doping of graphene by using physisorbed self-assembled networks. *Nanoscale* **2016,** *8* (48), 20017-20026.

87. Fears, K. P.; Creager, S. E.; Latour, R. A., Determination of the surface pk of carboxylic- and amine-terminated alkanethiols using surface plasmon resonance spectroscopy. *Langmuir* **2008,** *24* (3), 837-843.

88. Davis, T. C.; Bechtold, J. O.; Hayes, T. R.; Villarreal, T. A.; Claridge, S. A., Hierarchically patterned striped phases of polymerized lipids: Toward controlled carbohydrate presentation at interfaces. *Faraday Discussions* **2019**.

89. Kuo, W. H.; Wang, M. J.; Chien, H. W.; Wei, T. C.; Lee, C.; Tsai, W. B., Surface modification with poly(sulfobetaine methacrylate-co-acrylic acid) to reduce fibrinogen adsorption, platelet adhesion, and plasma coagulation. *Biomacromolecules* **2011,** *12* (12), 4348-4356.

90. Bieser, A. M.; Tiller, J. C., Mechanistic considerations on contact-active antimicrobial surfaces with controlled functional group densities. *Macromolecular Bioscience* **2011,** *11* (4), 526-534.

91. Firouzjaei, M. D.; Seyedpour, S. F.; Aktij, S. A.; Giagnorio, M.; Bazrafshan, N.; Mollahosseini, A.; Samadi, F.; Ahmadalipour, S.; Firouzjaei, F. D.; Esfahani, M. R.; Tiraferri, A.; Elliott, M.; Sangermano, M.; Abdelrasoul, A.; McCutcheon, J. R.; Sadrzadeh, M.; Esfahani, A. R.; Rahimpour, A., Recent advances in functionalized polymer membranes for biofouling control and mitigation in forward osmosis. *Journal of Membrane Science* **2020,** *596*.

92. Howarth, N. M.; Lindsell, W. E.; Murray, E.; Preston, P. N., Lipophilic peptide nucleic acids containing a 1,3-diyne function: Synthesis, characterization and production of derived polydiacetylene liposomes. *Tetrahedron* **2005,** *61* (37), 8875-8887.

93. Lee, J. P.; Hwang, H.; Chae, S.; Kim, J. M., A reversibly mechanochromic conjugated polymer. *Chemical Communications* **2019,** *55* (63), 9395-9398.

94. Thakar, R.; Baker, L. A., Lithography-free production of stamps for microcontact printing of arrays. *Analytical Methods* **2010,** *2* (8), 1180-1183.

APPENDIX A. SUPPORTING INFORMATION FOR CHAPTER 2

Hierarchically Patterned Striped Phases of Polymerized Lipids: Toward Controlled Carbohydrate Presentation at Interfaces

Experimental Methods

Materials

Chloroform (≥99.5 % purity), undec-10-ynoic acid (95 %), dec-1-yne (98 %), iodine (99.8 %), copper iodide (99.5 %), morpholine (99 %), potassium hydroxide, hydroxylamine hydrochloride (98 %), ethylamine (70 % (*v/v*) solution in water), sulfuric acid (95.0–98.0 %), sodium thiosulfate, and sodium sulfate, were all purchased from Sigma Aldrich (St. Louis, MO) and used as received. Absolute ethanol (100 % purity) was purchased from Decon Laboratories, Inc. (King of Prussia, PA) and used as received. Methanol, diethyl ether (anhydrous), hexanes, THF, and toluene were purchased from Fisher Scientific (Hampton, NH) and used as received. Silica gel was purchased from Macherey-Nagel (Bethlehem, PA) and used as received. 1,2-Bis(10,12-tricosadiynoyl)-*sn*-glycero-3-phosphoethanolamine (diyne PE, >99.0 % purity), 1,2bis(10,12-tricosadiynoyl)-*sn*-glycero-3-phosphocholine (diyne PC, >99.0 % purity), and 1,2-distearoyl-*sn*-glycero-3phosphoinositol (ammonium salt) (PI, >99.0 % purity) were purchased from Avanti Polar Lipids (Alabaster, AL) and used as received. Commercially available fatty acids 10,12-tricosadiynoic acid (TCDA, ≥ 98.0 % purity) and 10,12pentacosadiynoic acid (PCDA, ≥ 97.0% purity) were purchased from Sigma-Aldrich (St. Louis, MO), and 10,12nonacosadiynoic (NCDA, >97.0% purity) was purchased from Tokyo Chemical Industry Co., Ltd. (Montgomeryville, PA). All fatty acids were dissolved in chloroform and filtered through 0.2-μm syringe filters to eliminate oligomers prior to use. For preparation of the poly(dimethylsiloxane) (PDMS) elastomer stamps, SYLGARD 184 silicone elastomer kits containing base and curing (crosslinking) agent were purchased from Dow Chemical Company (Midland, MI). When water was experimentally required, Milli-Q water (≥18.2 MΩ·cm resistivity) was used. Ultrahigh purity nitrogen (UHP N_2, 99.999 % purity) was purchased from Indiana Oxygen Company (Indianapolis, IN). Lipids were deposited on 1 cm × 1 cm highly oriented pyrolytic graphite (HOPG) substrates (MicroMasch, Watsonville, CA), which were freshly cleaved immediately prior to transfer. All initial steps in the transfer process were carried out under UV-filtered light to prevent

polymerization in solution. PELCO conductive liquid silver paint, standard SEM pin stub mounts, and double-coated carbon conductive tape were purchased from Ted Pella, Inc. (Redding, CA). Silicon wafers photolithographically patterned with arrays of 5 μm × 5 μm × 5 μm recessed cubes with a 10 μm pitch were provided by Prof. Wei-Ssu Liao (National Taiwan University).

General procedure for synthesis of 1-iododec-1-yne

Synthesis was carried out using a modification of previously published procedures,[1] described briefly here. A solution of morpholine (44 mmol) in toluene (34.8 mL) was treated with iodine (6.16 mmol), shielded from light and stirred for 1 h at 45 °C. A solution of dec-1-yne (4.4 mmol) in toluene (3.48 mL) was then added and the reaction mixture stirred continuously at 45 °C for 1 h. The reaction mixture was cooled to room temperature and filtered to remove the iodomorpholine salt. The filtrate was poured over a mixture of diethyl ether (50 mL) and a saturated aqueous solution of $Na_2S_2O_3$ (50 mL) and shaken until the organic layer was colorless. The organic layer was separated, washed again with a saturated aqueous solution of $Na_2S_2O_3$ (50 mL), dried over anhydrous Na_2SO_4, filtered, concentrated, and purified via column chromatography, with hexane as an eluent, to afford a 1-iododec-1-yne as a colorless oil (typical yield ~70 %).

Synthesis of 10,12-henicosadiynoic acid (HCDA)

Synthesis was carried out using a modification of published procedure,[1-2] described briefly here. Undec-10-ynoic acid (1.9 mmol) was dissolved in THF (14 mL) and CuI (0.43 mmol) was dissolved in 70% (*v/v*) ethylamine in water (14 mL). The undec-10-ynoic acid solution and the CuI solution were combined with ethanol (14 mL). Subsequently, 1 M KOH in water (6 mL) was added to the reaction mixture along with hydroxylamine hydrochloride (0.33 mmol). The reaction was cooled to 0 ˚C. A solution of 1-iododec-1-yne (5.1 mmol) dissolved in THF (10 mL) was then added dropwise, causing a precipitate to form. The reaction was allowed to warm to room temperature and proceed for a further 24 h. If the solution turned blue, additional aliquots of hydroxylamine hydrochloride were added. The reaction was quenched by the addition of a 10% aqueous solution of sulfuric acid to achieve neutral pH (typical required volume ~4 mL). Crude product was extracted with diethyl ether (3 × 50 mL) and then washed with water (3 × 50 mL) and

brine (3 × 50 mL). The organic layer was dried over anhydrous Na_2SO_4, filtered, and the ether was removed by rotary evaporator. The crude product was purified by recrystallization from hexanes to yield a fatty acid with an internal diyne, as a white solid (typical yield ~30 %).

Preparation of PDMS Stamps

Stamps were prepared by mixing SYLGARD 184 silicone elastomer base and curing (crosslinking) agent at the desired ratio (*e.g.* 10:1 *m/m*, or as described in Chapter 2). After the components were thoroughly mixed (approximately 5 min), the mixture was poured onto a photolithographically etched silicon wafer resting in a petri dish. The mixture was then deaerated in a vacuum desiccator until no bubbles remained. Subsequently, the petri dish was placed in an oven to allow the PDMS to cure for 24 h at 60 °C. After curing, crosslinked PDMS was peeled from the silicon wafer and cut to the desired size using a razor blade. PDMS stamps were cleaned by soaking them in Milli-Q water for 1 h, followed by sonication in a 1:1:1 (*v/v/v*) mixture of ethanol, methanol, and Milli-Q water for 30 min. The sonication step is crucial. Following sonication, stamps were placed in an oven for 1 h at 60 °C to allow residual polar solvent mixture to evaporate. Stamps were then soaked in hexanes for 6 h, replacing the hexanes every 2 h. Finally, the stamps were dried for 24 h at 60 °C and placed, pattern side up, in a covered petri dish prior to use. The cleaning procedure was repeated in preparation for each use of the stamp.

Ultraviolet ozone (UVO) plasma processing to increase PDMS stamp hydrophilicity

PDMS stamps hydrophilicity was increased using a Herrick PDC-3XG Plasma Cleaner with an oxygen flow rate of 150 cc/min and the RF level set to high for 60 min, unless otherwise stated in Chapter 2.

Inking of PDMS Stamp

For inking, a cleaned PDMS stamp was first rinsed briefly with ethanol and blown dry with UHP N_2. The patterned surface of the stamp was immersed in a solution of the chosen amphiphile. Solutions of amphiphiles were prepared first at 2.5 mg/mL in either $CHCl_3$ (for phospholipids) or 3:2 (*v:v*) hexane:IPA (for fatty acids). The solution was then dissolved to the desired concentration (stated in Chapter 2) with ethanol. This procedure was followed in order to maintain amphiphile

solubility, while achieving a relatively low concentration of hexanes and $CHCl_3$ in the inking solution, since these solvents are known to swell PDMS and distort features. After 30 s of immersion in the dilute lipid solution in the carrier solvent mixture, the stamp was removed, blown dry with UHP N_2 and placed pattern side up for 1 h at room temperature to allow additional carrier solvent to evaporate from the stamp.

Transfer of amphiphiles from PDMS to HOPG

After inking and subsequent drying for 1 h, the patterned side of the PDMS stamp was brought into contact with a freshly cleaved HOPG substrate, using one of the methods described below. In the 'flat contact' method, the stamp was lowered gently onto the HOPG surface. The PDMS stamp typically wet the HOPG surface; light tapping pressure with tweezers was applied to restore contact if needed. PDMS–HOPG contact was maintained for 30 s (unless otherwise specified) before the stamp was carefully lifted from the surface. In the 'rolled contact' method, the stamp was mounted on a copper cylinder 2.54 cm in diameter, 6.8 cm in length, and 300 g in mass. Double-sided tape was placed around the diameter of the copper cylinder, and the back side of the stamp was affixed to the tape. In one fluid motion (typically lasting approximately 3 s), the stamp was rolled across the surface of a freshly cleaved HOPG substrate. After both 'flat contact' and 'rolled contact' transfers, the functionalized HOPG was placed under a hand-held UV lamp (254 nm, 8 W) for 1 h with ~2 cm between the lamp and the substrate, to induce diyne photopolymerization, stabilizing the transferred molecular layer.

SEM imaging

Molecular layers on HOPG were imaged using a Teneo VS SEM (FEI Company, Hillsboro, OR). Images were acquired at a working distance of ~5 mm using the segmented in-lens T3 detector. A beam current of 3.2 nA was selected for optimal image resolution, utilizing a 32-µm diameter aperture with an accelerating voltage of 5 kV. All substrates were affixed to standard SEM pin stub specimen mounts with double-sided conductive carbon tape. To further enhance substrate–mount conductivity, a small amount of colloidal silver paint (PELCO, Ted Pella, Inc.) was applied along the perimeter of the substrate, providing electrical contact with the underlying pin stub.

Image analysis

Images were processed using Gwyddion scanning probe microscopy data visualization and analysis software[3] and ImageJ analysis software[4] to perform median line corrections, plane flattening, scar artifact removal, and contrast adjustment. Transfer fidelity and domain area measurements were performed using Adobe Photoshop to identify domain boundaries and calculate transfer coverage.

Energy minimization

Software packages Maestro and Macromodel (Schrödinger, Cambridge MA) were used, respectively, to visualize molecular structures and to perform force field minimizations. Models were minimized using the OPLS_2005 force field, with extended cutoffs for Van der Waals, electrostatic, and hydrogen bonding interactions. The dielectric constant of the simulation was set to 80.1. Minimizations were performed using the Polak-Ribiere conjugate gradient (PRCG) algorithm and gradient method with 50000 runs and a convergence threshold of 0.05.

Comparison of PCDA transfer from PDMS stamps with base:crosslinker ratios of 10:5 to 10:1

Because the local surface roughness of HOPG is lower than that of Au substrates commonly used in microcontact printing of alkanethiols, we examined whether this led to differences in PDMS rigidity required for optimal molecular transfer to HOPG. The elastomer base and curing (crosslinking) agent are typically mixed in a 10:1 (*m/m*) ratio for transfer of alkanethiols to Au; here, we prepared PDMS stamps with ratios from 10:5 to 10:1. High crosslinker ratios (*e.g.* 10:5) produce more rigid stamps with high elastic moduli, possibly useful for improving stamping fidelity of small features, given the limited need of the stamp to deform on the fairly flat HOPG substrate. Simultaneously, high curing agent ratios have been observed in other systems to limit the ability of the stamp to absorb molecular ink. Stamps were cleaned as described in the Experimental Methods, and an ink solution of 1.1 mM PCDA in the carrier solvent mixture was applied. Figure S.A.1 shows SEM images of PCDA transferred to HOPG from the three stamps. Stamps prepared with a base:crosslinker ratio of 10:5 (Figure S.A.1a,b) produce a high degree of molecular deposition both inside and outside the contact area. The intermediate 10:2 ratio (Figure S.A.1c,d) produces desirable transfer characteristics: a high degree of striped phase coverage in

the contact area, with limited transfer outside the contact area. In general, stamps prepared at a ratio of 10:1 (Figure S.A.1e,f) resulted in a somewhat increased range of transfer outside the stamp contact area, and in some cases, increased PDMS deposition (black spots) within the contact area. However, overall, both 10:2 and 10:1 base:crosslinker ratios produce reasonable transfer, and in many cases we tested stamps prepared in both ratios, for comparison with common stamp preparation conditions used in the assembly of standing phases on gold.

Representative SEM images for microcontact transfer of lipids to HOPG at concentrations from 2.1 – 0.045 mM

Previously, ink concentration has been found to be an important factor in producing high density molecular coverage in the stamp contact area, while limiting transfer outside the contact area, with concentrations in the range of 1–10 mM producing optimal transfer for standing phases, depending on the structure of the molecular ink. In lying-down striped phases, molecular footprints are much larger than for similar molecules assembled in a standing orientation (*e.g.*, 154 $Å^2$ for PCDA in a lying-down phase *vs.* ~25 $Å^2$ when assembled as a standing phase), requiring, in the case of PCDA, ~1/6 as many molecules to transfer per unit surface area. Figure S.A.2 illustrates SEM images of HOPG substrates that have been exposed to PDMS stamps carrying PCDA in carrier solvent at concentrations ranging from 2.1 to 0.045 mM, using the conditions described above. Patterns of squares representing deposited PCDA appear in higher contrast due to enhanced electron scattering relative to the conductive HOPG substrate, in agreement with previous SEM images acquired from PCDA monolayers assembled through LS transfer.[5-6] Higher-resolution SEM imaging of a single contact area at each concentration (Figure 1-3b,d,f,h) illustrates that at 1.1 mM, the entire contact area is functionalized with PCDA, with a narrow band of continuously functionalized surface up to 600 nm outside the contact area, and a low fractional coverage of long narrow molecular domains between contact areas. At 0.045 mM PCDA in the ink solution (Figure S.A.2g,h), the contact area is only partially functionalized, although individual domains are larger (typical length 1–2 μm) than those observed for transfer at 1.1 mM PCDA, which is reasonable given that lower monomer concentrations result in fewer but larger molecular islands in the submonolayer island nucleation and growth model. For this transfer condition, substantial areas of PDMS deposition (black spots) are also observed in the contact area. Even at 2.1 mM PCDA in the transfer solution, some PDMS deposition can be observed; the amount of PDMS impurity

deposited can vary from transfer to transfer. Overall, 2.1 mM PCDA produced the greatest extent of PCDA transfer outside the contact area. Based on these findings, we utilized amphiphile ink solutions prepared with 1.1 mM alkyl chain concentrations (*i.e.*, 1.1 mM PCDA; 0.5 mM diyne PC), unless otherwise described in Chapter 2.

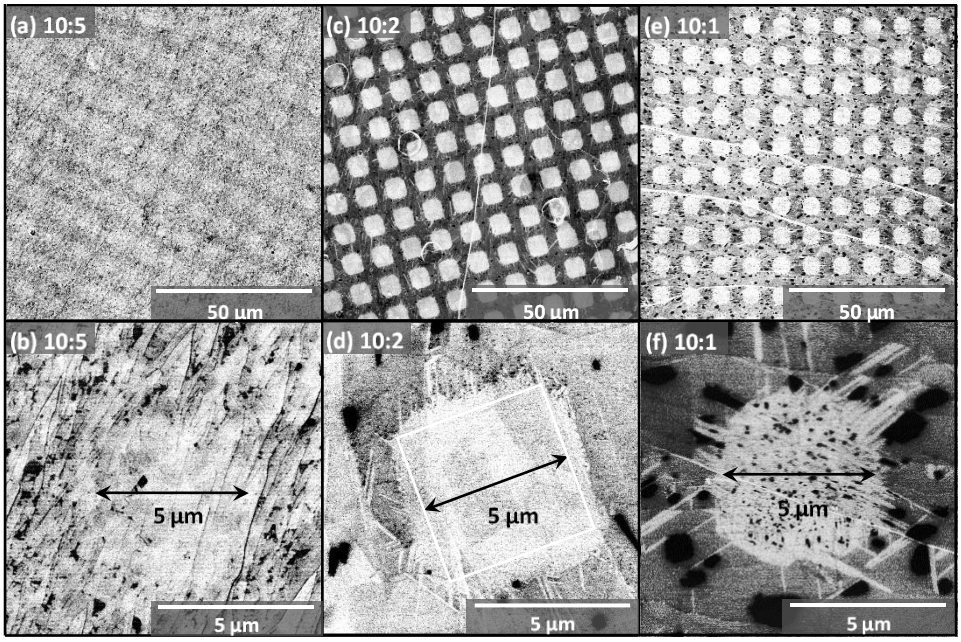

Figure S.A. 1 SEM images of PCDA transferred to HOPG from PDMS stamps prepared at elastomer base:crosslinker ratios of (a,b) 10:5, (c,d) 10:2, and (e,f) 10:1.

Comparisons of AFM and SEM images to examine orientation of transferred molecules

Because molecular domains produced by microcontact printing are relatively small (edge lengths *ca.* 100 nm), we utilized AFM imaging in addition to SEM imaging to characterize transfer, in order to examine the density of molecular domains produced under different transfer conditions. Figure S.A.3 compares SEM and AFM micrographs of microcontact printed squares of PCDA produced using 1.1 mM PCDA in ethanol. We have previously observed that striped monolayers of diacetylene amphiphiles can exhibit cracking defects following polymerization, which are emphasized in SEM images (presumably due to further polymerization and restructuring under the electron beam).[5] The presence of these defects makes it possible to infer the directionality of molecular rows within ordered domains. Cracking defects of this type were observed in SEM

images of diynoic acids deposited by microcontact printing, pointing to the assembly of ordered lamellar phases; AFM imaging was additionally utilized to quantify the presence of any areas of standing phase molecules based on topographic height (up to 3 nm for standing phases; 0.5–1.0 nm for typical lying down phases, dependent upon molecular orientation).

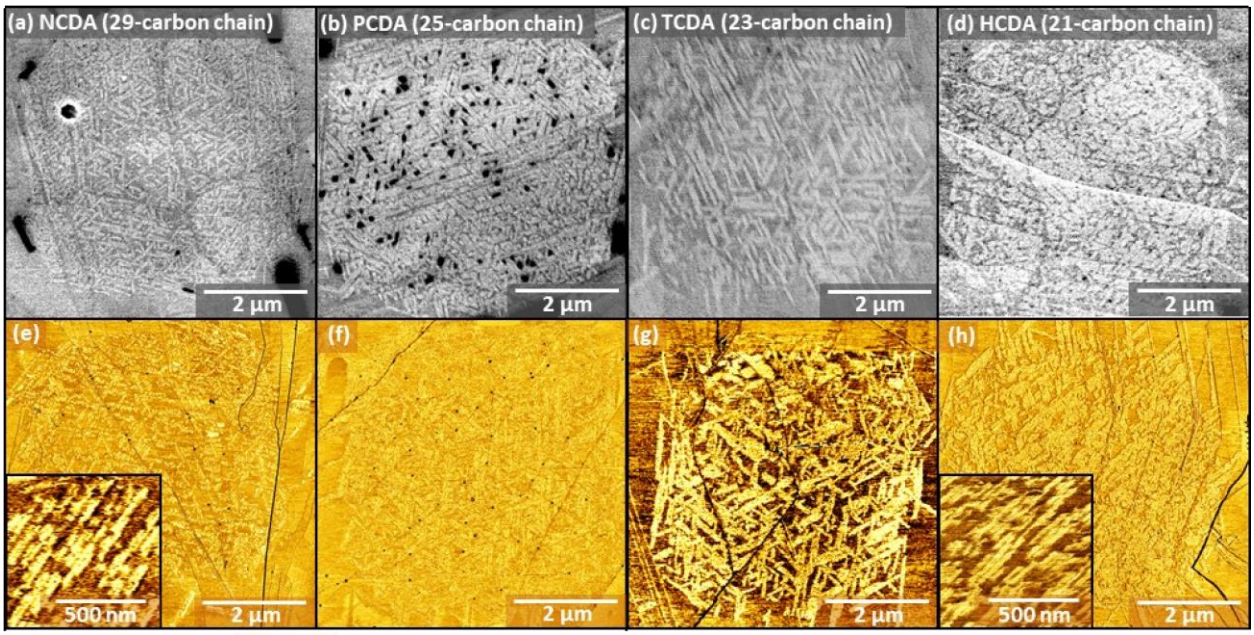

Figure S.A. 2. SEM and AFM images of microcontact printed diynoic acids with chains 29 to 21 carbons in length: (a,e) 10,12nonacosadiynoic acid (NCDA, 29-carbon chain); (b,f) 10,12-pentacosadiynoic acid (PCDA, 25-carbon chain); (c,g) 10,12tricosadiynoic acid (TCDA, 23-carbon chain); (d,h) 10,12-henicosadiynoic acid (HCDA, 21-carbon chain).

Figure S.A. 4 shows example SEM and AFM images of phospholipids deposited on HOPG by microcontact printing, to illustrate the distinction between standing and lying-down phases. Diyne PE was deposited using a flat contact geometry, with a contact time of 30 s; diyne PC was deposited utilizing rolled contact. Both phospholipids were deposited from a 0.55 mM transfer solution. The bright contrast in the SEM images of diyne PE (Figure S.A.4a,b) is characteristic of amphiphiles assembled in a standing phase, and is consistent with height profiles observed in AFM topography images. Diyne PC, deposited utilizing the rolled contact geometry, exhibits primarily ordered striped phases in the stamp contact areas (see Chapter 2 for diyne PC images).

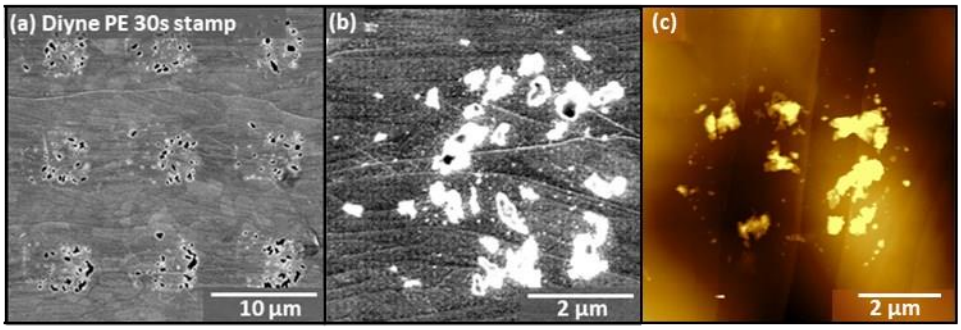

Figure S.A. 3. (a,b) SEM and (c) AFM images of diyne PE transferred to HOPG using a conventional flat stamping geometry, illustrating transfer of standing phase.

Comparison of HOPG surfaces brought into contact with un-inked PDMS stamps prepared at elastomer base:crosslinker ratios of 10:5 to 10:1

For optimizing the delivery of amphiphiles to the substrate, stamps with a range of base:crosslinker ratios (10:5 to 10:1) (*m/m*) were examined. Figure S.A.5 compares the transfer of PDMS impurities. Stamps were exposed to just the solvent components of the ink solution and allowed to dry as described in the Experimental Methods. Areas of dark contrast in SEM images of substrates prepared in this way (such as those in Figure S.A.5) were consistent with those observed following transfer of single-chain and dual-chain amphiphiles. The extent of impurity transfer varied; there was no observed correlation with base:crosslinker ratio. Figure S.A.6 shows AFM phase micrographs of substrates exposed to 1.1 mM PCDA during transfer and illustrates the deposition of PDMS on the HOPG surface.

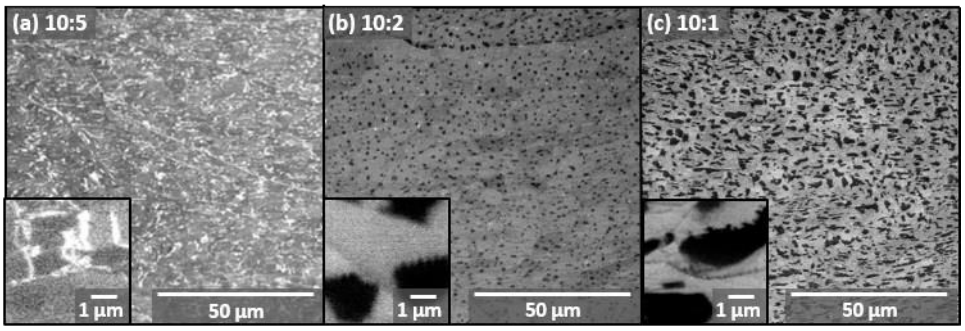

Figure S.A. 4. SEM images of HOPG placed in contact with PDMS stamps prepared at (a) 10:5, (b) 10:2, and (c) 10:1 ratios of elastomer base to curing agent and exposed to solvent only.

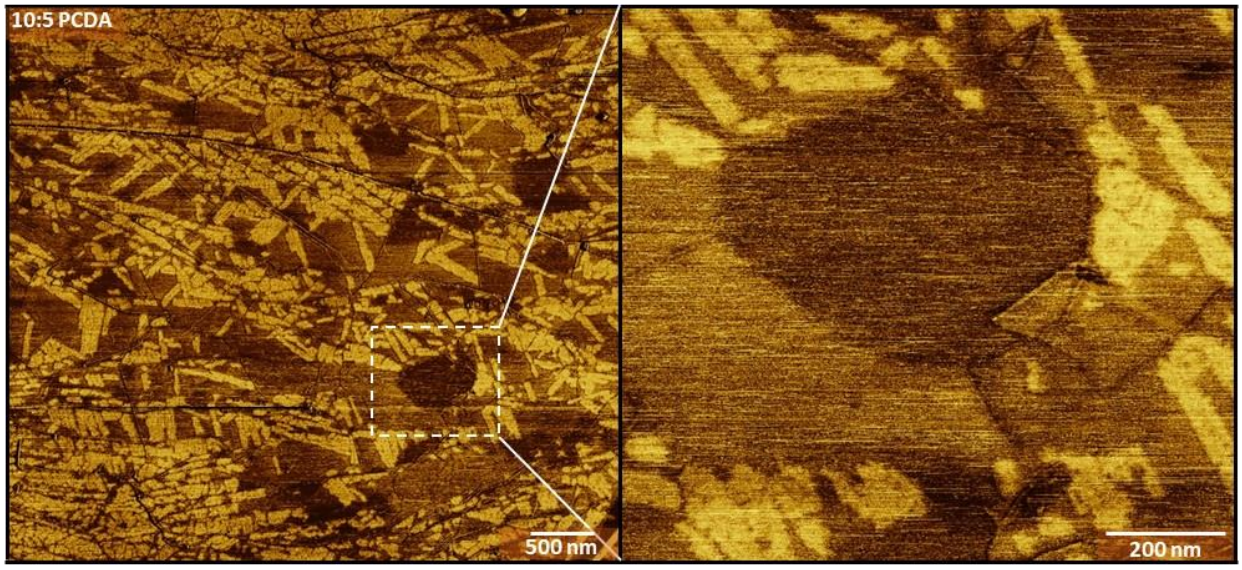

Figure S.A. 5. AFM images of PCDA transferred at 1.1 mM concentration in the ink solution, with a stamp prepared at 10:5 base:crosslinker ratio, resulting in transfer of both striped phase PCDA domains (light regions), and PDMS impurities (dark regions).

Representative images of 10:1 base:crosslinker ratio of 0.5 mM diyne PC

Chapter 2 shows representative images of diyne PC transferred from PDMS stamps prepared at a 10:2 base:crosslinker ratio. Figure S.A.7 shows representative images of diyne PC transferred from stamps prepared at a 10:1 base:crosslinker ratio; similar images were used to calculate domain number densities and diffusion distances.

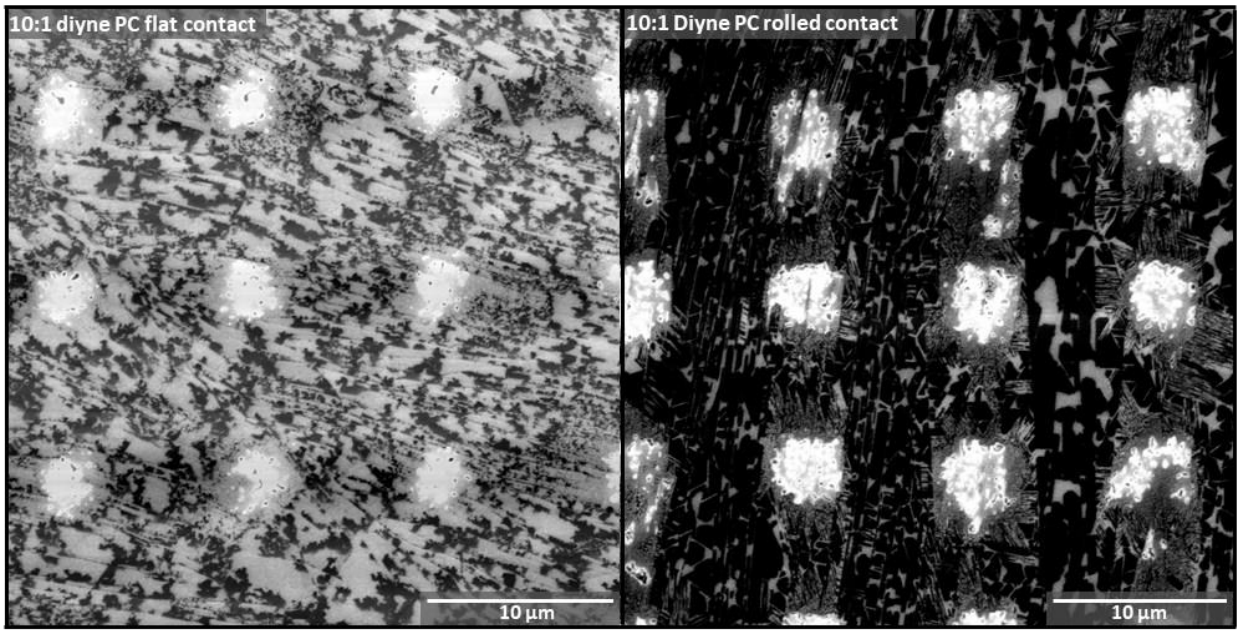

Figure S.A. 6. SEM images of HOPG after rolled and flat contact transfer of diyne PC.

Image segmentation and analysis examples

Figure S.A. 8 illustrates how manual image segmentation was performed to compare the assembly of striped phases and standing phases for the tested molecules (*e.g.* PCDA, diyne PE) using transfer conditions described in Chapter 2 and Experimental Methods. The figure illustrates an SEM image of diyne PC transferred to HOPG using a PDMS stamp prepared at a 10:1 base:crosslinker ratio, using rolled transfer. Striped phases can typically be identified based on rectangular domain geometries with linear edges, and/or the presence of long linear defects within the domain that appear during SEM imaging. The percent of the transfer resulting in striped phase domains is calculated by taking the difference of the area of the standing phase (Figure S.A.8c) from the total area occupied by the lipids (Figure S.A.8b). This gives the area of striped phase, which can then be divided by the total lipid-functionalized area to give the percentage of striped phase coverage. The diffusion distance was calculated by taking the total area occupied by the lipid (Figure S.A.8b) and subtracting the theoretical contact area (25 μm^2). This difference is the overfill (or underfill), which can then be used to calculate the diffusion distance.

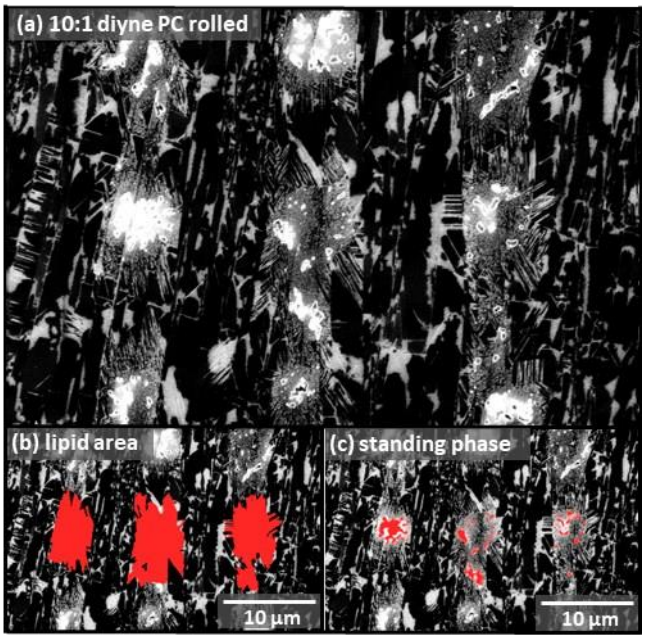

Figure S.A. 7. Sample SEM images showing segmentation (red highlighted areas) utilized for calculations of % striped phase (*vs.* standing phase) molecular transfer.

Molecular domains created through microcontact printing are frequently small relative to size scales that are straightforward to identify utilizing SEM images. Thus, for some image analyses, we utilized AFM images, which typically provide higher resolution at smaller scales. Figure S.A.9 shows example AFM images of NCDA and HCDA transferred to HOPG using PDMS stamps prepared at 10:2 base:crosslinker ratios. Red lines indicate domains tabulated for number density measurements.

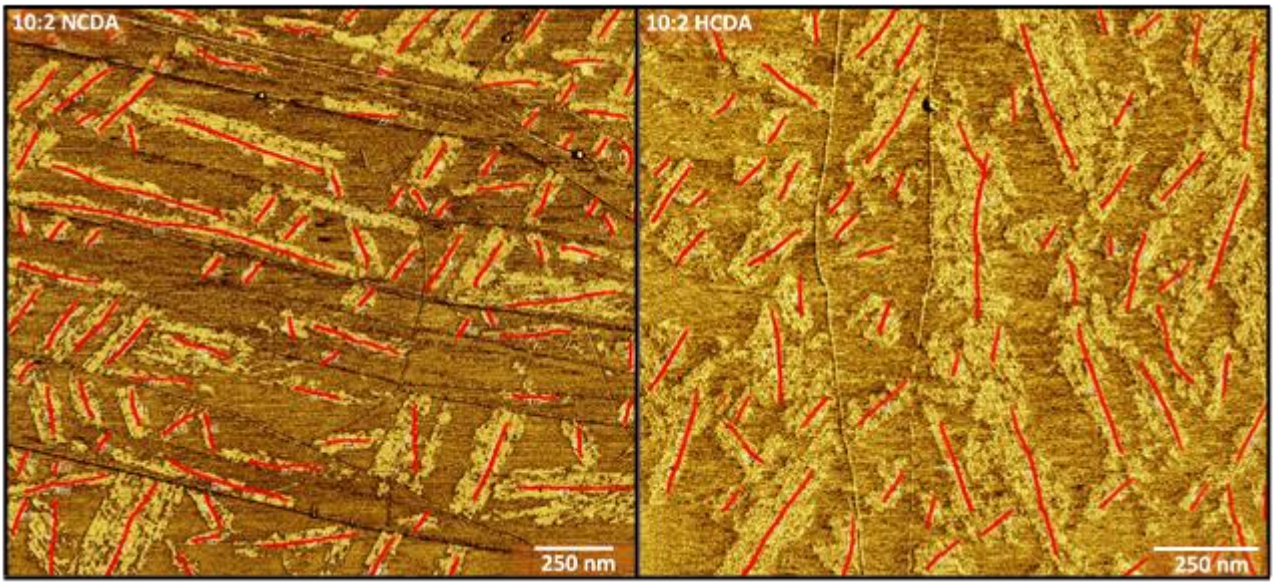

Figure S.A. 8. AFM images showing example domain number density measurements (red lines highlighting each domain) utilized for average domain number density per μm^2 calculations.

Large-scale versions of SEM images shown in Chapter 2

In Chapter 2, several SEM images are shown at small scale to facilitate comparison between molecular transfer conditions. Here, we show SEM images of larger areas of the surface and/or larger image sizes, to increase visibility of features within individual images. Figure S.A.10 shows a mm-scale area of the HOPG surface with areas of transferred PCDA striped phase. The square pattern is faintly visible at this scale, in addition to a large set of HOPG terraces in the lower left quadrant of the image; such features are common on cleaved HOPG. Figure S.A.11 shows an image of a section of the surface from Figure S.A.10, illustrating the degree of fidelity of pattern transfer, and the presence of narrow linear molecular domains (brighter) and amorphous impurities (darker) in the regions between stamp contact areas.

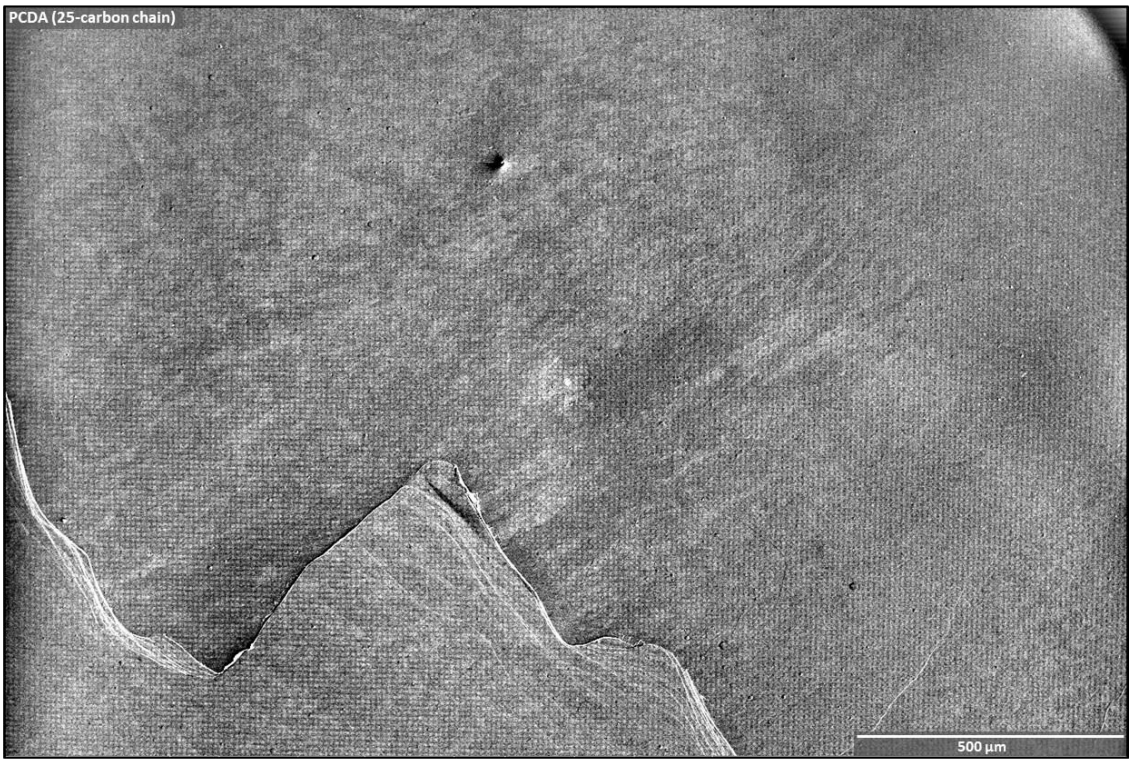

Figure S.A. 9. SEM images of HOPG after stamping with PDMS, illustrating long-range patterning and surface defects common on cleaved HOPG substrates.

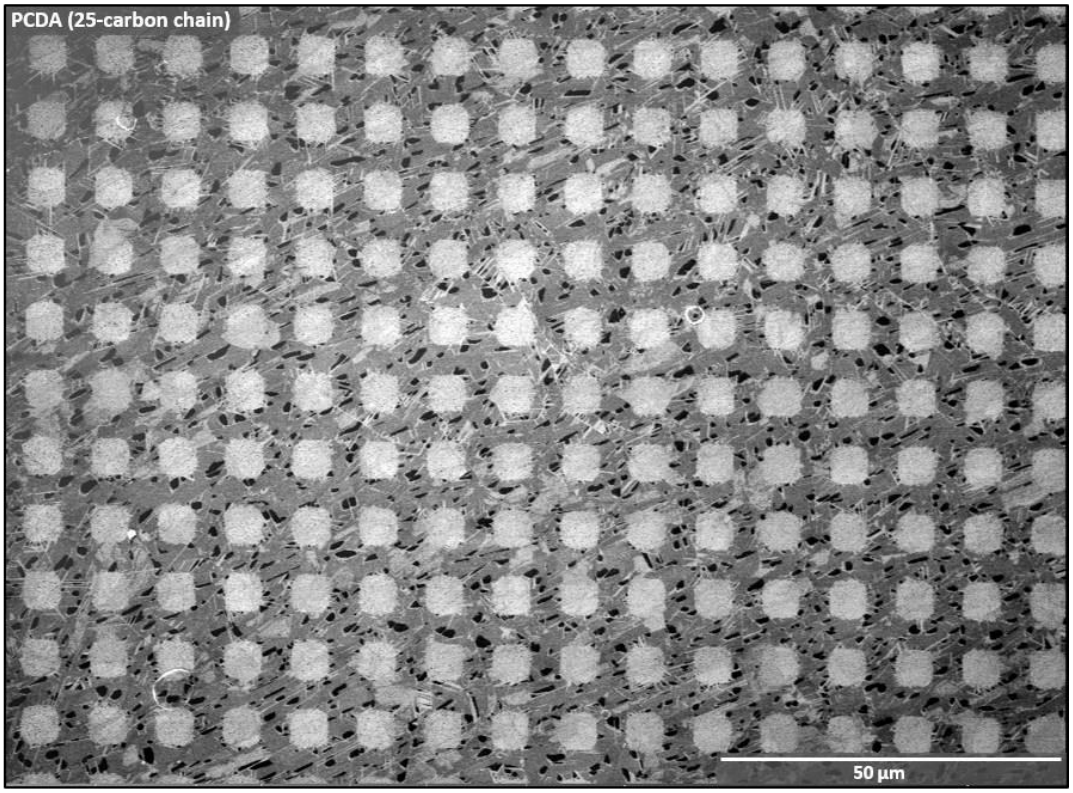

Figure S.A. 10. SEM image of HOPG after stamping with PDMS, illustrating rounded edges of square features in stamp following transfer, and narrow linear molecular domains extending between stamped areas.

Larger versions of images in Chapter 2 illustrating fidelity and quality of transfer

In Chapter 2, individual square areas of deposited NCDA, PCDA, and HCDA are shown in Figure. 2-4. Here, Figure S.A.12–15 show larger areas around the selected squares for visual comparison. Larger scale images of Diyne PE, Diyne PC, and PI from Figure 2-5–2-7 are shown here in Figure S.A.16–21.

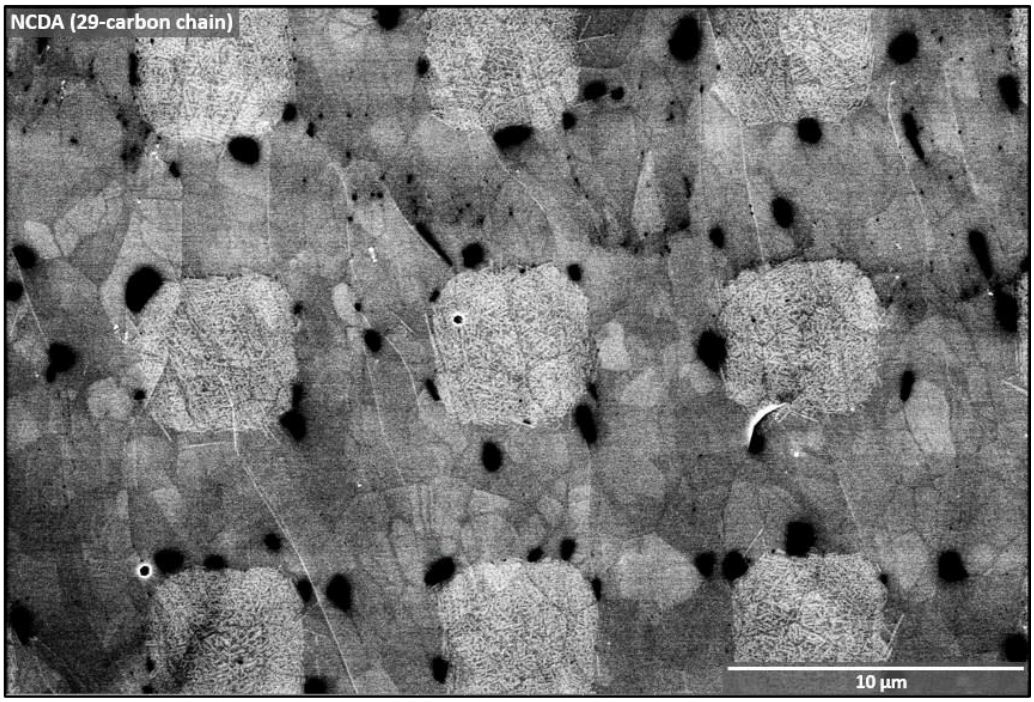

Figure S.A. 11. SEM image of HOPG after stamping with NCDA.

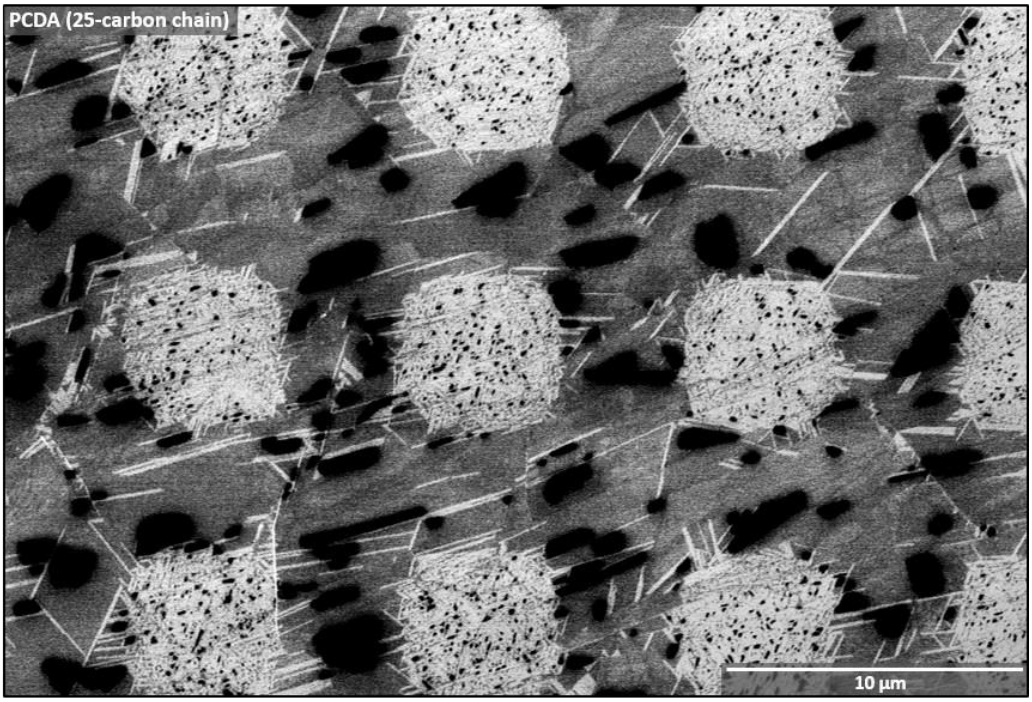

Figure S.A. 12. SEM image of HOPG after stamping with PCDA

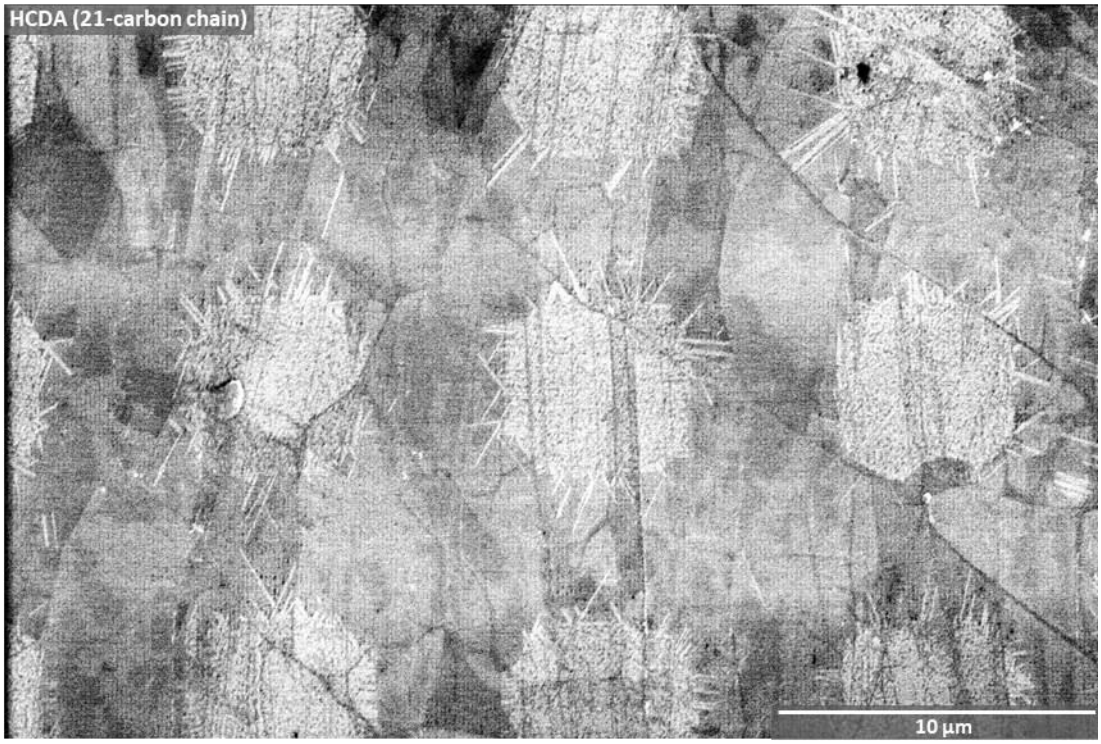

Figure S.A. 13. SEM image of HOPG after flat contact stamping with HCDA.

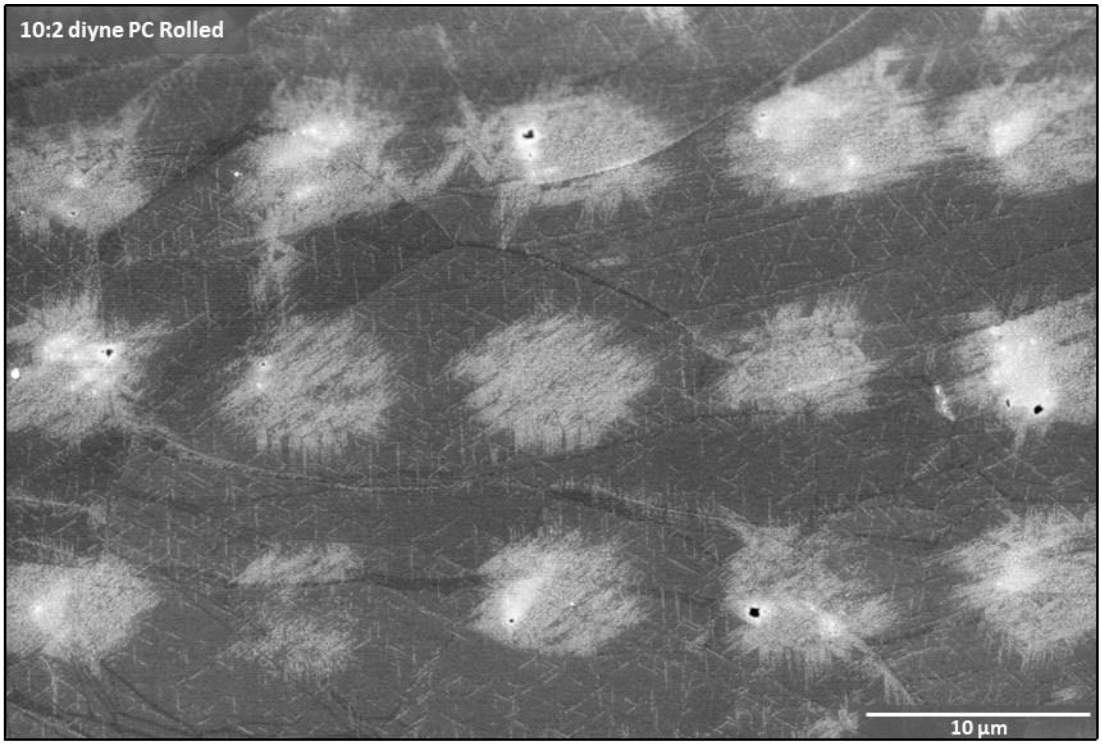

Figure S.A. 14. SEM image of HOPG after rolled contact stamping with Diyne PC.

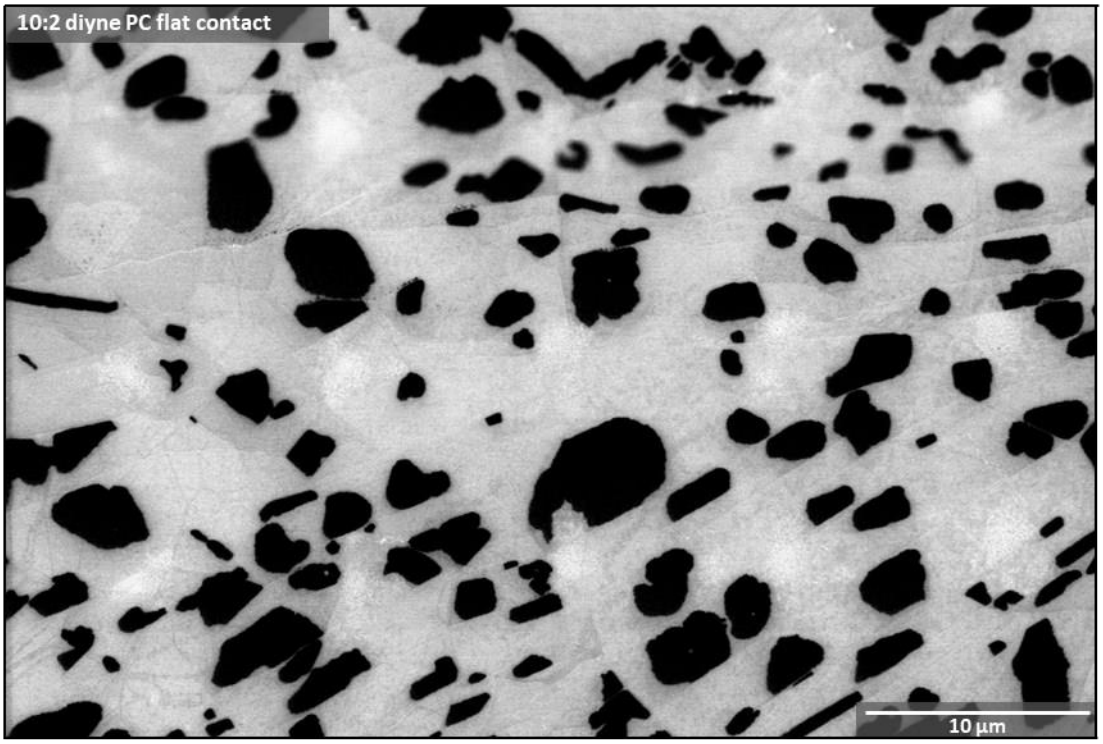

Figure S.A. 15. SEM image of HOPG after flat stamping with Diyne PC.

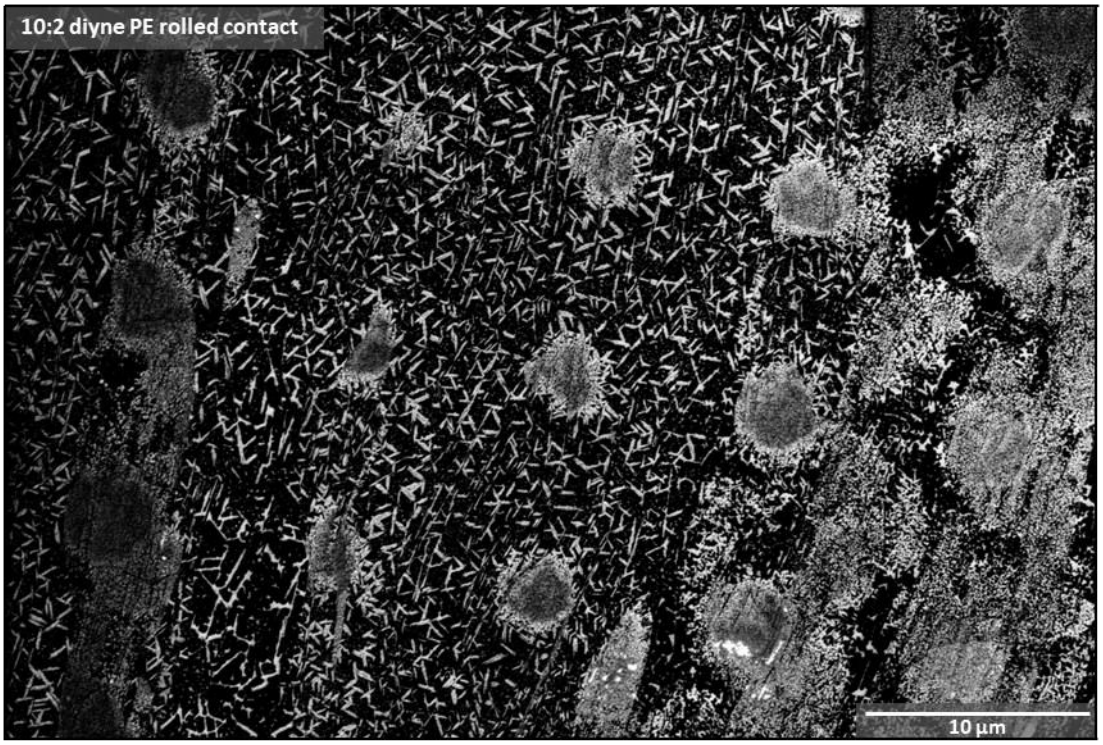

Figure S.A. 16. SEM image of HOPG after rolled contact stamping with Diyne PE.

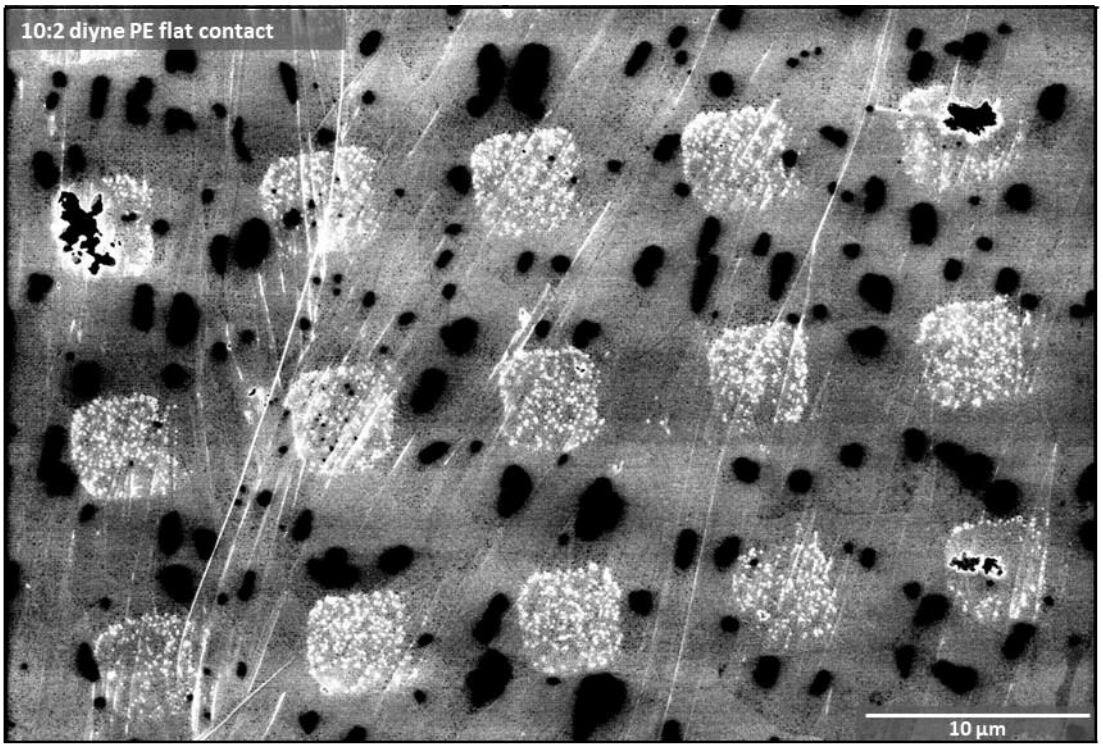

Figure S.A. 17. SEM image of HOPG after flat stamping with Diyne PE.

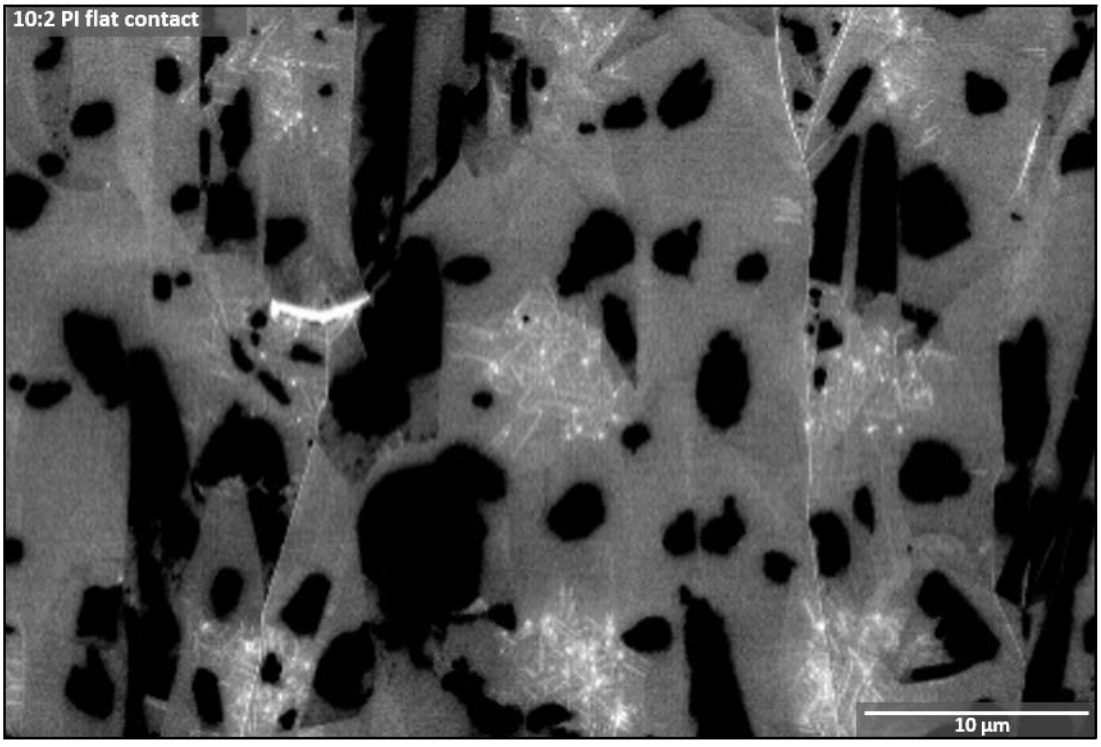

Figure S.A. 18. SEM image of HOPG after flat stamping with PI.

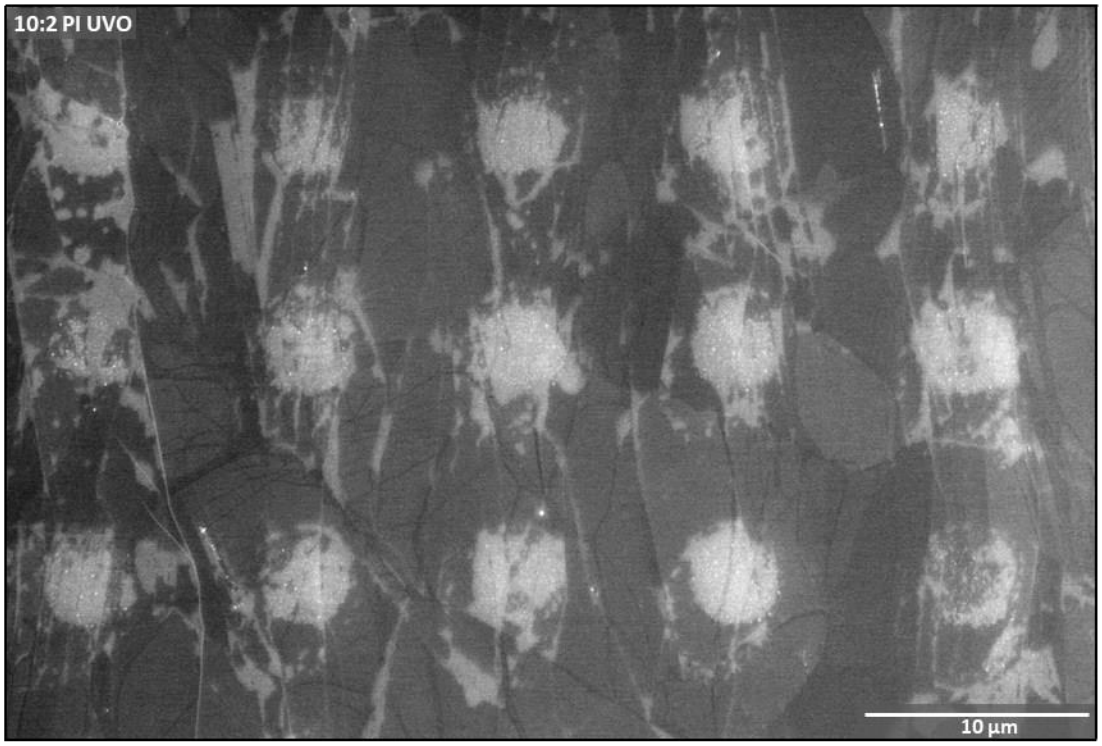

Figure S.A. 19. SEM image of HOPG after flat + UVO contact stamping with PI.

APPENDIX B. SUPPORTING INFORMATION FOR CHAPTER 3

Experimental Methods

Materials

Chloroform (≥99.5 % purity), poly (sodium 4-styrenesulfonate) (PSS) (Mw ≈1,000,000), poly (acrylic acid) (PAA) (Mw≈450,000), and octadecylamine (ODAm (≥99.0 % purity) were purchased from Sigma Aldrich (St. Louis, MO) and used as received. Absolute ethanol (100 % purity) was purchased from Decon Laboratories, Inc. (King of Prussia, PA) and used as received. Calcium chloride dihydrate was purchased from Fisher Scientific (Hampton, NH) and used as received. Albumin from bovine serum (BSA) tetramethylrhodamine conjugate was purchased from Thermo Fisher Scientific, Hillsboro, OR) and used as received. 1,2-Bis(10,12-tricosadiynoyl)-*sn*-glycero-3-phosphocholine (dPC, >99.0 % purity) was purchased from Avanti Polar Lipids (Alabaster, AL) and used as received. For transfer to polydimethylsiloxane (PDMS), SYLGARD 184 silicone elastomer kits containing base and curing (crosslinking) agent were purchased from Dow Chemical Company (Midland, MI). Lipids were deposited on 1 cm × 1 cm highly oriented pyrolytic graphite (HOPG, MicroMasch, Watsonville, CA) substrates. Substrates were cleaved immediately prior to sample deposition. All initial steps in the transfer process were carried out under UV-filtered light to prevent unwanted polymerization. PELCO conductive liquid silver paint, standard SEM pin stub mounts, AFM specimen discs (alloy 430), PELCO Formvar/carbon 400 mesh TEM grids, and double-coated carbon conductive tape were purchased from Ted Pella, Inc. (Redding, CA).

General procedure for the synthesis of a 10,12-diynamine from a 10,12-diynoic acid

10,12-Pentacosadiynamine (PCD-NH_2) and 10,12-tricosadiynamine (TCD-NH_2) were prepared from a 10,12-diynoic acid (i.e.,10,12-pentacodiynoic acid (PCDA) and 10,12-tricosadiynoic acid (TCDA) respectively) using a modification of previously reported literature[92-93] procedures described briefly here. First, 10,12-diynoic acid (1 eq) was dissolved in anhydrous DCM under N_2 atmosphere. Oxalyl chloride (1.3 eq) and DMF (N, N-dimethylformamide) (2 drops) were added to the solution. The reaction mixture was stirred at room temperature overnight

and concentrated under reduced pressure to obtain 10,12-diynoyl chloride as a yellow oil which was used for the next step without further purification. Next, in a round-bottom flask, 28-30 % aqueous ammonium hydroxide (1.3 eq) was added. 10,12-Diynoyl chloride (1 eq) was dissolved in THF and the resulting solution was added to the ammonium hydroxide solution at 0 °C. The reaction mixture was stirred at room temperature for 6 h. The product was extracted with DCM (3 × 50 mL) and combined organic extract was dried over anhydrous Na_2SO_4. The DCM was evaporated under reduced pressure to yield 10,12-diynoyl amide as a white solid. 10,12-Diynoyl amide (1 eq) was placed in a round-bottom flask. Anhydrous diethyl ether was added to the flask under N_2 atmosphere, yielding a white suspension. Subsequently, $LiAlH_4$ (10 eq) was added to the suspension at 0 °C and the reaction mixture was stirred at room temperature for 20 h. After the reaction was complete, the mixture was cooled to 0 °C and treated with sequential dropwise addition of water, aqueous NaOH (15 % w/w) and water. The mixture was filtered to remove inorganic impurities. Finally, the filtrate was dried over anhydrous Na_2SO_4 to yield 10,12-diynamine as a white solid.

PCD-NH_2 and TCD-NH_2 were dissolved in chloroform and filtered using a 13-mm syringe filter with a PTFE membrane and 0.2-μm pores (VWR, Radnor, PA) prior to use.

Langmuir–Schaefer transfer

Unless otherwise stated in Chapter 3, TCD-NH_2, PCD-NH_2, ODAm, and dPC were prepared using a previously reported temperature-controlled Langmuir–Schaefer conversion process that utilizes a custom-built temperature-controlled transfer stage.[14] This was utilized in conjunction with a MicroTrough XL Langmuir–Blodgett trough. HOPG substrates mounted on a standard 12-mm diameter stainless-steel AFM specimen disc were mounted on a magnet recessed in the temperature-controlled stage. Conductive carbon tape was used to affix the HOPG to the specimen disk surface to ensure temperature uniformity was achieved across the substrate surface. The temperature of the substrate was measured using a thermocouple prior to dipping.

TCD-NH_2 and PCD-NH_2 films were created at the air–water interface by depositing 36 μL of 0.75 mg/mL chloroform solution on a Milli-Q water subphase of 40 mM $CaCl_2$ at 30 °C. Barriers were swept inward at 6.23 mm/min to achieve the target mean molecular area (*e.g.,* 30 $Å^2$/chain) and subsequently switched to maintain the surface pressure measured at the target mean molecular area. The HOPG substrate was freshly cleaved and heated to 70 °C by the thermally controlled

stage and lowered (at 2 mm/min) into contact with the subphase for 2 min. The HOPG was then lifted out of contact at 2 mm/min.

ODAm films were created at the air–water interface by depositing 18 μL of 0.5 mg/mL chloroform solution on a subphase of 40 mM $CaCl_2$ at 30 °C. The trough barrier motion was 3.0 mm/min and moved inward to the target mean molecular area of 30 $Å^2$/chain and subsequently switched to target the surface pressure measured at 30 $Å^2$/chain. The HOPG substrate was freshly cleaved and heated to 35 °C by the thermally controlled stage and lowered (at 2 mm/min) into contact with the subphase for 2 min. The HOPG was then lifted out of contact at 2 mm/min.

The dPC films were created at the air–water interface by depositing 36 μL of 0.6 mg/mL chloroform solution on a subphase of Milli-Q water at 30 °C. The trough barrier motion was 6.23 mm/min and moved inward to a target surface pressure of 30 mN/m. The HOPG substrate was freshly cleaved and heated to 50 °C by the thermally controlled stage and lowered (at 2 mm/min) into contact with the subphase for 2 min. The HOPG was then lifted out of contact at 2 mm/min.

For all films, the chloroform solution was allowed 15 min to evaporate before the trough barriers were slowly moved inward. After contact with the subphase was broken, the HOPG substrate was blown dry with UHP N_2. Finally, unless otherwise stated in the Chapter 3, the HOPG substrate was placed under a hand-held UV lamp (254 nm, 8 W) for 1 h with ∼2 cm between the lamp and the substrate to induce diyne photopolymerization.

AFM imaging

All AFM measurements were performed using a Bruker (Bruker Instruments, Billerica, MA) MultiMode AFM, equipped with an E scanner, under ambient conditions utilizing Bruker RFESP-75 tips (nominal force constant 3 N/m and radius of curvature <10 nm). Micrographs were collected in tapping mode and tip broadening was corrected using the equation below where w_0 is the corrected width, w_{exp} is the experimentally measured width, and r_o is the AFM tip radius of curvature.

$$w_0 = w_{exp} - 2(h * [2r_0 - h])^{1/2}$$

Image Analysis

Images were processed using ImageJ analysis software and Gwyddion scanning probe microscopy data visualization and analysis software to preform plane flattening, median line corrections, scar artifact removal, contrast adjustment and pixel counting. Adsorption weight was quantified by digital image analysis within ImageJ after the raw bitmap files were processed by mean plane subtraction, median row alignment, and horizontal scar correction using Gwyddion. The pixels/nm scale was calibrated for individual micrographs then the pixels representing polymers in the micrograph were manually highlighted and subsequently measured for length in nm. The total weight of polyelectrolyte adsorption was calculated using the total polymer length in a micrograph divided by the length of the polyelectrolyte monomer and converted to total grams of monomer present. At least 3 images were analyzed for each data point graphed.

SEM imaging

SEM imaging of microcontact printed dPC square arrays under high magnification was performed using a Teneo VS SEM (FEI Company, Hillsboro Oregon) at a working distance of ~ 7mm using the segmented in-lens T3 secondary electron (SE) detector. For best resolution, image acquisition beam currents of 0.10nA or 25pA were utilized with a 32 µm diameter aperture at an accelerating voltage of 5kV. Substrates were mounted with conductive carbon tape to standard SEM pin stub specimen mounts where a small amount of colloidal silver paint (PELCO®, Ted Pella, Inc.) was applied along the perimeter of the HOPG to enhance substrate-mount conductivity.

Molecular Modeling

Software packages Maestro and Macromodel (Schrödinger, Cambridge, MA) were used respectively to visualize molecular structures and to perform force field minimizations. Energy minimizations on all models was performed using OPLS_2005 force field, with normal cutoffs for van der Waals, electrostatic, and hydrogen-bonding interactions. Minimizations were performed using the Polak−Ribiere conjugate gradient (PRCG) algorithm and gradient method with 50 000 runs and a convergence threshold of 0.05.

Contact Angle Titration

Contact angle titrations were performed using an Attension Theta optical tensiometer (Biolin Scientific, Espoo, Finland). Buffers with 20mM buffering capacity at a range of pH values from 2 to 12 were purchased from Sigma-Aldrich and used as received. For each measurement, both HOPG and PDMS substrates, a 3 μL droplet of a buffer solution was applied to the substrate. At the stated pH the buffer droplet was recorded by the tensiometer within 10s of deposition and recorded as the advancing contact angle. Subsequently the buffer droplet was withdrawn using a 32-gauge needle syringe until the droplet front on the substrate receded and recorded as the receding angle. Each contact angle graphed is the average of 27 data points distributed across 3 substrates from 3 sample sets. Typically, 9 measurements were recorded from the 1 × 1 cm samples.

Preparation of PDMS Stamps

Stamps were prepared by mixing SYLGARD 184 silicone elastomer base and a curing (crosslinking) agent at a 10:1 m/m ratio. After thoroughly mixing the components, the mixture was poured onto Formvar-and-carbon-coated copper 400 mesh TEM grids, with the Formvar side down in a glass Petri dish.[94] The mixture was then deaerated in a vacuum desiccator until no bubbles remained. The PDMS was cured for 24 h at 60 °C; the TEM grids were then gently peeled from the PDMS, generating a micropatterned surface. The micropatterned stamps were cleaned by sonication in a 1:1:1 (*v/v/v*) mixture of ethanol, methanol, and Milli-Q water for 60 min and subsequently placed in an oven for 1 h at 60 °C to allow residual polar solvent mixture to evaporate. The micropatterned stamps were then soaked in hexanes for 6 h, replacing the solvent with fresh hexanes every 2 h. Finally, the micropatterned stamps were dried for 24 h at 60 °C and then stored covered in a petri dish pattern side up prior to use.

Microcontact Printing of dPC

Inking and printing steps were performed following a previously published procedure,[88] described briefly here. The molecular ink solution was prepared at 2.5 mg/mL in $CHCl_3$ and diluted to 0.4 mg/mL with ethanol. Prior to inking, the PDMS stamp was rinsed with ethanol and blown dry with ultra-high purity (UHP) N_2. The stamp was then immersed for 1 min in the ink solution,

removed and blown dry with UHP N_2, and placed pattern side up at room temperature for 1 h. The pattern side of the PDMS stamp was brought into contact with a freshly cleaved HOPG substrate for 1 min and carefully lifted off the surface. The microcontact printed HOPG substrate was then exposed to UV, to induce diyne photopolymerization, for 1 h under a held UV lamp (254 nm, 8 W) for 1 h with ∼2 cm between the lamp and substrate surface.

Covalent transfer of polymerized diyne amphiphile striped phase from HOPG to PDMS

The covalent transfer from HOPG to PDMS was performed following a previously published procedure, described briefly here.[18] SYLGARD 184 silicone elastomer base and curing (crosslinking) agent were mixed at a 10:1 (m/m) ratio. The components were thoroughly mixed for 5 min, and the mixture was poured onto the HOPG substrate functionalized with a polymerized polydiacetylene amphiphile film. The mixture was then deaerated in a vacuum desiccator to remove all air bubbles. The PDMS was cured for 24 h at 60 °C. The cured PDMS was then carefully peeled away from the HOPG substrate.

Wide-field fluorescence microscopy

Wide-field fluorescence micrographs were obtained using an Olympus BX-51 optical microscope with an Olympus DP71 color camera. Images were acquired using either a 40X (metallographic, plan-fluorite aberration correction, NA = 0.75, infinity corrected optics) or a 100X (metallographic, apochromatic and flat field correction, NA = 0.95) brightfield objective. A UMWB2 filter cube was utilized with a 460–490 nm excitation band-pass filter, a dichroic filter wavelength of 500 nm and a long-pass emission filter wavelength of 520 nm. Typical dwell times for imaging ranged from 1/1.5 to 5s with a resolution of 1024 × 1024 pixels.

Confocal fluorescence microscopy and spectral imaging

Confocal micrographs and associated spectra were acquired utilizing a Zeiss LSM 880, Axio Examiner upright confocal microscope. Unless otherwise stated in the supplemental, excitation was provided by a 488 nm Ar laser set to 100 % power. Data was obtained using a 20X objective (plan-apochromatic, dry, NA = 0.80), with a 0.17-mm cover glass placed on the sample, and a 32-channel GaAsP spectral photomultiplier tube detector. Micrographs and corresponding

spectra were obtained at a resolution of 2856 x 718 pixels, a bit depth of 8 bits, a dwell time of 11.75 μs/pixel (using unidirectional scanning and averaging 16 times per line), and a pinhole set to 1 Airy unit. For detection, 23 of the 32 channels were used to collect data, with bins centered at values from 495–691 nm and a resolution (bin width) of 8.9 nm. Bare PDMS emits a strong peak at 513 nm which was not included in the monolayer's spectra. Therefore, we normalized the data to the bare PDMS spectra to observe the difference in emission from TCD-NH_2/PDMS.

Polyelectrolyte Deposition

Polyelectrolyte solutions were prepared in Milli-Q water at concentrations outlined in Chapter 3. For polyelectrolyte adsorption, substrates were hand-lowered until immersed in a polyelectrolyte solution, at a slight angle, for a specified time interval outlined in Chapter 3. The substrates were lifted out of the solution, dried with UHP N_2, and stored under ambient conditions.

To deposit a full coating of a polyelectrolyte film, substrates were hand-lowered until immersed in an aqueous 1 mg/mL PSS solution for 10 min, removed from the solution and blown dry with UHP N_2, followed by washing with Milli-Q water for 5 min twice and blown drying with N_2 between washings. This process was then repeated, and the substrates stored under ambient conditions.

BSA Deposition

Solutions of albumin from Bovine serum (TRITC-BSA) Tetramethylrhodamine conjugate were prepared at 0.5 mg/mL in 10mM Potassium Phosphate solution. Substrates were prepared and cut to a 0.5 cm × 0.5 cm area and placed on a glass slide. A 0.1 mL droplet of the BSA Tetramethylrhodamine solution was deposited on the substrates and covered under a petri dish for 10 min. The droplets were withdrawn off the substrates and subsequently washed with a 10mM potassium phosphate solution for 30s and then blown dry with UHP N_2.

Larger AFM and SEM images illustrating the LS assembly of striped phase films of PCD-NH_2, ODAm, TCD-NH_2, and dPC on HOPG

In Chapter 3 Figure 3.2 showed AFM and SEM images illustrating the lamellar and domain structure for striped phase films. Here, we show larger AFM and SEM images (Figure S.B. 1 and S.B. 2) to demonstrate the length scale of ordering that is possible to achieve using thermally regulated Langmuir–Schaefer (LS) conversion. Within Figure S.B. 1, AFM images of (a) PCD-NH_2, (b) ODAm, (c) TCD-NH_2, and (d) dPC. exhibit long-range ordered striped phase domains of length scales > 100 nm. Highlighted in the image are long linear features generally crossing the entire image from left to right, which correspond to HOPG step edges.

Figure S.B. 2 shows an SEM image of PCD-NH_2 striped phase assembly on HOPG. Long-range cracking defects are visible at length scales >20 μm (Figure S.B. 2 left) indicating the extended domain ordering of the assembled monolayer. In other experiments we utilize conditions that result in rounded or oval microscopic vacancies in the monolayer (Figure S.B. 2, right). Here, the darker areas in the image correspond to vacancies in the monolayer. The vacancies within the monolayer provide contrast after the polydiacetylene-on-amorphous material transfer (PATRN) for distinguishing functionalized from unfunctionalized areas of the PDMS surface.

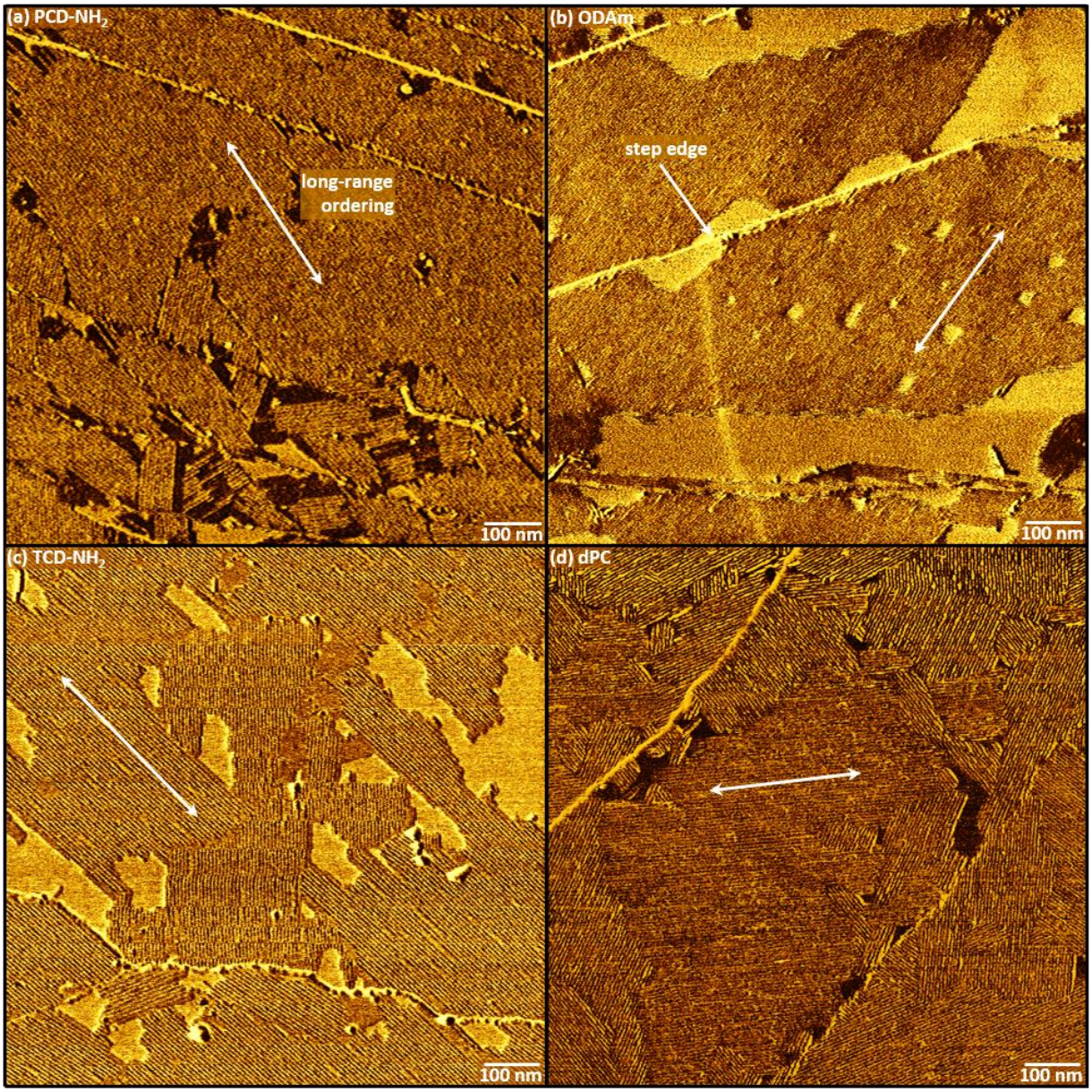

Figure S.B. 1 AFM micrographs illustrating the long-range ordering of striped domains of (a) PCD-NH_2 (b) ODAm (c) TCD-NH_2 and (d) dPC on HOPG.

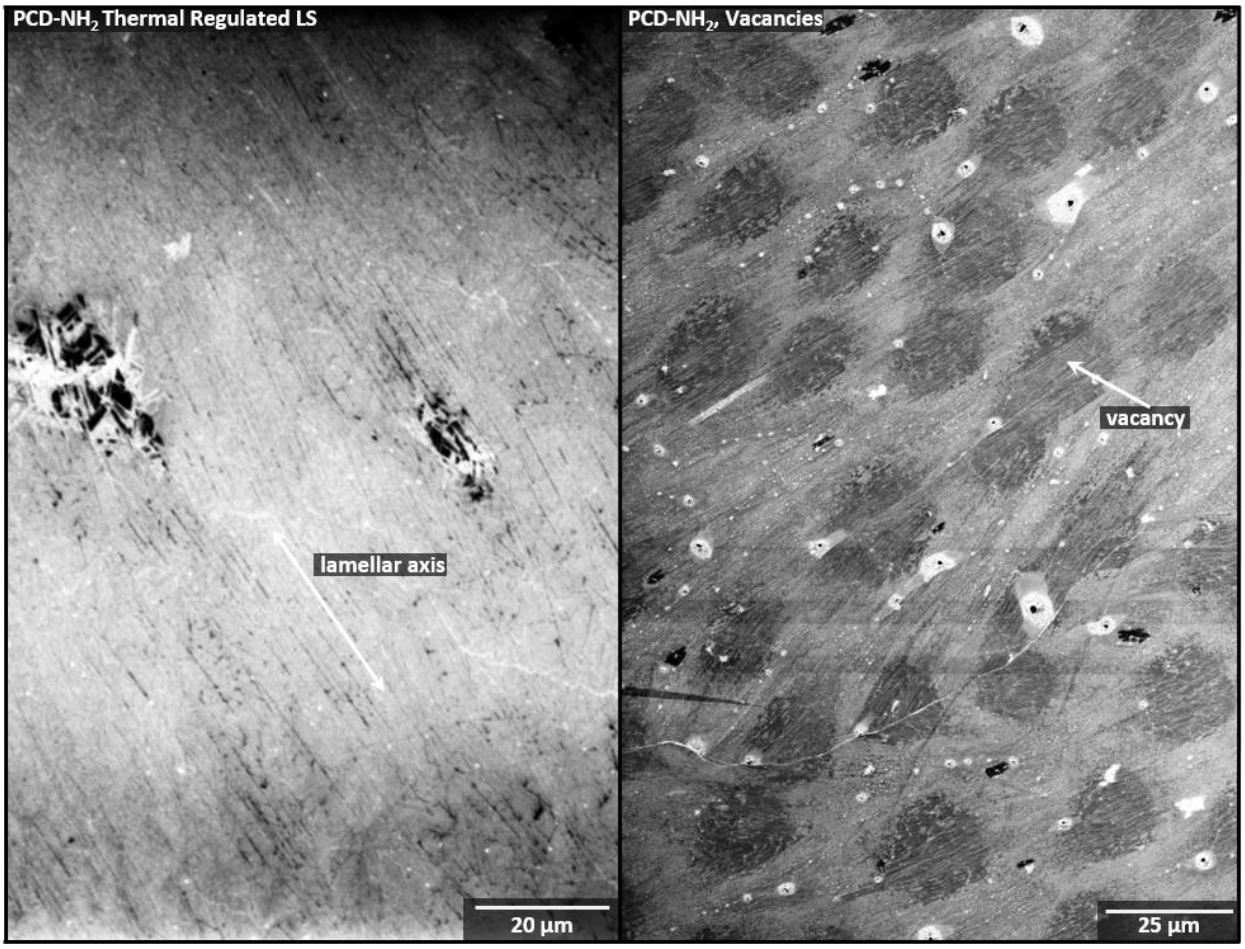

Figure S.B. 2 SEM images of PCD-NH_2 illustrating (a) the long-range ordering of striped phase domains and (b) monolayer coverage with oval vacancies.

Larger AFM micrographs illustrating the adsorption of polyelectrolytes

In Chapter 3, Figure 3.3 contained AFM micrographs of polyelectrolyte adsorption on striped phases of PCD-NH_2 and ODAm. Here, we show larger AFM micrographs of the striped phase domains and the PSS adsorption from spin coating and dip coating deposition. Highlighted in the micrographs are regions of PSS polymers exhibiting anisotropic conformations parallel to the lamellar axis of the PCD-NH_2 striped phase. In Figure S.B. 3, we highlight PSS bundles separating into individual polymer chains when aligned epitaxially with the underlying PCD-NH_2 template. Dip coated samples of PCD-NH_2 shown in Figure S.B. 3b exhibit reduced anisotropic adsorption of PSS and minor disordering of the striped phase template. Figure S.B. 3c show PSS spin coated to ODAm films which exhibit anisotropic adsorbed polymers. ODAm dip coated

samples (Figure S.B. 3d), however, exhibit less anisotropic alignment and larger monolayer vacancies.

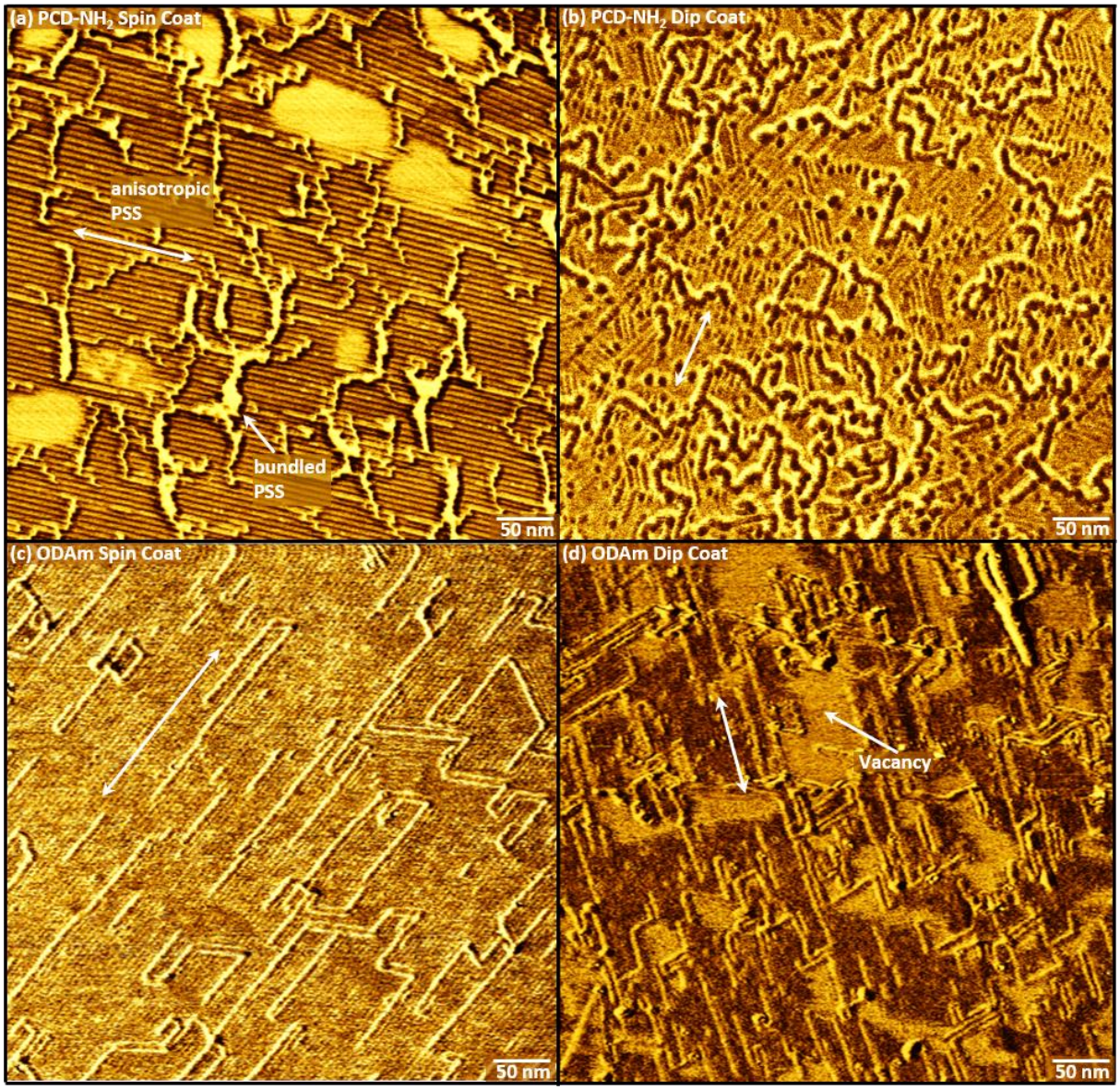

Figure S.B. 3 AFM micrographs illustrating the anisotropic adsorption of PSS in epitaxy with ordered rows of (a,b) PCD-NH_2 and (c,d) ODAm. Dip coated samples (b,d) illustrate monolayer disordering and desorption cause from PSS solution exposure.

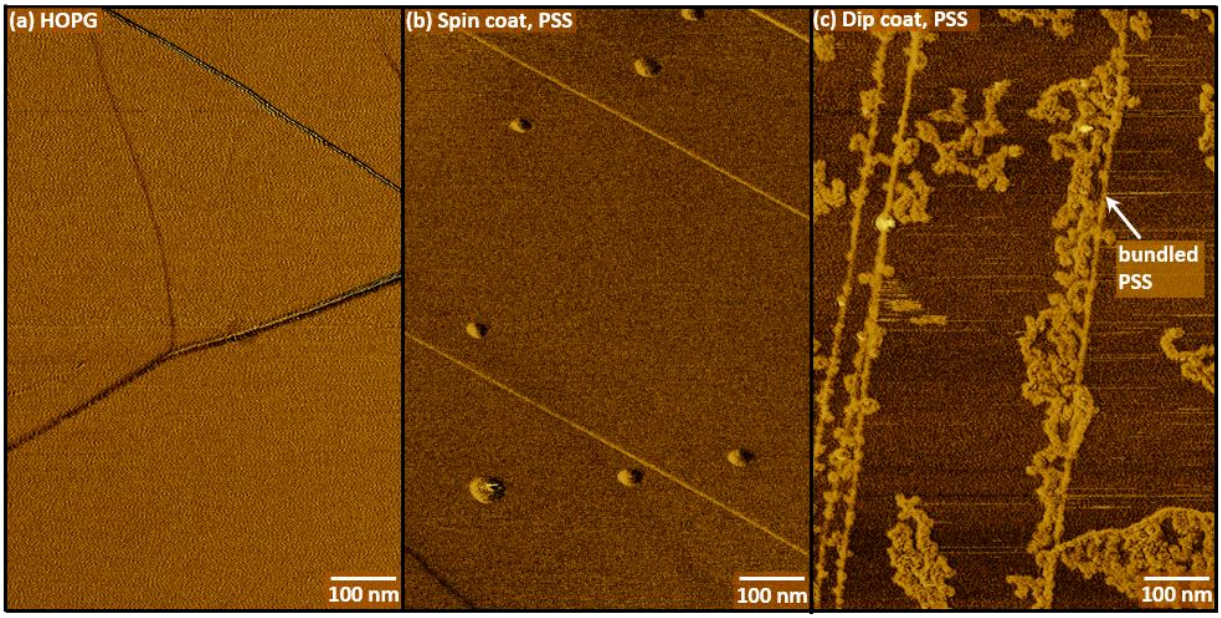

Figure S.B. 4 AFM micrographs of (a) bare HOPG and the surface after exposure to (b) PSS spin coated (b) PSS dip coated.

In Figure 3.5 of Chapter 3, we illustrated polyelectrolyte adsorption on functionalized PDMS. Here, in Figure S.B. 5 we provide enlarged AFM micrographs of bare PDMS substrates illustrating the minimal polyelectrolyte adsorption we observe. To ensure topographical consistency between the control and functionalized samples, the 10:1 base:crosslinker bare PDMS was cured in contact with a bare HOPG substrate as shown in Figure S.B. 5a. Figure S.B. 5b shows an AFM micrograph of bare PDMS dip coated under the same LBL related conditions as the TCD-NH_2 functionalized PDMS (TCD-NH_2/PDMS), shown in Figure 3.6 of Chapter 3. Unlike the extensive PSS adsorption shown in Figure 3.6, we observe minimal PSS adsorption on the bare PDMS surface after 2 min of exposure. Figure S.B. 5c–d show enlarged micrographs of the PDMS controls for both PSS (strong) and PAA (weak) polyelectrolytes where we observe minimal adsorption to the surface after 2 min exposure.

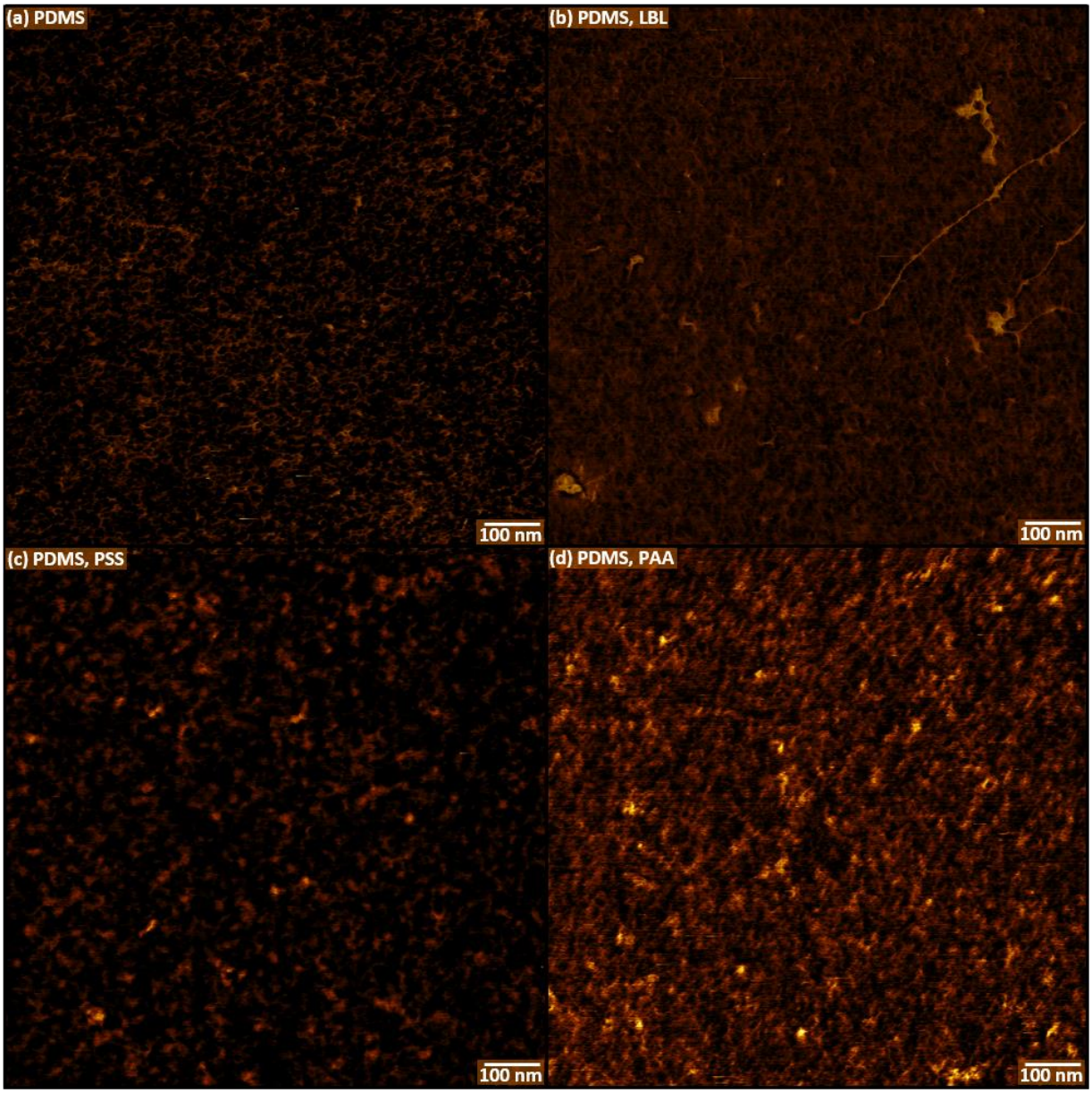

Figure S.B. 5 AFM micrographs of PDMS illustrating the surface after exposure to polyelectrolyte solutions. (a) bare PDMS (b) PDMS dip coated under conditions similar to LBL in PSS solution, (c) PDMS dip coated in PSS solution, and (d) PDMS dip coated in PAA solution.

In Chapter 3, we demonstrated polyelectrolyte adsorption on functionalized PDMS in Figure 3.5. Here we provide enlarged AFM micrographs of polyelectrolyte adsorption on TCD-NH_2/PDMS samples in Figure S.B. 6. For comparison, we show the TCD-NH_2/PDMS in Figure S.B. 6a prior to polyelectrolyte exposure. After 2 min exposure to PSS and PAA solutions, we

observe the adsorption of polyelectrolytes to the surface as illustrated in Figure S.B. 6b–c. Here, we observe both PSS and PAA adsorbates on the surface as described in the Chapter 3. The TCD-NH_2/PDMS film facilitates polyelectrolyte adsorption in contrast to the minimal adsorbed mass on bare PDMS. Figure S.B. 6d, illustrates the extensive adsorption (~ 50 % coverage) of PSS following repeated dip coating depositions at conditions similarly used for LBL fabrication.

For PDMS functionalized with PCD-NH_2 (PCD-NH_2/PDMS) (Figure S.B. 7), we observe similar polyelectrolyte adsorption as illustrated in the enlarged AFM micrographs. Prior to polyion adsorption, we characterize the PCD-NH_2/PDMS surface as shown in Figure S.B. 7a. We then expose the PCD-NH_2/PDMS surface to polyelectrolyte solutions under similar conditions. Here, in Figure S.B. 7b–c we observe PSS and PAA adsorption on PCD-NH_2/PDMS after 2 min dip coating exposure.

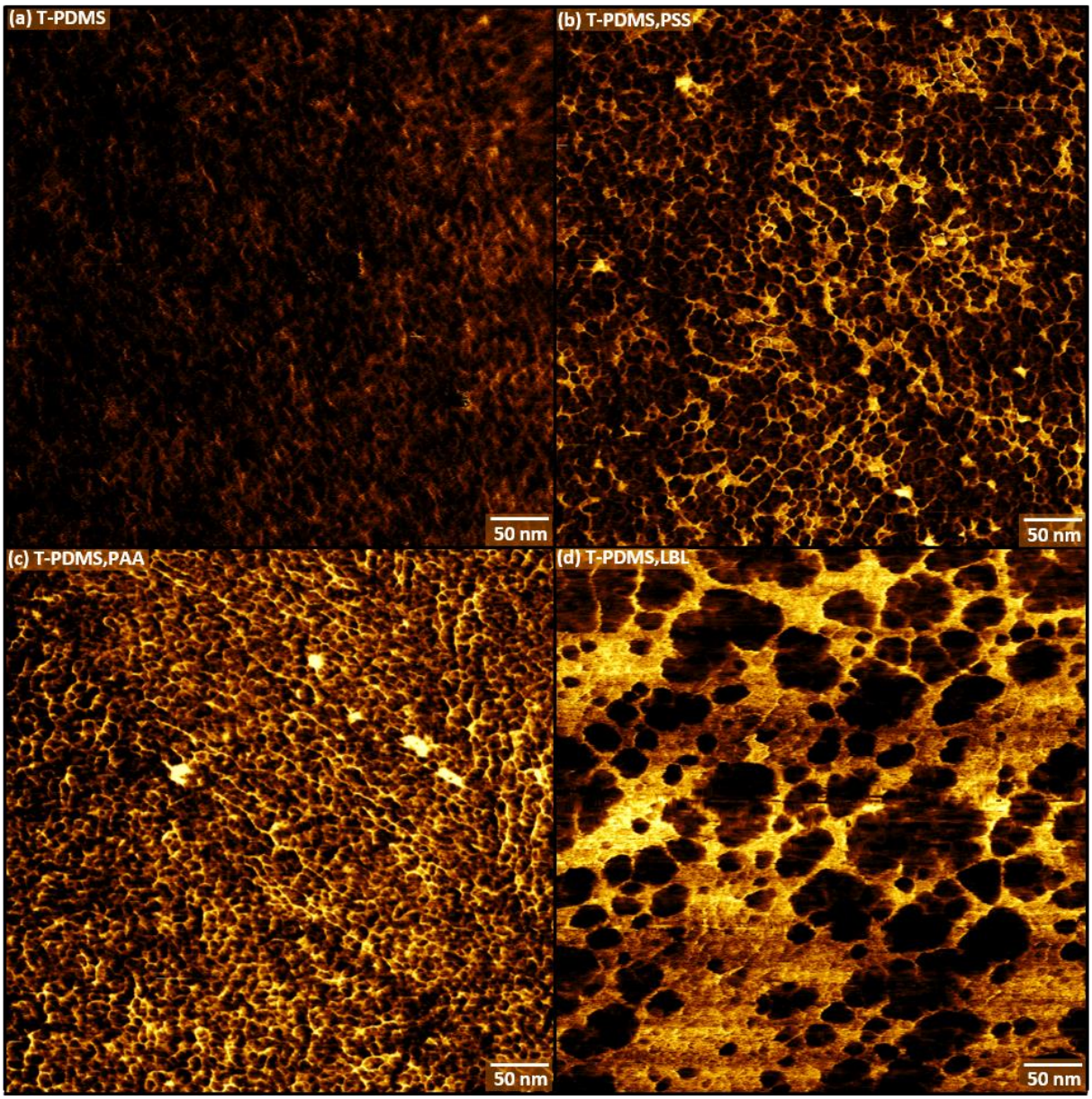

Figure S.B. 6 AFM micrographs of PDMS functionalized with (a–d) TCD-NH_2 illustrating the surface after exposure to (b) PSS dip coated (c) PAA dip coated (d) PSS LBL deposition.

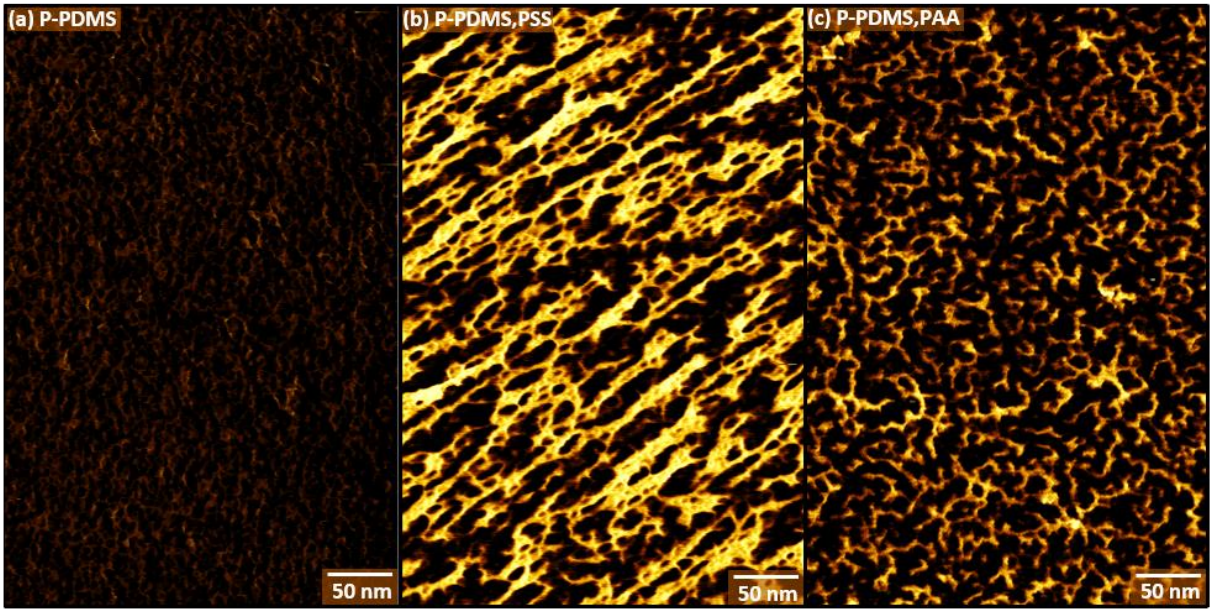

Figure S.B. 7 AFM micrographs of (a) PCD-NH_2/PDMS and the surface after exposure to (b) PSS dip coated (b) PAA dip coated.

Larger SEM and fluorescence images illustrating the PATRN transfer of stiped phase films to PDMS

In Chapter 3, we assembled striped phase monolayers of various characteristics. Here, we show enlarged SEM and fluorescence images of the monolayer morphologies. In Figure S.B. 8, we show SEM images of μCP dPC illustrating three distinct phases of dPC: standing, lying-down, and low number-density (LND). Here, we highlight the LND molecular domains within the channel region as described Chapter 3. After transfer to PDMS we observe only standing and lying-down phases in the enlarged fluorescence image (Figure S.B. 8b). This is due to the low density of the fluorescent PDA groups in the channel region. These images illustrate the transfer of μCP dPC features from HOPG to PDMS through the PATRN process.

For TCD-NH_2 we assembled oval vacancies in the monolayer to facilitate characterization *via* SEM or fluorescence microscopy. Here in Figure S.B. 9a, the SEM image illustrates the monolayer vacancies assembled with the LS transfer conditions similar to the PCD-NH_2 film in Figure 3.2. In Figure S.B. 9b–c, we show enlarged fluorescence images of oval vacancies transferred to PDMS for TCD-NH_2 and PCD-NH_2 films. Here, we observe dark oval features on the functionalized PDMS exhibiting low fluorescence intensity consistent with the oval vacancies observed in the SEM (Figure S.B. 2 & Figure S.B. 9a).

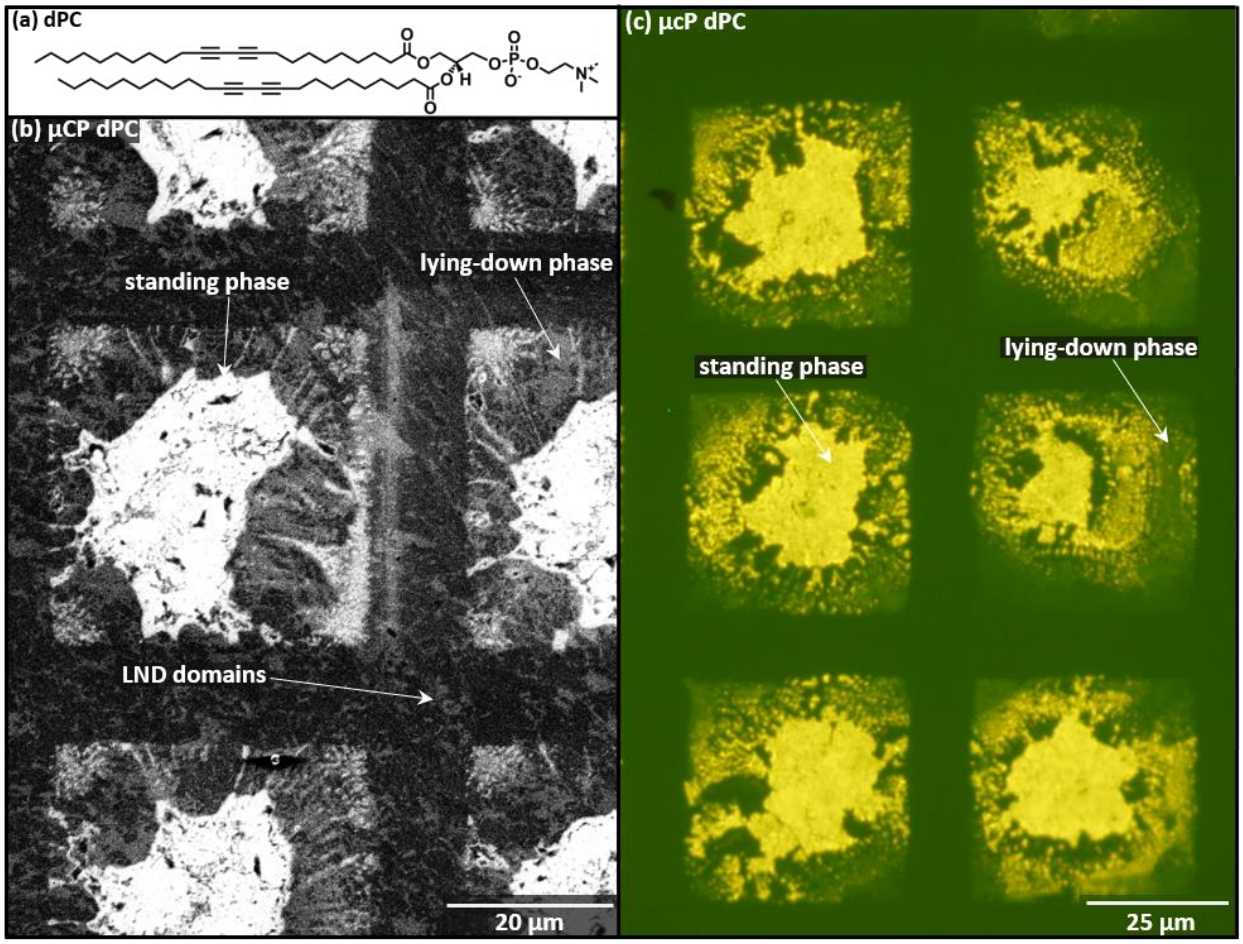

Figure S.B. 8 (a) Structure of dPC. (b,c) SEM and fluorescence image illustrating congruence of µCP dPC domain structure before and after transfer to PDMS. (Left) SEM image of µCP dPC on HOPG highlighting standing phase, lying-down phase, and LND domains. (Right) Fluorescence image of µCP dPC on PDMS.

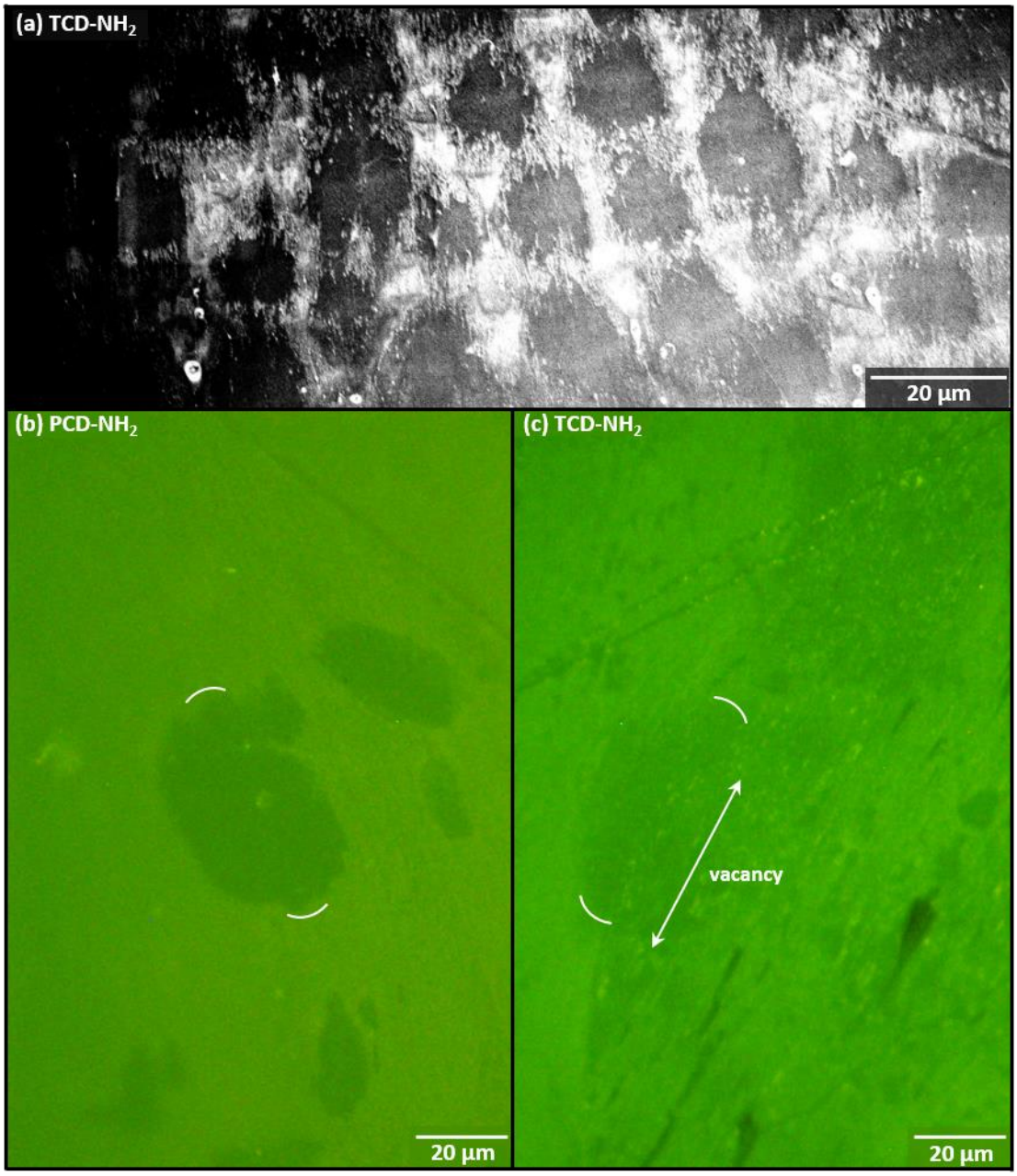

Figure S.B. 9 SEM and fluorescence image illustrating congruence of PCD-NH_2 and TCD-NH_2 vacancy domain structure after transfer to PDMS. SEM image of vacancies in (a) TCD-NH_2/HOPG. Fluorescence image of vacancies within (b) PCD-NH_2/PDMS and (c) TCD-NH_2/PDMS

Fluorescence imaging of TRITC-BSA

In Chapter 3, we estimated the BSA adsorption to functionalized PDMS substrates. Here, in Figure S.B. 10 we show enlarged fluorescence images of bare and functionalized PDMS from Figure 3-6. Figure S.B. 10a–c fluorescence images taken with a 500 nm dichroic filter showing the emission from the PDA groups and PDMS substrate were taken as a control prior to BSA adsorption. In Chapter 3, we described the difference in the fluorescence spectra observed for TCD-NH_2/PDMS substrates compared to bare PDMS. Figure S.B. 10d–f presents the full collected images from the Zeiss upright confocal microscope, which represents the full-collected bandwidth of the substrate emission can be broken down by wavelength range. The measured emission from 500–700 nm (Figure S.B. 10e) illustrates the surface features of the transferred films producing novel fluorescence emission from the PDMS surface. Finally, we demonstrate the lack of 572 nm emission fluorescent material on the surface prior to TRITC-BSA adsorption with a 520 nm long-pass emission filter to observe the fluorescence. For Figure S.B. 10g–i, we observe no 572 nm emission produced on the surface, supporting our claim in Chapter 3 that the fluorescence observed in Figure 2.6 is produced from adsorbed fluorescent labeled BSA proteins.

With Figure S.B. 11, we show enlarged fluorescence images of the PDMS substrates after TRITC-BSA adsorption. In Figure S.B. 11a–b, we show BSA adsorption on TCD-NH_2/PDMS as well as PSS dip coated TCD-NH_2/PDMS substrates (TCD-NH_2/PDMS+PSS). On bare PDMS, we observe the highest adsorbed mass of BSA as illustrated by the fluorescence image in Figure S.B. 11c. The adsorption of BSA, as shown in Figure S.B. 11d, on µCP dPC illustrate reduced rates of adsorption on the three distinct regions of the surface in comparison to bare PDMS. Overall, we observe a reduction in the adsorption of BSA for all functionalized PDMS substrates in comparison to bare PDMS.

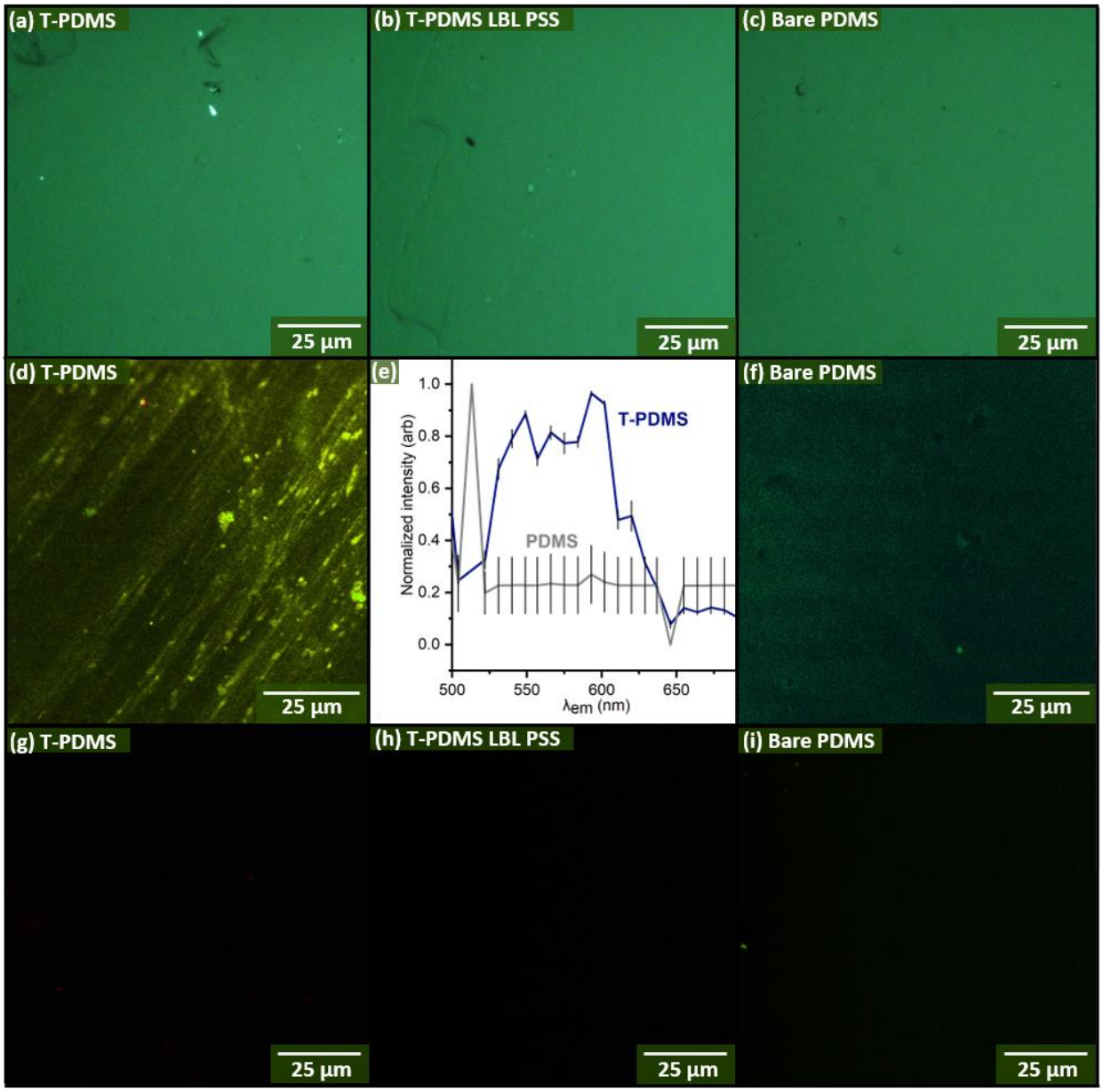

Figure S.B. 10 Fluorescence micrographs illustrating functionalized PDMS with (a) TCD-NH_2/PDMS, (b) TCD-NH_2/PDMS+PSS, and (c) bare PDMS. Fluorescence spectra (e) and images for (d) TCD-NH_2/PDMS, and (f) bare PDMS of fluorescence emission detected from 495–691 nm. Fluorescence images utilizing the 520 nm long-pass emission filter to capture red emission on (g) TCD-NH_2/PDMS, (h) TCD-NH_2/PDMS+PSS, and (i) bare PDMS substrates prior to TRITC-BSA adsorption.

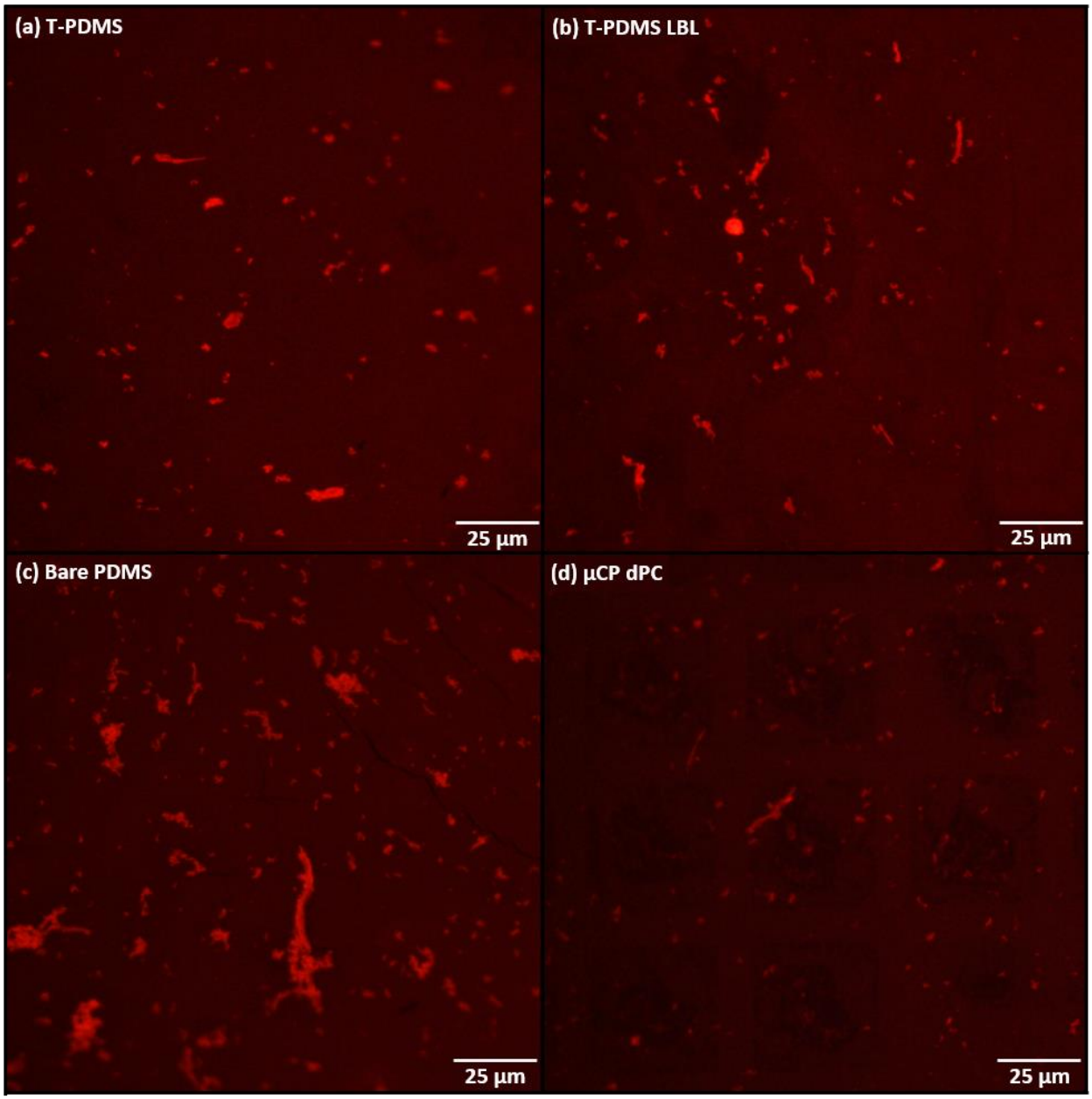

Figure S.B. 11 Fluorescence images illustrating TRITC-BSA adsorption on functionalized PDMS with (a) TCD-NH_2/PDMS (b) TCD-NH_2/PDMS+PSS, (c) bare PDMS, and (d) µCP dPC film.